Title
Development of a Light Actuated Drug Delivery-on-Demand System

Author
Linsley, Chase Schilling

Publication Date
2015

Peer reviewed|Thesis/dissertation

UNIVERSITY OF CALIFORNIA

Los Angeles

Development of a Light Actuated Drug Delivery-on-Demand System

A dissertation submitted in partial satisfaction of the requirements for the degree Doctor of Philosophy in Biomedical Engineering

by

Chase Schilling Linsley

2015

ABSTRACT OF THE DISSERTATION

Development of a Light Actuated Drug Delivery-on-Demand System

by

Chase Schilling Linsley

Doctor of Philosophy in Biomedical Engineering

University of California, Los Angeles, 2015

Professor Benjamin M. Wu, Chair

The need for temporal-spatial control over the release of biologically active molecules has motivated efforts to engineer novel drug delivery-on-demand strategies actuated via light irradiation. Many systems, however, have been limited to *in vitro* proof-of-concept due to biocompatibility issues with the photo-responsive moieties or the light wavelength, intensity and duration. To overcome these limitations, the objective of this dissertation was to design a light actuated drug delivery-on-demand strategy that uses biocompatible chromophores and safe wavelengths of light, thereby advancing the clinical prospects of light actuated drug delivery-on-demand systems. This was achieved by 1) characterizing the photothermal response of biocompatible visible light and near infrared-responsive chromophores, and demonstrating the feasibility and functionality of the light actuated on-demand drug delivery system *in vitro*; and 2) designing a modular drug delivery-on-demand system that could control the release of biologically active molecules over an extended period of time.

Three biocompatible chromophores – cardiogreen, methylene blue, and riboflavin – were identified and demonstrated significant photothermal response upon exposure to near infrared and visible light, and the amount of temperature change was dependent upon light intensity, wavelength as well as chromophore concentration. As a proof-of-concept, pulsatile release of a model protein from a thermally responsive delivery vehicle fabricated from poly (N-isopropylacrylamide) was achieved over four days by loading the delivery vehicle with cardiogreen and irradiating with near infrared light. To extend the useful lifetime of the light actuated drug delivery-on-demand system, a modular, reservoir-valve system was designed. Using poly (ethylene glycol) as a reservoir for model small molecule drugs combined with a poly (N-isopropylacrylamide) valve spiked with chromophore-loaded liposomes, pulsatile release was achieved over seven days upon light irradiation. Ultimately, this drug delivery strategy has potential for clinical applications that require explicit control over the presentation of biologically active molecules. Further research into the design and fabrication of novel biocompatible thermally responsive delivery vehicles will aid in the advancement of the light actuated drug delivery-on-demand strategy described here.

The dissertation of Chase Schilling Linsley is approved.

James C.Y. Dunn

Adrienne G. Lavine

Min Lee

Benjamin M. Wu, Committee Chair

University of California, Los Angeles

2015

DEDICATION

To Dad, Mom, Chelsea and Grandma too!

TABLE OF CONTENTS

LIST OF FIGURES

LIST OF TABLES

ACKNOWLEDGEMENTS

This dissertation would not have been possible without the support of Professor Benjamin Wu. Thank you for your guidance and for allowing me the freedom to make mistakes. I would also like to thank Prof. James Dunn, Prof. Min Lee and Prof. Adrienne Lavine for being part of my committee and helping make this a more complete dissertation. Additionally, special thanks to my co-advisor, Professor Bill Tawil, for your mentorship over the years and teaching me everything I know about fibrin.

Helpful advice and technical insight from my labmates over the years have helped make this dissertation possible. Thank you to: Helena Chia, Eric Tsang, Chris Walthers, Arnold Suwarnasarn, Yulong Zhang, Cheng-Han Chen, and Stephanie Reed. A special thanks to Abigail Parks (née Corrin) whose advice and friendship has been indispensable since we started this journey at CLU all those years ago. I would also like to thank Zhongkai Cui from Prof. Lee's lab for sharing his time and extensive knowledge in liposome fabrication with me.

A lot of time spent in the lab collecting data by my undergraduate research assistants has made this dissertation possible. Thank you to Gaurav Agrawal for your help collecting the chromophore characterization data. Thank you to Elyse Hartnett for your help designing the electrophoresis setup that was used to load cardiogreen into the NiPAAm hydrogels. Thank you to Viola Quach for all your help collecting the light actuated drug release data. For all the students who made their way through the Wu, Dunn and Lee labs during my time here, I look forward to being able to say, "I knew them when…"

Nearly every academic quarter while I was a graduate student at UCLA was spent serving as a Teaching Assistant. This not only allowed me to grow as an educator but was also my primary source of funding. Big thanks are owed to the professors who hired me as their TA, especially Prof. Don Browne. Your advice and mentorship over the years is greatly appreciated and will not be forgotten. I would also like to thank the University of California, Los Angeles Graduate Division for the Dissertation Year Fellowship.

Keeping me sane during these many years of graduate school were my friends. Thank you, thank you, THANK YOU for all the laughs: Josh, Katie, Dave, Jaclyn, Lauren, Jen, Greg, Steven, Madison, Nick, Katie, Eric, Julisa, Amanda and Jerry. I appreciate your patience and understanding when I had to miss out on the fun. I am undeserving of your friendship and lucky to have you all as cheerleaders!

Support from my family throughout this process has been unwavering and I will forever be in their debt. To my California family – Aunt Dorothy, Rachel, Darrell and Scott – thank you for the fun adventures as well as the room and board over the years. To Mom, Dad, Chelsea and Grandma, thank you for being my source of inspiration and courage. I love you all very much!

VITA

Education

University of California, Los Angeles, Los Angeles, CA — Sep. 2008 – Dec. 2009
Henry Samueli School of Engineering and Applied Sciences
Biomedical Engineering Interdepartmental Program
Master of Science

California Lutheran University, Thousand Oaks, CA — Aug. 2004 – May 2008
College of Arts and Sciences
Bioengineering
Bachelor of Science

Teaching Experience

Teaching Fellow — Apr. 2013 – Jun. 2014
Henry Samueli School of Engineering and Applied Sciences
University of California, Los Angeles

Teaching Associate — Sep. 2010 – Mar. 2013
Henry Samueli School of Engineering and Applied Sciences
University of California, Los Angeles

Teaching Assistant — Apr. 2009 – Aug. 2010
Henry Samueli School of Engineering and Applied Sciences
University of California, Los Angeles

Publications

Journal Publications

Linsley C, Wu B, Tawil B. The Effect of Fibrinogen, Collagen Type I and Fibronectin on Mesenchymal Stem Cells Growth and Differentiation into Osteoblasts. Tissue Engineering Part A. June 2013, 19(11-12): 1416-1423. doi:10.1089/ten.tea.2012.0523.

Publications in Submission

Linsley C, Wu B, Tawil B. Mesenchymal Stem Cell Growth On and Mechanical Properties of Fibrin-Based Biomimetic Bone Scaffolds. Submitted.

Linsley C, Quach V, Agrawal G, Hartnett E, Wu B. Visible light and near infrared-responsive chromophores for drug delivery-on-demand applications. Submitted.

Editorial

Linsley C, Boardman L, Tawil B. Fibrin-Based Matrices for Tissue Engineering. Austin Journal of Biomedical Engineering. 2014, 1(2): 2.

Proceedings

Linsley C, Tawil B. Cellular Response of Mesenchymal Stem Cells in Three-Dimensional Fibrin-Collagen-Calcium Phosphate Scaffolds. Oral presentation at Tissue Engineering and Regenerative Medicine International Society, Washington, DC, December 2014.

Linsley C, Wu B, Tawil B. Mechanical Properties of and Mesenchymal Stem Cell Growth on Three-Dimensional Biomimetic Bone Scaffolds. Poster presentation at Tissue Engineering and Regenerative Medicine International Society, Atlanta, Georgia, November 2013.

Linsley C, Hung M, Tawil B, Wu B. DNA for Drug Delivery-On-Demand Applications. Oral presentation at the 7th Nagoya University-UCLA International Symposium & Hokkaido University and Nagoya University Global COE Joint Symposium, Sapporo, Japan, September 2012.

Linsley C, Fard R, Wu B, Tawil B. Fabrication and Characterization of Multi-Component Biomimetic Scaffold for Bone Tissue Engineering. Poster presentation at Tissue Engineering and Regenerative Medicine International Society, Houston, Texas, December 2011.

Linsley C, Wu B, Tawil B. Osteogenic Differentiation of Mesenchymal Stem Cells on Various 2-D Substrates. Poster presentation at Tissue Engineering and Regenerative Medicine International Society, Orlando, Florida, December 2010.

CHAPTER ONE: INTRODUCTION

1.1 BACKGROUND

The path from drug discovery and development to market is challenging. A majority of drugs fail due to safety and efficacy issues that arise in the Food and Drug Administration's (FDA) Phase II and Phase III trials which become apparent as the number of patients increases as well as the length of the trials [1]. Many of these failures can be attributed to the fact that traditional methods of drug delivery flood the body with concentrations of drug required to reach the target area and have a therapeutic effect. The drawbacks to this approach include problems with drug instability, toxicity and overcoming barriers to the target area from the circulation system [2]. This contributes to the 13 year average for a new drug to reach the market with a 95% failure rate at an average cost of US$2 billion [3].

These figures have motivated efforts to streamline the process of getting new therapeutics to market. Recently, the National Institute of Health (NIH) established the National Center for Advancing Translational Sciences (NCATS) to help expedite the process for delivering new treatments to patients. One of the NCATS pilot programs, called Discovering New Therapeutic Uses for Existing Molecules, is designed to repurpose drugs that had passed safety testing but failed to achieve intended clinical outcomes. Advanced drug delivery systems are one way to rescue failed drugs. They aim to improve safety and efficacy by localizing drug delivery to the target site, having a rapid onset of action, reducing the amount of drug required for a therapeutic effect, and improving patient compliance.

Commercial and research interest in novel drug delivery systems has been growing in recent decades and is expected to continue rising. In 2013, advanced drug delivery systems made up a US$182 billion market globally and are projected to grow to US$213 billion market in 2018

[4]. Contributing to this demand for new methods of controlled delivery are the development of new pharmaceuticals out of macromolecules such as proteins, peptides, oligonucleotides, and plasmids [5]. These biologically active agents, termed 'biologics', account for 30% of licensed pharmaceutical products [6], and, in addition to traditional small molecule drugs, require delivery systems that overcome obstacles associated with poor solubility, degradation, unfavorable pharmacokinetics, poor biodistribution, lack of selectivity, and administration frequency. To date, there are a number of technologies that have been developed to meet these challenges.

1.2 CONTROLLED RELEASE TECHONLOGY

A couple of the earliest controlled release delivery systems designed to extend efficacy and reduce unwanted side effects were the oral osmotic delivery system and slow-release polymer-matrix systems. The use of an oral osmotic delivery system to slowly release oxprenolol, a non-selective beta blocker, demonstrated a blood plasma concentration of drug that persisted longer than the conventional regimen and reduced exercise induced tachycardia [7, 8]. Similarly, the controlled delivery of the drug pilocarpine from the Ocusert® system – a slow-release polymer matrix system – reduced ocular pressure caused by ocular hypertension and glaucoma to the same extent as eye drops of the drug administered four times a day [9, 10]. Both of these systems demonstrate zero order release where the drug release rate is independent of the starting drug concentration rather it is dependent on diffusion through a membrane. The Ocusert® system used poly (ethylene-co-vinyl acetate) as a membrane to control diffusion of the drug from a reservoir and the oral osmotic delivery system works by controlling the diffusion of water though a water-permeable jacket. As the osmotic pressure of water entering the tablet increases, drug is pushed through a laser cut hole in the jacket and released and other cardiovascular drugs

like methylphenidate, nifedipine, and oxybutynin have been delivered using the same system [11]. Current research efforts not only use diffusion as the mechanism to control the release of drugs but also utilize degradation of the carriers as well as drug-carrier affinity [12].

Degradation of the delivery vehicle is one of the release mechanisms for drugs that are uniformly distributed in a matrix, specifically in cases where degradation of the delivery vehicles occurs faster than diffusion [13]. Degradation can either be due to bulk or surface erosion. In bulk erosion, material is lost uniformly throughout the volume of the construct, and in surface erosion, there is a loss in volume and degradation only occurs at the surface [14]. The rate of release from the polymeric delivery vehicle is a function of the material properties (composition, hydrophobicity/hydrophilicity, molecular weight), which influence the susceptibility of the polymer bonds to hydrolysis, especially in polyesters and polyanhydrides [14, 15]. A well-known example of these types of delivery systems is the Gliadel® wafers. Approved in 2006 by the FDA for the treatment of malignant gliomas, they are a biodegradable polyanhydride copolymer of 20:80 molar ratio poly [bis (p-carboxyphenoxy) propane: sebacic acid] that is implanted in the tumor cavity for the local delivery of the anticancer drug carmustine [16]. Release occurs via erosion of the surface layer of the wafer and, as the eroding front advances, the surface of interior pores begin eroding as well [17]. This leads to an increase in the release rate overtime. The resulting degradation products are then cleared from the body via urine or exhaled as CO_2 [16]. For any delivery system that uses degradation as the release mechanism (or degradable materials in general), knowledge of what the degradation products are and evaluation of the *in vivo* effects of each degradation products is needed to insure to that they don't cause unwanted side effects.

Affinity-controlled release systems are less dependent on the properties of the polymer matrix (e.g. degradation rate, pore size, etc.) [18]; instead, they utilize molecular interactions between the drug of interest and the delivery vehicle to modulate drug delivery. These interactions include hydrogen bonding, van der Waals forces, ionic interactions and hydrophobic interactions, and are observed in many biological processes, such as receptor-ligand binding [19]. For an affinity-controlled release system, the association constant describes how readily a drug will be released. Taking advantage of the interactions that naturally occur in the body, delivery vehicles made out of a variety of materials, including extracellular matrix (ECM) proteins and synthetic polymers, have been fitted with heparin for the controlled release of heparin-binding growth factors, such as basic fibroblast growth factor (bFGF). For example, fibrin matrices functionalized with heparin released bioactive bFGF to enhance neurite extension. In this system, release occurred due to dissociation of the bFGF from heparin (independent of cells) as well as enzymatic degradation of both the fibrin and heparin (cell mediated) [20]. There are a number of different delivery systems, beyond heparin, that utilize affinity between the drug and delivery vehicle to control release. For instance, cyclodextrin-based polymers have a cup-shape architecture with a hydrophobic cavity that complexes with hydrophobic drugs [21], and molecular imprinting fits polymers with recognition elements for the drug of interest to lock it in place and slowly release [22]. Regardless of the approach used, the main advantages of using affinity-controlled systems are 1) capacity to deliver multiple drugs at different rates as long as each drug has a different affinity for the delivery vehicle and 2) ability to reload the delivery vehicle with drug by a single injection [18].

Overall, these controlled release systems aim to maintain a constant drug concentration – defined by a therapeutic window where high drug concentration results in unwanted side effects

and low concentration has no therapeutic effect – by the sustained release of drug overtime. However, different applications require different release profiles and it is not always desirable to have prolonged exposure to a biologically active molecule. For some applications, it is more advantageous to have explicit control on when a drug is released and when it is not.

1.3 BIOMEDICAL APPLICATIONS REQUIRING DELIVERY-ON-DEMAND

Chronotherapy uses the body's rhythmic cycles to deliver drugs at times when the body is most receptive to treatment, thereby maximizing their therapeutic effects. There are numerous examples where chronotherapy has been shown to improve the efficacy of therapeutics, including hypertension, asthma, duodenal ulcer, hypercholesterolemia, and neurological disorders [23]. For patients with diabetes, the delivery of insulin is required when there is a spike in blood sugar concentration. Rheumatoid arthritis patients have increased levels of interleukin-6 (IL-6) during the night. This contributes to morning stiffness and inflammation to a greater extent since cortisol levels don't increase for another 3 hours [24]. Therefore, properly timed delivery of prednisone, an immunosuppressant drug, can be used to help alleviate morning stiffness. Drug delivery-on-demand systems are uniquely suited to these applications since release is dependent upon the intensity and/or duration of each stimulus and is marked by sharp increases in the amount released upon stimulation and little-to-no release in the absence of stimulation.

One such applications is the delivery of human parathyroid hormone fragment (1-34) [hPTH(1-34)], which has been FDA approved since 2002 to treat osteoporosis. Current treatment requires daily injections since *sustained* exposure to hPTH(1-34) promoted osteoclast activity whereas *intermittent* injections promoted osteoblast activity [25, 26]. In 2012, clinical trials began for an implantable, wirelessly controlled drug delivery device that would deliver hPTH(1-

34) in a pulsatile manner in lieu of daily injections for osteoporosis treatment. The device (54 mm x 31 mm x 11 mm, l x w x h) delivered daily doses of 40 µg for 3 weeks in seven postmenopausal women with osteoporosis [26]. While the device was able to release active drug and subsequently promote bone growth, there is room for improvement. The device is made of non-biodegradable materials (i.e. silicone and titanium) and requires removal after the drug reservoirs are depleted. This would require multiple replacement procedures – subcutaneous implantation in the abdomen – over the approved 2-year treatment period for hPTH(1-34) [27]. Additionally, the tissue capsule that forms around implants can interfere with drug release. Despite these limitations, the delivery-on-demand approach has a customizable release profile to achieve the desired efficacy without the need for repeated needle injections.

Another area where drug delivery-on-demand is applicable is in cancer treatment. A study on the sensitivity of C57BL/6J male mice to the anticancer drug cyclophosphamide showed that mice treated at the time of dark-to-light transition had a 20% survival rate while mice treated at the time of light-to-dark transition had an 80% survival rate [28]. In this particular case, the difference in cyclophosphamide sensitivity resulted from circadian control of lymphocyte survival/recovery [28]. Similar outcomes likely exist for the numerous types of cancers and their numerous treatment options since the expression of growth factors at different times of the day can change the sensitivity of cancer cells to a chemotherapy agent and/or the survivability healthy cells. However, there is still relatively little known about the mechanism of action for such treatments which has limited its practice [29].

As evident by these clinical examples, timing is everything, and traditional methods of drug delivery (e.g. bolus injections, pills, and inhalants) fail to account for biological differences throughout the day. These differences are controlled by the suprachiasmatic nucleus (SCN) of

the hypothalamus via the expression of *period* and *cryptochrome* genes in the neurons of SCN, which are regulated by the transcription factors: CLOCK and BMAL1. Biological functions, such as body temperature, blood pressure, immune activity, enzyme and hormone production, are regulated by this internal clock and can thereby influence cells' sensitivity to different therapeutic agents [29]. The failure to account for these temporal differences results is a decrease in the efficacy of treatment and an increase in wasted drug. Drug delivery-on-demand systems are well suited for these applications since they allow for explicit temporal and spatial control and subsequently enhance the therapeutic effect while decreasing the amount of drug required. To date, many systems have been engineered to meet this clinical need (Table 1). These systems modulate release as a function of a specific stimuli and they work in either a closed or open circuit [2, 30].

1.4 DELIVERY-ON-DEMAND SYSTEMS

Closed-loop systems are self-regulated and have no external intervention to control release [31]. Instead, these systems respond to changes in the physiological environment [32]. Approaches used to trigger release in closed-loop systems include: changes in pH, temperature changes, and the presence or absence of biological molecules. For example, the pH of inflammatory tissue, tumors (pH~6.8) and the lysosome (pH ~5-6) is lower than physiological pH of 7.4, thereby providing a localized trigger for release from pH sensitive delivery vehicles [33]. Many of the pH sensitive delivery systems use hydrazone as the linker, which is stable at neutral pH (such as in the blood) but undergoes hydrolysis in acidic conditions (such as in lysosomes) [34]. However, closed-loop systems have several shortcomings. In diseased state models, closed-loop systems may fail due to an overproduction or absence of local triggering molecules. Additionally, systemic infections could non-specifically trigger release from pH and

temperature sensitive carriers. Finally, these systems need to be tailored to a specific application and, therefore, lack versatility. For example, colon-specific delivery systems often utilize polysaccharides as the delivery vehicle because they are degraded by enzymes like dextranase and glycosidase, which are native to the colon [35]. This system, however, could not be readily translated to applications for bone tissue, which has alkaline phosphatase and cathepsin K as local enzymes [36].

Open-loop systems are independent of the physiological environment and release biologically active molecules in response to a remote or external stimulation. Unlike closed-loop systems, open-loop systems release biologically active molecules in response to external stimulation instead of physiological variables. The release profile from open-loop systems is dependent upon the intensity and/or duration of each stimulus and is marked by a sharp increase in the amount released upon stimulation and little to no release in the absence of stimulation [2, 31, 32]. There are numerous publications which have studied different external stimulations to trigger release, including light irradiation, heat, magnetic field, and ultrasound. For example, ultrasound waves have been an attractive stimulus to mediate drug delivery due to their widespread use and deep-tissue penetration. The mechanisms for drug release from ultrasound waves include cavitation, streaming and hyperthermia and the delivery vehicles range from liposomes and micelle nanocarries to microbubbles [37]. Other groups have fabricated drug delivery systems that respond to the application of a magnetic field. Recently, Fe_3O_4 nanoparticles trapped within hollow nanocapsules with a porous silica shell were used to successfully deliver the hydrophobic drug camptothecin by using magnetic hyperthermia to induce the diffusion of drug [38]. Despite the *in vitro* proof-of-concept successes of open-loop systems, few have been tested in animal models and only thermosensitive liposomes and iron

oxide nanoparticles have reached clinical trials partly due to the complex design of many of these systems [39]. A concise summary of additional limitations of open-loop systems are presented in Table 2.

Light actuated delivery-on-demand systems are plagued by many of these limitations. This is unfortunate since light as the external stimulus is advantageous for a number of reasons, including its non-invasive nature, high spatial resolution and temporal control, as well as convenience and ease of use. Many light actuated systems use ultraviolet (UV) light to act upon photo-responsive moieties within the polymeric drug delivery vehicles, and the mechanisms for release include isomerization and cleavage [40]. For example, groups have created liposomes using azobenzene, which undergo a *trans-cis* isomerization when exposed to 340-380 nm irradiation, in the lipid backbone, and exposure to UV light causes the tightly packed *trans* form of azobenzene to adopt a *cis* conformation, thereby creating a leaky lipid bilayer that allows for release [41]. Additionally, ortho-nitrobenzyl moieties have been included in hydrogel networks to act as the photodegradable functionality after exposure to 365 nm light in order to facilitate release, both spatially and temporally [42]. However, the reliance on UV radiation hinders translation to *in vivo* due to mutagenicity and low tissue transparency in the UV region [43]. Also, azobenzene and some of its degradation products, including nitrobenzene, are considered toxic by the FDA [2, 44]. As such, light actuated drug delivery-on-demand systems currently serve as *in vitro* models only due to biocompatibility issues with the photo-responsive moieties or the light wavelength, intensity and duration.

1.5 DISSERTATION OBJECTIVES AND SPECIFIC AIMS

To overcome the obstacles to get light actuated delivery systems to the clinic, research is needed in developing strategies that use safe wavelengths of light as well as biocompatible

photo-responsive materials. Visible and near infrared (NIR) light are safe stimuli for *in vivo* applications. Additionally, non-toxic and biocompatible chromophores for visible and NIR light can be employed to release biologically active molecules from thermally responsive polymeric delivery vehicles via the photothermal effect and eliminate the need for toxic photo-responsive materials. Therefore, the objective was to design a light actuated drug delivery-on-demand system that uses biocompatible chromophores and safe wavelengths of light, thereby advancing the clinical prospects of light actuated drug delivery-on-demand systems.

This objective was achieved by completing the following specific aims:

1. Characterizing the photothermal response of biocompatible visible light and NIR-responsive chromophores for drug delivery-on-demand applications, and demonstrating the feasibility and functionality of the light actuated on-demand drug delivery system *in vitro*.
2. Designing a modular drug delivery-on-demand system that can control the release of biologically active molecules over an extended period of time.

1.6 TABLES

Table 1. Select drug delivery-on-demand systems since 2010

Classification	Stimulus	Payload	Delivery Vehicle	Reference
Closed-Loop	Biomarker	Insulin *hormone*	Nanogel containing a glucose-sensitive PBA moiety	[45]
		siRNA *gene silencing*	PEG-PCL micelles containing MMP-2-degradable peptide PLG*LAG	[46]
		DPAP inhibitor *antimalarial drug*	Fe^{II}-sensitive 1,2,4-trioxolane ring	[47]
	pH	Doxorubicin *chemotherapeutic agent*	PEG-PbAE block co-polymer micelles	[48]
		AAV2 *gene therapy*	Poly(PEG-ApIm-PEG-Asp) and PEI_{800} matrix	[49]
		Serum albumin *model protein*	PEG-PbAE block co-polymer micelles	[50]
Open-Loop	Heat	Doxorubicin *chemotherapeutic agent*	DPPC-based liposome modified with ELP	[51]
		PTHrP 107–111 *hormone peptide*	DPPC-based liposome with MSPC	[52]
	Electrical	Daunorubicin *chemotherapeutic agent*	Polypyrrole nanoparticles	[53]
		Ketoprofen *anti-inflammatory drug*	PEO/PETA matrix with multi-walled carbon nanotubes	[54]
	Light	Fluorophores *model compounds*	PLGA capsules	[55]
		Doxorubicin *chemotherapeutic agent*	PEG-coated HAuNS	[56]
		Aspart *insulin*	ethylcellulose matrix containing HAuNS & NG	[57]

	Magnetic	Doxorubicin *chemotherapeutic agent*	USPIO loaded polymersomes	[58]
		Nimesulide *anti-inflammatory drug*	$Fe_3O_4/Cu_3(BTC)_2$ nanocomposites	[59]
		Camptothecin *chemotherapeutic agent*	$SAIO@SiO_2$	[60]
	Ultrasound	Mitoxantrone *chemotherapeutic agent*	ionically cross-linked polymers	[61]
		Doxorubicin *chemotherapeutic agent*	Liposome-loaded microbubbles	[62]

*Acronyms: phenylboronic acid, PBA; small interfering RNA, siRNA; poly(ethylene glycol), PEG; poly(ε-caprolactone), PCL; matrix metalloproteinase 2, (MMP-2); Pro–Leu–Gly–Leu–Ala–Gly, PLG*LAG; parasite cysteine protease dipeptidyl aminopeptidase, DPAP; ferrous iron, Fe^{II} ; poly(β-amino ester), PbAE; recombinant adeno-associated virus serotype 2, AAV2; 1-(3-aminopropyl)imidazole, ApIm; DL-aspartic acid, Asp; polyethyleneimine, PEI_{800}; dipalmitoylphosphatidylcholine, DPPC; elastin-like polypeptide, ELP; parathyroid hormone-related protein, PTHrP; 1-monostearoyl phosphatidylcholine, MSPC; polyethylene oxide, PEO; pentaerythritol triacrylate, PETA; poly(lactic-co-glycolic acid), PLGA; hollow gold nanospheres HAuNS; copolymer nanogel comprised of N-isopropylacrylamide, N-isopropylmethacrylamide, and acrylamide, NG; ultrasmall superparamagnetic iron oxide nanoparticles, USPIO; benzene-1,3,5-tricarboxylate, BTC; iron oxide/silica core–shell nanocarries, $SAIO@SiO_2$.*

Table 2. Limitations of open-loop drug delivery-on-demand systems

Stimulus	Limitations	Reference
Electrical	Risk of damage to healthy tissue from electric source needed for deep tissue penetration (attenuation of stimulus)	[39]
Heat	Risk of superficial tissue damage from external heating source needed for deep tissue penetration (attenuation of stimulus)	[63]
Light	Questionable safety and/or biodegradability of materials	[2]
	Safety risks and/or low tissue penetration for UV-Vis light	[39]
Magnetic	Potential toxicity from iron oxide	[64]
	Requires complex equipment set-up for adequate focusing, intensity and penetration depth	[39]
Ultrasound	Low drug carrier stability	[37]
	Minimal safety risks with *low* intensity and *short* exposures	[65]

Acronyms: ultraviolet, UV; visible, Vis.

1.7 REFERENCES

[1] J. Arrowsmith, P. Miller, Phase II and Phase III attrition rates 2011-2012, Nature Reviews Drug Discovery, 12 (2013) 568-568.

[2] C. Alvarez-Lorenzo, L. Bromberg, A. Concheiro, Light-sensitive Intelligent Drug Delivery Systems, Photochemistry and Photobiology, 85 (2009) 848-860.

[3] F.S. Collins, Reengineering Translational Science: The Time Is Right, Science Translational Medicine, 3 (2011) 6.

[4] S.S. Dewan, Global Markets and Technologies for Advanced Drug Delivery Systems, in, Business Communications Company, Wellesley, MA, 2014, pp. 218.

[5] T.M. Allen, P.R. Cullis, Drug delivery systems: entering the mainstream, Science, 303 (2004) 1818.

[6] J.G. Sathish, S. Sethu, M.-C. Bielsky, L. de Haan, N.S. French, K. Govindappa, J. Green, C.E.M. Griffiths, S. Holgate, D. Jones, I. Kimber, J. Moggs, D.J. Naisbitt, M. Pirmohamed, G. Reichmann, J. Sims, M. Subramanyam, M.D. Todd, J.W. Van der Laan, R.J. Weaver, B.K. Park, Challenges and approaches for the development of safer immunomodulatory biologics, Nature Reviews Drug Discovery, 12 (2013) 306-324.

[7] W.J. Leahey, J.D. Neill, M.P.S. Varma, R.G. Shanks, Comparison of the activity and plasma-levels of oxprenolol, slow release oxprenolol, long-acting propranolol and sotalol, European Journal of Clinical Pharmacology, 17 (1980) 419-424.

[8] M.J. West, M.J. Kendall, M. Mitchard, E.B. Faragher, Comparison of slow release with conventional oxprenolol - plasma concentrations and clinical effects, British Journal of Clinical Pharmacology, 3 (1976) 439-443.

[9] H.A. Quigley, I.P. Pollack, T.S. Harbin, Pilocarpine ocuserts - long-term clinical trials and selected pharmacodynamics, Archives of Ophthalmology, 93 (1975) 771-775.

[10] M.F. Armaly, K.R. Rao, Effect of pilocarpine ocusert with different release rates on ocular pressure, Investigative Ophthalmology, 12 (1973) 491-496.

[11] H. Rosen, T. Abribat, The rise and rise of drug delivery, Nature Reviews Drug Discovery, 4 (2005) 381-385.

[12] C.J. Kearney, D.J. Mooney, Macroscale delivery systems for molecular and cellular payloads, Nature Materials, 12 (2013) 1004-1017.

[13] K.S. Soppimath, T.M. Aminabhavi, A.R. Kulkarni, W.E. Rudzinski, Biodegradable polymeric nanoparticles as drug delivery devices, Journal of Controlled Release, 70 (2001) 1-20.

[14] A. Gopferich, Mechanisms of polymer degradation and erosion, Biomaterials, 17 (1996) 103-114.

[15] M. Lee, T.T. Chen, M.L. Iruela-Arispe, B.M. Wu, J.C.Y. Dunn, Modulation of protein delivery from modular polymer scaffolds, Biomaterials, 28 (2007) 1862-1870.

[16] M. Panigrahi, P.K. Das, P.M. Parikh, Brain tumor and Gliadel wafer treatment, Indian Journal of Cancer, 48 (2011) 11-17.

[17] W.B. Dang, T. Daviau, H. Brem, Morphological characterization of polyanhydride biodegradable implant GLIADEL(R) during in vitro and in vivo erosion using scanning electron microscopy, Pharmaceutical Research, 13 (1996) 683-691.

[18] A.S. Fu, H.A. von Recum, Affinity-Based Drug Delivery, in: R.A. Bader, D.A. Putnam (Eds.) Engineering Polymer Systems for Improved Drug Delivery, John Wiley & Sons, Inc., Hoboken, New Jersey, 2014, pp. 429-452.

[19] N.X. Wang, H.A. von Recum, Affinity-Based Drug Delivery, Macromolecular Bioscience, 11 (2011) 321-332.

[20] S.E. Sakiyama-Elbert, J.A. Hubbell, Development of fibrin derivatives for controlled release of heparin-binding growth factors, Journal of Controlled Release, 65 (2000) 389-402.

[21] M.E. Davis, M.E. Brewster, Cyclodextrin-based pharmaceutics: Past, present and future, Nature Reviews Drug Discovery, 3 (2004) 1023-1035.

[22] M.E. Byrne, K. Park, N.A. Peppas, Molecular imprinting within hydrogels, Advanced Drug Delivery Reviews, 54 (2002) 149-161.

[23] B.B.C. Youan, Chronopharmaceutics: gimmick or clinically relevant approach to drug delivery?, Journal of Controlled Release, 98 (2004) 337-353.

[24] F. Buttgereit, G. Doering, A. Schaeffler, S. Witte, S. Sierakowski, E. Gromnica-Ihle, S. Jeka, K. Krueger, J. Szechinski, R. Alten, Targeting pathophysiological rhythms: prednisone chronotherapy shows sustained efficacy in rheumatoid arthritis, Annals of the Rheumatic Diseases, 69 (2010) 1275-1280.

[25] T. Uzawa, M. Hori, S. Ejiri, H. Ozawa, Comparison of the effects of intermittent and continuous administration of human parathyroid hormone(1-34) on rat bone, Bone, 16 (1995) 477-484.

[26] R. Farra, N.F. Sheppard, Jr., L. McCabe, R.M. Neer, J.M. Anderson, J.T. Santini, Jr., M.J. Cima, R. Langer, First-in-Human Testing of a Wirelessly Controlled Drug Delivery Microchip, Science Translational Medicine, 4 (2012).

[27] C. Deal, J. Gideon, Recombinant human PTH 1-34 (Forteo): An anabolic drug for osteoporosis, Cleveland Clinic Journal of Medicine, 70 (2003) 585-586.

[28] V.Y. Gorbacheva, R.V. Kondratov, R.L. Zhang, S. Cherukuri, A.V. Gudkov, J.S. Takahashi, M.P. Antoch, Circadian sensitivity to the chemotherapeutic agent cyclophosphamide depends on the functional status of the CLOCK/BMAL1 transactivation complex, Proceedings of the National Academy of Sciences of the United States of America, 102 (2005) 3407-3412.

[29] L.N. Fu, C.C. Lee, The circadian clock: Pacemaker and tumour suppressor, Nature Reviews Cancer, 3 (2003) 350-361.

[30] D.A. LaVan, T. McGuire, R. Langer, Small-scale systems for in vivo drug delivery, Nature Biotechnology, 21 (2003) 1184-1191.

[31] J. Kost, R. Langer, Responsive polymeric delivery systems, Advanced Drug Delivery Reviews, 46 (2001) 125-148.

[32] S. Sershen, J. West, Implantable, polymeric systems for modulated drug delivery, Advanced Drug Delivery Reviews, 54 (2002) 1225-1235.

[33] O. Onaca, R. Enea, D.W. Hughes, W. Meier, Stimuli-Responsive Polymersomes as Nanocarriers for Drug and Gene Delivery, Macromolecular Bioscience, 9 (2009) 129-139.

[34] A.M. Wu, P.D. Senter, Arming antibodies: prospects and challenges for immunoconjugates, Nature Biotechnology, 23 (2005) 1137-1146.

[35] A. Jain, Y. Gupta, S.K. Jain, Perspectives of biodegradable natural polysaccharides for site-specific drug delivery to the colon, Journal of Pharmacy and Pharmaceutical Sciences, 10 (2007) 86-128.

[36] M.J. Seibel, Biochemical markers of bone turnover: part I: biochemistry and variability, The Clinical biochemist. Reviews / Australian Association of Clinical Biochemists, 26 (2005) 97-122.

[37] S.R. Sirsi, M.A. Borden, State-of-the-art materials for ultrasound-triggered drug delivery, Advanced Drug Delivery Reviews, 72 (2014) 3-14.

[38] S.D. Kong, C. Choi, J. Khamwannah, S. Jin, Magnetically Vectored Delivery of Cancer Drug Using Remotely On-Off Switchable NanoCapsules, Ieee Transactions on Magnetics, 49 (2013) 349-352.

[39] S. Mura, J. Nicolas, P. Couvreur, Stimuli-responsive nanocarriers for drug delivery, Nature Materials, 12 (2013) 991-1003.

[40] I. Tomatsu, K. Peng, A. Kros, Photoresponsive hydrogels for biomedical applications, Advanced Drug Delivery Reviews, 63 (2011) 1257-1266.

[41] N. Fomina, J. Sankaranarayanan, A. Almutairi, Photochemical mechanisms of light-triggered release from nanocarriers, Advanced Drug Delivery Reviews, 64 (2012) 1005-1020.

[42] A.M. Kloxin, A.M. Kasko, C.N. Salinas, K.S. Anseth, Photodegradable Hydrogels for Dynamic Tuning of Physical and Chemical Properties, Science, 324 (2009) 59-63.

[43] T. Tadokoro, N. Kobayashi, B.Z. Zmudzka, S. Ito, K. Wakamatsu, Y. Yamaguchi, K.S. Korossy, S.A. Miller, J.Z. Beer, V.J. Hearing, UV-induced DNA damage and melanin content in human skin differing in racial/ethnic origin, Faseb Journal, 17 (2003) 1177-1179.

[44] J.M. Joseph, H. Destaillats, H.M. Hung, M.R. Hoffmann, The sonochemical degradation of azobenzene and related azo dyes: Rate enhancements via Fenton's reactions, Journal of Physical Chemistry A, 104 (2000) 301-307.

[45] L. Zhao, C. Xiao, J. Ding, P. He, Z. Tang, X. Pang, X. Zhuang, X. Chen, Facile one-pot synthesis of glucose-sensitive nanogel via thiol-ene click chemistry for self-regulated drug delivery, Acta Biomaterialia, 9 (2013) 6535-6543.

[46] H.-X. Wang, X.-Z. Yang, C.-Y. Sun, C.-Q. Mao, Y.-H. Zhu, J. Wang, Matrix metalloproteinase 2-responsive micelle for siRNA delivery, Biomaterials, 35 (2014) 7622-7634.

[47] E. Deu, I.T. Chen, E.M.W. Lauterwasser, J. Valderramos, H. Li, L.E. Edgington, A.R. Renslo, M. Bogyo, Ferrous iron-dependent drug delivery enables controlled and selective release of therapeutic agents in vivo, Proceedings of the National Academy of Sciences of the United States of America, 110 (2013) 18244-18249.

[48] W. Song, Z. Tang, M. Li, S. Lv, H. Yu, L. Ma, X. Zhuang, Y. Huang, X. Chen, Tunable pH-Sensitive Poly(beta-amino ester)s Synthesized from Primary Amines and Diacrylates for Intracellular Drug Delivery, Macromolecular Bioscience, 12 (2012) 1375-1383.

[49] S.J. Tseng, I.M. Kempson, S.-F. Peng, B.-H. Ke, H.-H. Chen, P.-F. Chen, Y. Hwu, Environment acidity triggers release of recombinant adeno-associated virus serotype 2 from a tunable matrix, Journal of Controlled Release, 170 (2013) 252-258.

[50] G.H. Gao, M.J. Park, Y. Li, G.H. Im, J.-H. Kim, H.N. Kim, J.W. Lee, P. Jeon, O.Y. Bang, J.H. Lee, D.S. Lee, The use of pH-sensitive positively charged polymeric micelles for protein delivery, Biomaterials, 33 (2012) 9157-9164.

[51] M.S. Kim, D.-W. Lee, K. Park, S.-J. Park, E.-J. Choi, E.S. Park, H.R. Kim, Temperature-triggered tumor-specific delivery of anticancer agents by cRGD-conjugated thermosensitive liposomes, Colloids and Surfaces B-Biointerfaces, 116 (2014) 17-25.

[52] A. Lopez-Noriega, E. Ruiz-Hernandez, E. Quinlan, G. Storm, W.E. Hennink, F.J. O'Brien, Thermally triggered release of a pro-osteogenic peptide from a functionalized collagen-based scaffold using thermosensitive liposomes, Journal of Controlled Release, 187 (2014) 158-166.

[53] J. Ge, E. Neofytou, T.J. Cahill, III, R.E. Beygui, R.N. Zare, Drug Release from Electric-Field-Responsive Nanoparticles, Acs Nano, 6 (2012) 227-233.

[54] J.S. Im, B.C. Bai, Y.-S. Lee, The effect of carbon nanotubes on drug delivery in an electro-sensitive transdermal drug delivery system, Biomaterials, 31 (2010) 1414-1419.

[55] M.L. Viger, W. Sheng, K. Dore, A.H. Alhasan, C.-J. Carling, J. Lux, C.d.G. Lux, M. Grossman, R. Malinow, A. Almutairi, Near-Infrared-Induced Heating of Confined Water in Polymeric Particles for Efficient Payload Release, Acs Nano, 8 (2014) 4815-4826.

[56] J. You, G. Zhang, C. Li, Exceptionally High Payload of Doxorubicin in Hollow Gold Nanospheres for Near-Infrared Light-Triggered Drug Release, Acs Nano, 4 (2010) 1033-1041.

[57] B.P. Timko, M. Arruebo, S.A. Shankarappa, J.B. McAlvin, O.S. Okonkwo, B. Mizrahi, C.F. Stefanescu, L. Gomez, J. Zhu, A. Zhu, J. Santamaria, R. Langer, D.S. Kohane, Near-infrared-actuated devices for remotely controlled drug delivery, Proceedings of the National Academy of Sciences of the United States of America, 111 (2014) 1349-1354.

[58] H. Oliveira, E. Perez-Andres, J. Thevenot, O. Sandre, E. Berra, S. Lecommandoux, Magnetic field triggered drug release from polymersomes for cancer therapeutics, Journal of Controlled Release, 169 (2013) 165-170.

[59] F. Ke, Y.-P. Yuan, L.-G. Qiu, Y.-H. Shen, A.-J. Xie, J.-F. Zhu, X.-Y. Tian, L.-D. Zhang, Facile fabrication of magnetic metal-organic framework nanocomposites for potential targeted drug delivery, Journal of Materials Chemistry, 21 (2011) 3843-3848.

[60] W.L. Tung, S.H. Hu, D.M. Liu, Synthesis of nanocarriers with remote magnetic drug release control and enhanced drug delivery for intracellular targeting of cancer cells, Acta Biomaterialia, 7 (2011) 2873-2882.

[61] N. Huebsch, C.J. Kearney, X. Zhao, J. Kim, C.A. Cezar, Z. Suo, D.J. Mooney, Ultrasound-triggered disruption and self-healing of reversibly cross-linked hydrogels for drug delivery and enhanced chemotherapy, Proceedings of the National Academy of Sciences of the United States of America, 111 (2014) 9762-9767.

[62] B. Geers, I. Lentacker, N.N. Sanders, J. Demeester, S. Meairs, S.C. De Smedt, Self-assembled liposome-loaded microbubbles: The missing link for safe and efficient ultrasound triggered drug-delivery, Journal of Controlled Release, 152 (2011) 249-256.

[63] T. Tagami, W.D. Foltz, M.J. Ernsting, C.M. Lee, I.F. Tannock, J.P. May, S.-D. Li, MRI monitoring of intratumoral drug delivery and prediction of the therapeutic effect with a multifunctional thermosensitive liposome, Biomaterials, 32 (2011) 6570-6578.

[64] Wahajuddin, S. Arora, Superparamagnetic iron oxide nanoparticles: magnetic nanoplatforms as drug carriers, International Journal of Nanomedicine, 7 (2012) 3445-3471.

[65] H. Shankar, P.S. Pagel, Potential Adverse Ultrasound-related Biological Effects A Critical Review, Anesthesiology, 115 (2011) 1109-1124.

CHAPTER TWO: VISIBLE LIGHT AND NEAR INFRARED-RESPONSIVE CHROMOPHORES FOR DRUG DELIVERY-ON-DEMAND APPLICATIONS

2.1 ABSTRACT

The need for temporal-spatial control over the release of biologically active molecules has motivated efforts to engineer novel drug delivery-on-demand strategies actuated via light irradiation. Many systems, however, have been limited to *in vitro* proof-of-concept due to biocompatibility issues with the photo-responsive moieties or the light wavelength, intensity and duration. To overcome these limitations, this paper describes a light actuated drug delivery-on-demand strategy that uses visible and near infrared (NIR) light and biocompatible chromophores: cardiogreen, methylene blue and riboflavin. All 3 chromophores are capable of significant photothermal reaction upon exposure to NIR and visible light, and the amount of temperature change is dependent upon light intensity, wavelength as well as chromophore concentration. Pulsatile release of bovine serum albumin (BSA) from thermally-responsive hydrogels was achieved over 4 days. These findings have the potential to translate light actuated drug delivery-on-demand systems from the bench to clinical applications that require explicit control over the presentation of biologically active molecules.

2.2 INTRODUCTION

Traditional methods of drug delivery, which load the body with high concentrations of drug, have problems with drug instability, toxicity and overcoming barriers to the target area from the circulation system [1]. To overcome these drawbacks, delivery systems were developed to localize the delivery, enable rapid onset of action, reduce the amount of drug required, and improve patient compliance. One approach is drug delivery-on-demand systems. These systems modulate the release of drugs as a function of stimuli intensity [1-4]. Stimuli that have been used

to control release include: light irradiation, heat, electrical or magnetic fields, mechanical compression and ultrasound. Light as the stimulus for drug delivery-on-demand systems is advantageous for a number of reasons: it is non-invasive, convenient, easy to use, and offers high spatial resolution and temporal control.

Many light actuated systems use ultraviolet (UV) light to act upon photo-responsive moieties within the polymeric drug delivery vehicles. The photo-responsive moieties use UV light for either isomerization or chemical reactions that facilitate release [5]. However, the reliance on UV radiation hinders clinical translation due to low tissue transparency in the UV region [6]. Additionally, repetitive low-dose (18 J/cm^2) exposure to UVA radiation (320-400nm) caused an increase in inflammatory infiltrates, depleted Langerhans cells and increased lysozyme deposition in human skin [7]. Furthermore, photo-responsive moieties (e.g. azobenzene) and some of their degradation products are considered toxic by the U.S. Food and Drug Administration (FDA) [1, 8]. For these reasons, light actuated drug delivery-on-demand systems only serve as proof-of-concept models due to the problems with mutagenicity, toxicity and biocompatibility. Despite these shortcomings, light actuated drug delivery-on-demand systems offer precise and explicit triggering of release as well as versatility in clinical applications. Therefore, the development of a light actuated system that improves upon the shortcomings of UV systems will advance the clinical applications of light actuated drug delivery-on-demand systems.

Visible and near infrared (NIR) light actuation eliminates the negative side effects that accompany UV irradiation, such as DNA and tissue damage [6, 9], thereby making them a safe stimulus for *in vivo* applications. Furthermore, utilizing non-toxic and biocompatible chromophores for visible and NIR light eliminates the need for toxic photo-responsive materials.

In this approach, the radiationless dissipation of a chromophore's excess energy from an absorbed photon can serve as a heat source, and this photothermal effect can be used to release biologically active molecules from a thermally responsive polymeric delivery vehicle.

This study aimed to characterize the photothermal effect of cardiogreen, methylene blue and riboflavin upon light irradiation, and demonstrate triggered release. Cardiogreen, methylene blue and riboflavin are non-toxic and biocompatible, unlike azobenzene and o-nitrobenzene used in UV systems. Cardiogreen has multiple medical diagnostic applications, such as measuring cardiac output [10]. Methylene blue is used in technologies that sterilize blood products through photo-inactivation [11, 12], and riboflavin is naturally occurring in the body as a constituent of the coenzymes flavin mononucleotide and flavin adenine dinucleotide [13]. Additionally, these chromophores have absorption peaks in the NIR or visible region. Cardiogreen has a NIR absorbance peak at 780 nm [10], and methylene blue absorbs in the red region with a major peak at 665 nm [12]. The absorption spectrum of riboflavin shows four distinct absorbance peaks with one of the peaks in the visible region at 445 nm [14]. Furthermore, the quantum efficiency of fluorescence for these chromophores is low, which suggests there is a high occurrence of radiationless transitions – one of which is heat generation – when these molecules are excited with light. Cardiogreen's quantum efficiency for fluorescence is 0.027 in water [10]. Methylene blue has a quantum efficiency of 0.01 in aqueous solutions [15], and the quantum efficiency of riboflavin is 0.26 at neutral pH in an aqueous solution [14]. By selecting these biocompatible chromophores, biologically active molecules can be photothermally released on-demand from thermally responsive delivery vehicles.

2.3 MATERIALS AND METHODS

2.3.1 Chromophores

Riboflavin was purchased from Acros Organics (CAS number 83-88-5; New Jersey, USA). Methylene blue was purchased from Thermo Fisher Scientific (CAS number 61-73-4; Massachusetts, USA). Cardiogreen was purchased from Sigma-Aldrich (CAS number 3599-32-4; Missouri, USA). Their absorption spectra and chemical structure are shown in Figure 1. All chromophores were used without further purification.

2.3.2 Chromophore-dependent temperature change

Aqueous solutions of each chromophore were prepared by dissolving the chromophores in deionized water. The final concentrations were 0.1, 0.05, and 0.01 mg/mL for cardiogreen, methylene blue and riboflavin. To measure the photothermal effect for each chromophore, 1 mL solutions of each chromophore were added to disposable cuvettes that were optically transparent for visible and NIR light (Figure 2A). The final molar concentrations were 12.9, 64.5, and 129 μM for cardiogreen; 31.3, 156, and 313 μM for methylene blue; and 26.6, 133 and 266 μM for riboflavin.

Wavelength- and power-dependent temperature change measurements were achieved by irradiating with a POLILIGHT® PL500 multi-wavelength light source (Rofin, Australia). The central wavelengths and corresponding bandwidths are listed in Supplement Table 1. A Fluke 54 Series II thermometer (Fluke Corporation, Washington, USA) was used to record rate of temperature change as well as the final temperature change after irradiation for all experiments. For power-dependent temperature change, the chromophore solutions at varying concentrations were irradiated by visible or NIR light at varying power intensities (100, 300, and 500mW) for 5 minutes. The light intensity used for each chromophore's wavelength-dependent temperature

change was 600mW and the light intensities for the rate of temperature change were 600mW and 750mW. The experiments were conducted in triplicate and the average values are represented with the standard error.

2.3.3 Photothermal-triggered release from thermally responsive NiPAAm

Poly (N-isopropylacrylamide) (NiPAAm) (CAS number 25189-55-3, Sigma-Aldrich, Missouri, USA) hydrogels were fabricated using the procedure previously described by Zhang, et al [16]. Briefly, NiPAAm was dissolved in 50:50 water and acetone solution along with the crosslinker N, N'-methylenebisacrylamide (MBA) (CAS number 110-26-9, Sigma-Aldrich, Missouri, USA). This mixture was polymerized with N, N, N', N'-tetramethylethylenediamine (TEMED) (CAS number 110-18-9, Acros Organics, New Jersey, USA) and 10% (w/v) ammonium persulfate (APS) (CAS number 7727-54-0, Sigma-Aldrich, Missouri, USA), and then soaked and stirred in deionized water (dH_2O) for at least 24-hours to leach away unreacted products.

Bovine serum albumin (BSA) (Fisher Scientific, New Jersey, USA) was used as a model drug (66 kDa) for triggered release. To load BSA, the NiPAAm hydrogels were incubated in a 60˚C water bath for 10 minutes to de-swell and then transferred to a 1% (w/v) BSA solution to soak at 4˚C for 24 hours.

Cardiogreen was loaded into the NiPAAm hydrogel via electrophoresis (Figure 2B). Briefly, two wells were separated by an impermeable divider that included the NiPAAm hydrogel. 10 mL of phosphate buffered saline (PBS, Thermo Fisher Scientific, Massachusetts, USA) solution was added to the well with the positive lead and 10 mL of the cardiogreen solution was added to the well with the negative lead. For control hydrogels, which contained no cardiogreen, tap water was used in place of the cardiogreen solution. A MicroJet III Controller

(MicroFab, Technologies, Inc., Texas, USA) was used to supply 140 V for 5 minutes and electrostatically load cardiogreen into the NiPAAm hydrogel (Supplement Figure 1).

In order to measure the release of BSA from the NiPAAm hydrogels, a modified conical tube and petri dish setup was designed (Figure 2C). Briefly, the NiPAAm hydrogel was placed at the mouth of a 15mL conical tube body to ensure the same surface was exposed to the supernatant for the duration of the experiment. The exposed surface of the NiPAAm hydrogel was submerged in 10 mL of dH_2O in a transparent petri dish. The conical tube body was held up by a modified petri dish cover and secured by rubber O-rings. The NIR light source was positioned below the setup. During the experiment, 1 mL samples of the supernatant were collected from the petri dish at designated time points. Specifically, at times 0, 1 and 60 minutes on day 1 and every 24 hours thereafter for 2 weeks. To keep the supernatant volume constant at 10 mL, 1 mL of fresh dH_2O was added to replace the volume taken at each time point.

For samples exposed to NIR light, the supernatant solution was heated to 27˚C – 5˚C below the lower critical solution temperature of NiPAAm – immediately prior to irradiation. Starting at the 24 hour time point, the NiPAAm hydrogels were irradiated with NIR light at 750mW or 1.2W for 1-2 minutes. The 1 mL supernatant sample was collected 5 minutes after light irradiation started. This process was repeated every 24 hours for 4 days.

The amount of BSA released at each time point was determined by using the BCA assay (Pierce, Thermo Scientific, Illinois, USA). Following the assay manufacturer's protocol, the absorbance was read on an Infinite F200 plate reader (Tecan, Männedorf, Switzerland). The experiments were conducted in two sets of duplicates for each experimental group and the average values are represented with the standard error.

2.4 RESULTS

2.4.1 Concentration- and power-dependent temperature changes

Aqueous solutions of cardiogreen, methylene blue and riboflavin were exposed to 3 power intensities (100mW, 300mW, and 500mW) of light that corresponded with the absorption peak of each chromophore. In addition, the effect of chromophore concentration (0mg/mL to 0.1mg/mL) on total temperature change was examined. The data shows that with increasing chromophore concentration and increasing light intensity there is an increase in the temperature rise. In all cases, the presence of a chromophore results in a greater temperature change when compared to water with no added chromophore (Figure 3).

Cardiogreen. The final temperature change of an aqueous solution of cardiogreen at 0.1mg/mL after exposure to 500mW of NIR light was 6.9˚C (±0.2˚C), whereas a 0.01mg/mL solution of cardiogreen at the same power intensity produced a final temperature change of 5.2˚C (±0.1˚C). Similar temperature changes were achieved when 0.05mg/mL and 0.1mg/mL solutions of cardiogreen were irradiated with 300mW (6.2˚C (±0.3˚C) and 6.3˚C (±0.4˚C), respectively). For all the solutions irradiated with 100mW of NIR light the change in temperature measured was less than 2˚C. The greatest temperature change in samples of water with no chromophore added was 3˚C at 300mW and 500mW (Figure 3A).

Methylene Blue. After exposure to 500mW of 650nm light, the final temperature change of an aqueous solution of methylene blue at 0.1mg/mL was 5.9˚C (±0.3˚C), and a 0.01mg/mL solution of methylene blue at the same power intensity produced a final temperature change of 5.5˚C (±0.1˚C) (Figure 3B). At each power intensity there is a similar temperature change achieved between the various concentrations of methylene blue solutions. For instance, methylene blue solutions irradiated with 300mW had temperature changes ranging between

3.5˚C to 4˚C. Additionally, for all the solutions irradiated with 100mW of 650nm light the change in temperature measured was less than 2˚C. This was greater than the temperature change caused by water with no chromophore added which increased in temperature by less than 1.5˚C even at 500mW.

Riboflavin. The final temperature change of an aqueous solution of riboflavin at 0.1mg/mL after exposure to 500mW of 450nm light was 7.4˚C (±0.1˚C), whereas a 0.01mg/mL solution of riboflavin at the same power intensity produced a final temperature change of 2.1˚C (±0.3˚C) (Figure 3C). A similar temperature change was achieved when 0.01mg/mL solutions of riboflavin were irradiated with 300mW (1.9˚C (±0.1˚C)). For all the solutions irradiated with 100mW of 450nm light the change in temperature measured was less than 2˚C. However, this was still greater than the temperature change caused by water with no chromophore added which increased in temperature by less than 1˚C even at 500mW.

2.4.2 Wavelength-dependent temperature change

As seen in Figure 1, each chromophore has an absorption peak either in the visible or NIR light region of the spectrum with cardiogreen's absorption peak in the NIR region between 780-900 nm, methylene blue's in between 580-680nm, and riboflavin's appearing in the blue region (400-500 nm). The greatest temperature change is observed near the absorption maxima while wavelengths outside the absorption bands produce smaller temperature changes (Figure 4).

Cardiogreen. The absorption maximum for cardiogreen is 780 nm. Exposure to 600mW of NIR light demonstrated a concentration dependent temperature change below 0.05mg/mL: 9.9˚C (±0.4˚C) (0.1mg/mL); 9.8˚C (±0.2˚C) (0.05mg/mL); and 7.7˚C (±0.1˚C) (0.01mg/mL). Outside the absorption band, the higher concentrations have a significant temperature change over water alone but less than the temperature change in the NIR region. Between 490 nm and

555 nm the change in temperature ranges from: 3.5˚C (0.05mg/mL) to 5.0˚C (0.1mg/mL). Cardiogreen has a second smaller peak between 400 nm and 500 nm. The temperature change in this region demonstrated concentration dependent temperature changes and ranged from 7.4˚C (±0.1˚C) (0.1mg/mL; 415nm) to 2.0˚C (±0.1˚C) (0.01mg/mL; 470nm). This is greater than the temperature change measured outside the absorption peaks but less than the larger absorption peak in the NIR region (Figure 4A).

Methylene blue. The absorption maximum for methylene blue is 665 nm. Exposure to 650 nm light (600mW) caused significant temperature changes at all concentrations: 11.4˚C (±0.2˚C) (0.1mg/mL); 11.2˚C (±0.2˚C) (0.05mg/mL); and 9.9˚C (±0.2˚C) (0.01mg/mL). Outside the absorption band, methylene blue demonstrates a significant temperature change over blank water samples, different from riboflavin but similar to cardiogreen. For example, at 415 nm (600mW) the measured temperature change was 4.6˚C (±0.4˚C) (0.1 mg/mL). The lowest concentration shown (0.01 mg/mL), however, follows a similar pattern where the greatest temperature change corresponds with the absorption max and little temperature change outside the absorption band (1.8˚C (±0.2˚C) at 415 nm) (Figure 4B). Since there was little difference in the measured temperature changes within the absorption band between the three concentrations of methylene blue, the concentration was lowered to evaluate how low the concentration of methylene blue could be and still have a meaningful temperature change over water. Two additional concentrations were measured, 0.005mg/mL and 0.001mg/mL. 0.001mg/mL had a temperature change of 3.8˚C (±0.1˚C) at 650 nm (600mW), nearly 2˚C more than water under the same conditions (Figure 4C). At 590 nm (600mW), the difference had decreased to 0.5˚C with methylene blue at 2.6˚C (±0.1˚C) and water at 2.1˚C (±0.2˚C) (Figure 4C).

Riboflavin. The absorption maximum for riboflavin is 445 nm. Exposure to 415 nm light (600mW) demonstrated a concentration dependent temperature change: 9.9˚C (±0.1˚C) (0.1 mg/mL); 8.1˚C (±0.2˚C) (0.05mg/mL); and 3.4˚C (±0.3˚C) (0.01mg/mL). Outside the absorption band, very little temperature change is measured starting at 530 nm where there is no difference between the different concentrations: 2.2˚C (±0.1˚C) (0.1mg/mL); 1.6˚C (±0.1˚C) (0.05mg/mL); and 1.7˚C (±0.2˚C) (0.01mg/mL) (Figure 4D).

2.4.3 Chromophore lifetime

To study each chromophore's lifetime for heat generation, cardiogreen, methylene blue and riboflavin underwent 5 minute exposures every 24 hours for 7 days to 600mW of NIR or visible light, corresponding with each chromophore's absorption max. The data shows that cardiogreen and methylene blue had no loss in their photothermal abilities between time points and showed a prolonged lifetime for heat generation while riboflavin had a steady decrease in heat generation over the 7 days. The temperature change of 1 mL aqueous solutions loaded with 0.1mg/mL of cardiogreen ranged between 9.9˚C and 12.6˚C (Figure 5A), and the methylene blue solutions had temperature changes that ranged between 7.1˚C and 8.3˚C (Figure 5B). The riboflavin solutions had a 7˚C (±0.2˚C) change in temperature at day 1 that decreased to 2.5˚C (±0.1˚C) by day 7. Decreasing the power of light to 500mW helped to prolong the lifetime for heat generation; however, at day 5 the temperature change caused by irradiating riboflavin with blue light dropped to 5.5˚C (±0.1˚C) and was down to 3.6˚C (±0.1˚C) at day 7 (Figure 5C).

2.4.4 Rate of chromophore-dependent temperature change

Figure 6 shows the rate of heat generation by cardiogreen, methylene blue and riboflavin (0.1mg/mL) upon irradiation with NIR or visible light. The temperature change of cardiogreen after 1 minute of NIR light exposure was 2.5˚C (±0.2˚C) and 4.4˚C (±0.3˚C) after 2 minutes of

exposure at 600mW with an average temperature change rate of 2.2˚C/min. For methylene blue, after 1 minute of exposure to 650 nm light, the temperature change was 2.7˚C (±0.1˚C) and 4.4˚C (±0.1˚C) after 2 minutes of exposure at 600mW with an average temperature change rate of 2.2˚C/min. Riboflavin generated 3.3˚C (±0.1˚C) of heat at 1 minute and 5.6˚C (±0.1˚C) after 2 minutes of exposure to 450 nm light at 600mW with an average temperature change rate of 2.8˚C/min (Figure 6A).

The advantage of NIR light over visible light is the limited light attenuation in tissues. However, water also absorbs NIR light more strongly. For *in vivo* applications, rapid temperature change over water is necessary for chromophore-dependent heat generation. The temperature change of cardiogreen after 1 minute of NIR light exposure at 750mW was 5.4˚C (±0.1˚C) and 9.4˚C (±0.1˚C) after 2 minutes of exposure with an average temperature change rate of 4.7˚C/min. For methylene blue, after 1 minute of exposure to NIR light, the temperature change was 3.7˚C (±0.1˚C) and 6.0˚C (±0.1˚C) after 2 minutes of exposure at 750mW with an average temperature change rate of 3.0˚C/min. Riboflavin generated 3.2˚C (±0.1˚C) of heat at 1 minute and 5.0˚C (±0.1˚C) after 2 minutes of exposure to NIR light at 750mW with an average temperature change rate of 2.5˚C/min, however this heat generation was due to water absorbing the NIR light (Figure 6B).

2.4.5 Photothermal-triggered release from thermally responsive NiPAAm

NiPAAm is a well-known temperature-sensitive hydrogel and exhibits a lower critical solution temperature (LCST) around 32˚C. As the temperature increases it becomes hydrophobic and expels water molecules, including the payload molecules, as it goes from a hydrogel to a globular structure. NiPAAm hydrogels were loaded with BSA and the release profile over four days was determined.

Figure 7A compares the release profiles of BSA due to diffusion and light actuation. All samples show an initial burst release within the first 24 hours – 43µg (±2µg) from the diffusion samples, 41µg (±5µg) from NIR light samples without cardiogreen, and 53µg (±4µg) from NIR light samples with cardiogreen. The first light exposure (1 minute at 750mW) triggered the release of 49µg of BSA from the hydrogels loaded with cardiogreen compared to 27µg from the NiPAAm hydrogels alone. The second, third and fourth exposure triggered the release of 50µg, 42µg and 47µg of BSA from the hydrogels loaded with cardiogreen and 32µg, 37µg and 44µg from the hydrogels alone, respectively. In total, 319µg (±9µg) of BSA was released after 4 days by the photothermal effect of cardiogreen acting upon the NiPAAm hydrogel compared to 223µg (±5µg) and 121µg (±7µg) of BSA from NIR light irradiation without cardiogreen and diffusion only, respectively.

The effect that increasing the light power from 750mW to 1200mW has on the release of BSA from NiPAAm hydrogels is seen in Figure 7B. Similar burst release within the first 24 hours due to diffusion is seen (46µg (±2µg)). The first light exposure triggered the release of 55µg (±8µg). The second, third and fourth exposure triggered the release of 40µg (±2µg), 41µg (±4µg) and 49µg (±6µg), respectively. In total, 274µg (±27µg) of BSA was released from NiPAAm hydrogels loaded with cardiogreen and irradiated with 1200mW of NIR light for 1 minute.

The effect that increasing the exposure time to 750mW of NIR light from 1 minute to 2 minutes has on the release of BSA from NiPAAm hydrogels is seen in Figure 7C. Again, there is an initial burst release within the first 24 hours due to diffusion (69µg (±12µg)). The first light exposure triggered the release of 69µg (±8µg) of BSA. The second, third and fourth exposure triggered the release of 56µg (±4µg), 36µg (±4µg) and 36µg (±2µg), respectively. In total,

288µg (±24µg) of BSA was released from NiPAAm hydrogels loaded with cardiogreen and irradiated with 750mW of NIR light for 2 minutes.

To determine the percent of BSA released from the NiPAAm hydrogels, the mass released at each timepoint, M_t, was divided by the mass released at time infinity, M_∞, which was set at day 14 (Figure 7D). After 4 days of 4x1 minute NIR light exposures at 750mW, 80% of the BSA had been released from the NiPAAm hydrogel. 13% of the loaded BSA is released from the initial burst release. The first light exposure triggers the release of 12% of the BSA, and the second, third and fourth exposures trigger 12%, 11% and 12% of the BSA to release, respectively.

2.5 DISCUSSION

The choice of cardiogreen, methylene blue and riboflavin as chromophores for drug delivery-on-demand applications via NIR and visible light actuation highlights the novelty of this study. The current biomedical application for riboflavin is to act as a type II photo-initiator for hydrogel polymerization reactions which uses riboflavin's absorption in the visible region as a safe alternative to using harmful UV irradiation [17, 18]. Methylene blue is actively researched for photo-inactivation technologies in European countries. Viruses, including Hepatitis B, Hepatitis C, HIV, B19 virus and West Nile virus, have been inactivated in fresh blood plasma with 1µM methylene blue and visible light exposure [11, 12, 19]. Finally, cardiogreen is the only FDA approved NIR dye for medical diagnosis [20]. Specifically, cardiogreen is clinically used to evaluate blood flow and liver function (i.e. clearance) [21, 22] although there is growing interest in using cardiogreen for tumor ablation [23]. Advancing the biomedical application of these chromophores, this study 1) characterized and identified the optimal photothermal response of these materials for drug delivery-on-demand applications; and 2) in the case of cardiogreen,

demonstrated triggered release of BSA from the thermally responsive delivery vehicle, NiPAAm. Specifically, this study achieved 5˚C temperature change rapidly (<2 minutes). Necessary since 5˚C above physiological temperature (37˚C) is the threshold for tissue damage from hyperthermia and prolonged light irradiation can lead to high temperatures that cause tissue ablation within seconds as well as raise the temperature of surrounding tissue via thermal conduction [24, 25]. Additionally, the rapid photothermal response of the chromophores, specifically cardiogreen, is necessary to outpace the heating due to absorption of NIR light by water which has a low absorption coefficient, but non-negligible, between 700-900nm [26, 27]. The key properties and photothermal results for the chromophores are summarized in Table 1. These conditions were used to uniformly trigger the release of BSA over 4 days from a rapidly responding NiPAAm hydrogel – prepared using a mixed solvent for the polymerization reaction that produced an expanded hydrogel structure that exhibits a rapid, thermodynamically driven phase transition [16].

The dose-dependent and power-dependent temperature change for each chromophore allows for these variables to be customized to applications requiring various changes in temperature. The results show that these temperature changes can be achieved by changing the concentration of chromophore as well as the power of light used. These have important considerations for the efficacy of the reported delivery-on-demand approach. For instance, according the inverse-square law, light intensity is proportional to the inverse square of the distance from the light source [28]. Additionally, light attenuation in biological tissues due to absorption by chromophores like hemoglobin and scattering by collagen fibers [9] limits the intensity of light in deeper tissues (Supplement Figure 2). As such, the operating parameters and

the precision necessary for future clinical applications will be dependent on the light power required to overcome the threshold for triggered release.

The *in vivo* effects of different wavelengths of light at specific power intensities will also impact future operating parameters. For instance, all three chromophores induce a significant change in temperature over water in the blue (400-500nm) region of light (riboflavin and cardiogreen have absorption peaks in this region and methylene blue demonstrates a blue shift in absorption due to dimerization at high concentrations [29]). This wavelength is strongly absorbed by hemoglobin and penetration depth into the body is limited to a few microns so clinical applications are limited to surfaces. However, visible light has been to shown to have a dose-dependent increase in reactive oxygen species generation in the range of solar irradiance [30] and the light intensities used for this study are greater than ambient light. Therefore, light power, time of exposure and wavelength are all variables that need to be considered when using light actuated drug delivery-on-demand systems.

The lifetime for the photothermal response of the chromophores studied varied and is dependent upon the photostability of each chromophore. This is because absorbed light causes electron excitation that can result in radical formation in the excited singlet and triplet states. Radicals are highly reactive species that can disrupt the conjugated double bonds responsible for the absorption of NIR or visible light. The prolonged photothermal response of cardiogreen seen in this study is due to the low quantum yield for triplet formation, which previous studies looking at the photostability of cardiogreen report in water and human plasma is 2.2×10^{-3} and 0.026, respectively [31]. Additionally, cardiogreen forms J-aggregates at higher concentrations (similar to the concentration used in this study) which protect it from conformational changes that lead to radical formation and subsequent degradation that occurs at lower concentrations [31, 32].

Similarly, methylene blue forms dimers at higher concentrations that help stabilize the molecules, which has a high quantum yield for triplet formation at low concentrations (0.52) [33]. Riboflavin also has a high quantum yield for triplet formation (0.6) [34]. Unlike cardiogreen and methylene blue, however, riboflavin undergoes photobleaching and is no longer sensitive to light. The main products from the photolysis of riboflavin are lumichrome and lumiflavin and are obtained by the oxidation of the ribityl side-chain [35]. Previous work has used citrate buffer to stabilize riboflavin against photolysis [36] and may have utility in drug delivery-on-demand applications by stabilizing the photothermal response of chromophores for long-term use, including cardiogreen and methylene blue, which may be less stable at lower concentrations.

Because these molecules have the potential to produce reactive oxygen species such as singlet oxygen or free radicals upon light irradiation, they can be toxic to cells and lead to irreversible damage [37]. For instance, previous studies looking at the reactive oxygen species generation of cardiogreen found that when irradiated with $2W/cm^2$ 808 nm laser for 5 minutes, the amount of reactive oxygen species was higher than the positive control of H_2O_2 and 3.4 times higher than the negative control [37]. Additionally, it was seen that increased riboflavin concentration and visible light exposure resulted in decreased cell viability [38]. This is from the generation of hydrogen peroxide – a common product of free radical generation in aqueous solutions [39]. To combat this deleterious outcome, the human eye has been used as inspiration, where excess vitamin C (ascorbic acid) is present to act as a free radical scavenger [40]. The effect of adding 2.5mM of ascorbic acid to the system was studied, and was shown not to influence the photothermal response of the chromophore (Supplement Figure 3). It is worth noting that for certain clinical indications it may be advantageous to allow free radical (and

subsequent H_2O_2) generation to occur (known as Photodynamic Therapy (PDT) and sometimes used to treat oncological, cardiovascular, and ophthalmic diseases [41]) and couple it with drug delivery-on-demand.

Cardiogreen irradiated with NIR light was selected for the triggered release because: 1) cardiogreen's safety - low quantum yield for triplet formation and subsequent free radical production; 2) cardiogreen's rapid photothermal response upon irradiation; 3) NIR light's greater penetration depth in tissues than visible light; and 4) cardiogreen's absorption peak in the NIR region. Uniform spikes in BSA release with 1 minute of 750mW NIR light exposure every 24 hours for 4 days were achieved. While the lifetime for the photothermal response of cardiogreen is ≥7 days, only 4 days' worth of triggered release was achieved. Cardiogreen, as well as methylene blue and riboflavin, are small molecules that can diffuse from the hydrogel and decrease the concentration of chromophore over time – eventually dropping below the lower limit required for heat generation within the delivery vehicle. The incorporation of chromophore reservoirs (micro-particles loaded with chromophore) could alleviate this limitation by delaying the diffusion of chromophore away from the scaffold and maintaining the threshold concentration for a therapeutically relevant timeline. Alternatively, these chromophores could also be chemically conjugated to the scaffold to prevent chromophore elution [41, 42].

The triggered release profiles showed no significant difference when there were changes in the amount of light exposure time as well as the light intensity. It is possible that there is no difference for the times studied. As the surface of the NiPAAm delivery vehicle is heated by the photothermal response of cardiogreen irradiated with NIR light, the network collapses and expels water and protein, but the collapsed network also stops the release of BSA from deeper inside the hydrogel network [43]. It is worth noting that the NiPAAm hydrogels fabricated for this study do

not form a dense skin layer that hinders the permeation of both water and BSA (thereby turning 'off' release upon light irradiation) but rather were prepared using a mixed solvent to prevent skin formation [16] and produce a rapidly and uniformly deswelling hydrogel for release via squeezing [44]. Increased power results in faster heating but after 1 minute both power intensities have raised the temperature above the LCST of NiPAAm and the heated region has transitioned from a hydrogel to a collapsed gel. Similarly, both hydrogels have been heated above the LCST of NiPAAm when the irradiation time is increased from 1 minute to 2 minutes. In both cases, there is more heat generated with greater light intensity and longer light exposure. In these cases where more heat is generated, more heat is transferred further into the gel. As a result, a larger zone of the gel collapses and releases the water and BSA occupying the space. This is supported by the greater amount of BSA release seen at the first light exposure in the samples irradiated with 1200mW and both the first and second light exposures in the samples irradiated for 2 minutes.

The delivery-on-demand results are compared with other NIR actuated systems in Table 2. Perhaps the most widely researched material for applications actuated by NIR light is gold nanoparticles; however, gold nanoparticles are limited by issues with toxicity both *in vitro* and *in vivo*. When delivered intravenously, gold nanoparticle accumulation has been seen in liver, lung, and spleen tissue and in heart, kidney and brain tissue to a small degree [45]. A study in BALB/c mice showed that 13nm-sized gold nanoparticles induced inflammation and apoptosis in liver tissue after 7 days [46]. Recently, a NIR actuated delivery system was designed where water was confined within poly (lactic-co-glycolic acid) (PLGA) particles and released fluorescein as the water was heated above the polymer's glass transition temperature [47]. A key strength of the system is the biocompatibility since PLGA is already used in FDA-approved implantable

devices; however, the system is slow to respond as it takes 5 minutes of light exposure to trigger release and all light cycles occurred within 90 minutes. In contrast, the reported system released BSA from NiPAAm within 1 minute of light exposure for 4 cycles over 4 days. Despite studies demonstrating NiPAAm's biocompatibility [48-50], there are concerns regarding the *in vivo* safety of NiPAAm due to the toxicity of the monomer [51, 52]. However, adaptation of the reported strategy for delivery-on-demand to novel biocompatible thermally responsive delivery vehicles, such as thermally responsive hydrogels based on polypeptides, may be used to overcome concerns regarding the biocompatibility and cytotoxicity of the reported delivery vehicle. One example is the block co-polymer (ethylene glycol)–(DL-alanine)–(L-alanine) whose hydrophilic-hydrophobic balance and block sequence with a flexibility gradient creates a thermo-sensitive polymer that is a hydrogel at 37˚C and a squeezed gel above 40˚C [53], and in addition to being biocompatible, is also biodegradable via enzymatic degradation. [54] Ultimately, further research into the design and fabrication of novel biocompatible thermally responsive delivery vehicles will aid in the advancement of the light actuated drug delivery-on-demand approach described here.

2.6 CONCLUSION

In this proof-of-concept study, a new strategy for triggered release via near infrared light (NIR) actuation for future biomedical applications is described. The data demonstrates the feasibility of and parameters for using irradiated riboflavin and methylene blue as actuators for the controlled delivery of biologically active molecules and demonstrates triggered release of protein from a thermally responsive delivery vehicle loaded with cardiogreen and irradiated with NIR light. Specifically, it was shown that each of these chromophores is capable of significantly increasing the temperature of aqueous solutions upon exposure to visible or NIR light. The

amount of temperature change is dependent upon light intensity, wavelength, as well as chromophore concentration. Finally, the rapid release of BSA upon NIR light exposure from NiPAAm was achieved over 4 cycles with 24 hours between light exposures. The amount of BSA released showed little dependence on the amount of light exposure time and light intensity for the conditions studied. Ultimately, this drug delivery strategy has potential for clinical applications that require explicit control over the presentation of biologically active molecules.

2.7 FIGURES

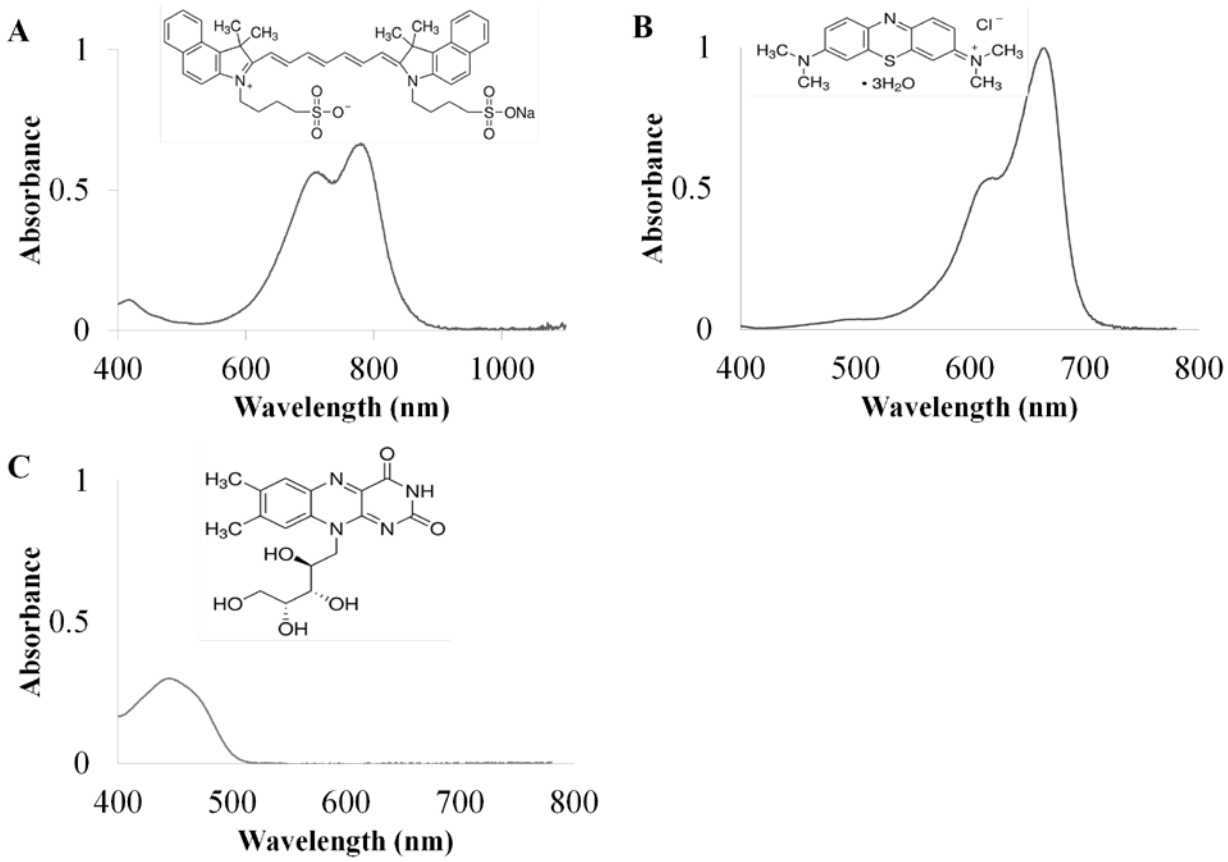

Figure 1. The absorbance spectra and chemical structures of (A) cardiogreen (13µM), (B) methylene blue (16µM), and (C) riboflavin (26µM) in water.

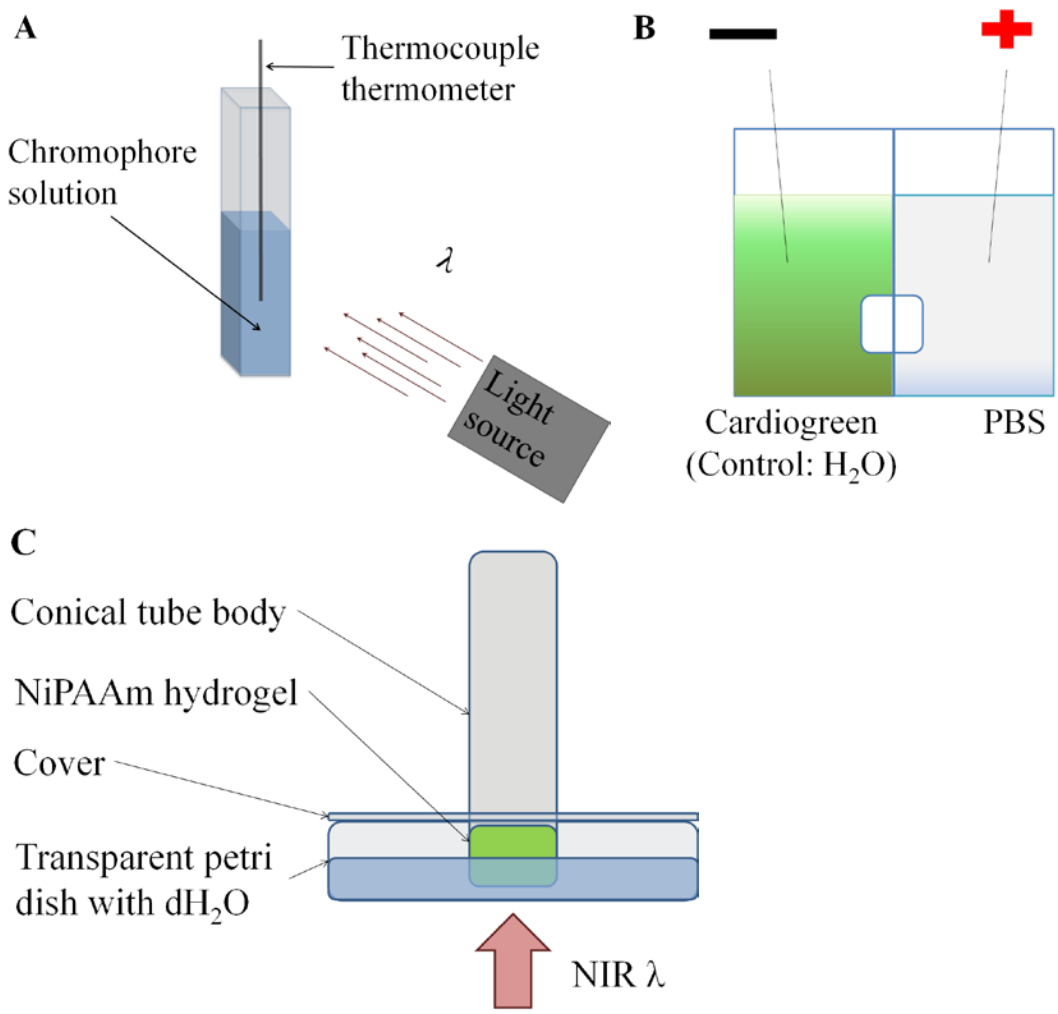

Figure 2. Illustrations of the experimental setup for (A) irradiating aqueous solutions of each chromophore with visible and NIR light; (B) loading cardiogreen into NiPAAm hydrogels via electrophoresis; and (C) measuring the light actuated of release of BSA from NiPAAm hydrogels.

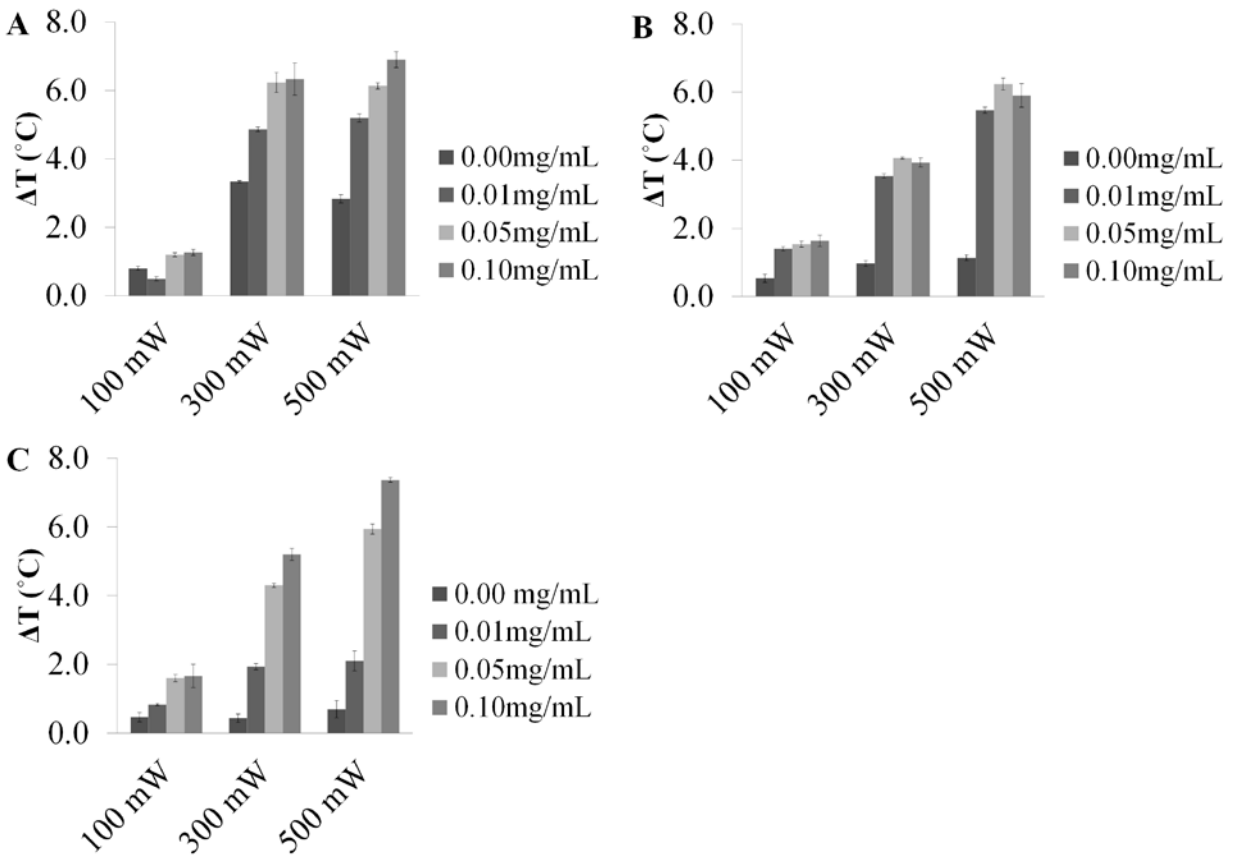

Figure 3. The measured temperature change of 1 mL aqueous solutions loaded with 0, 0.01, 0.05, and 0.1mg/mL of (A) cardiogreen, (B) methylene blue and (C) riboflavin after 5 minutes of light exposure (cardiogreen: 900 nm; methylene blue: 650 nm; and riboflavin: 450 nm) at 100, 300 and 500mW (n=3). For each chromophore studied, increasing the concentration of chromophore, the power of the light source, or both increased the measured temperature changes.

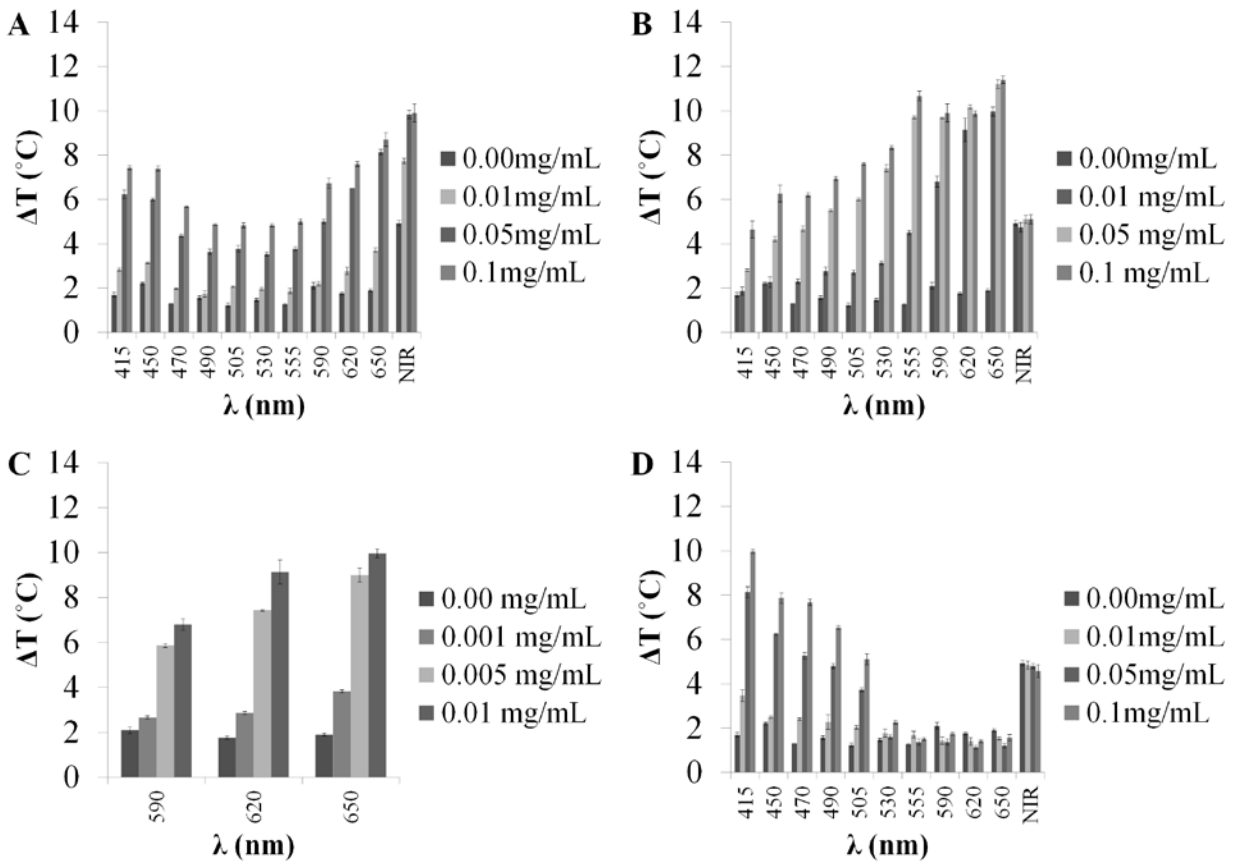

Figure 4. The measured temperature change of 1 mL aqueous solutions loaded with varying concentrations of (A) cardiogreen, (B–C) methylene blue, and (D) riboflavin after 5 minutes of exposure to varying wavelengths of visible and NIR light at 600mW (n=3). Chromophores show a wavelength dependent change in temperature with the greatest temperature change falling within the chromophore's absorption band.

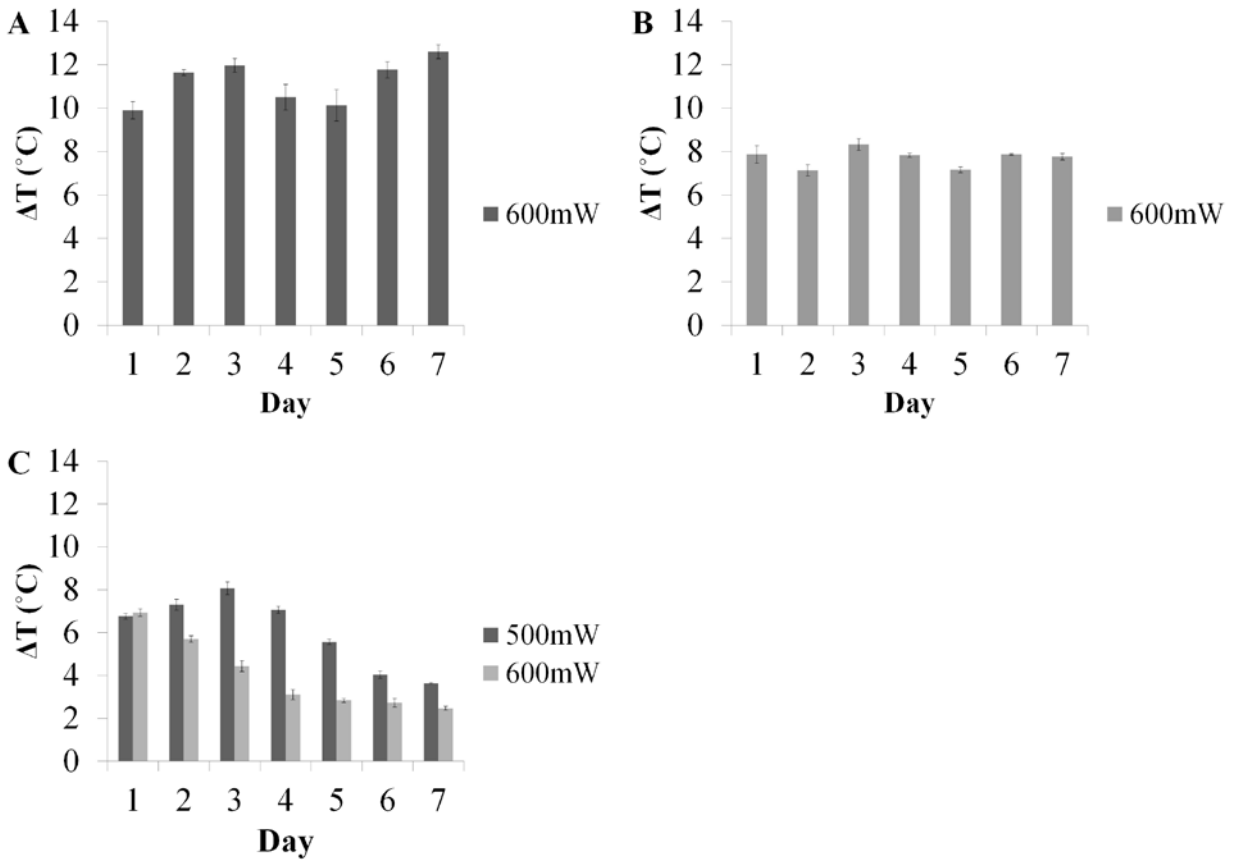

Figure 5. The measured temperature change of 1 mL aqueous solutions loaded with 0.1mg/mL of (A) cardiogreen, (B) methylene blue and (C) riboflavin after 5 minutes of light exposure every day for 7 days (cardiogreen: 900nm; methylene blue: 650nm; and riboflavin: 450nm) at 600mW (n=3). No loss in photothermal response from cardiogreen and methylene blue while the photothermal response steadily decreases for riboflavin after the first exposure. Decreasing the light power to 500mW prolongs the photothermal response but begins to decrease after the third exposure at day 3.

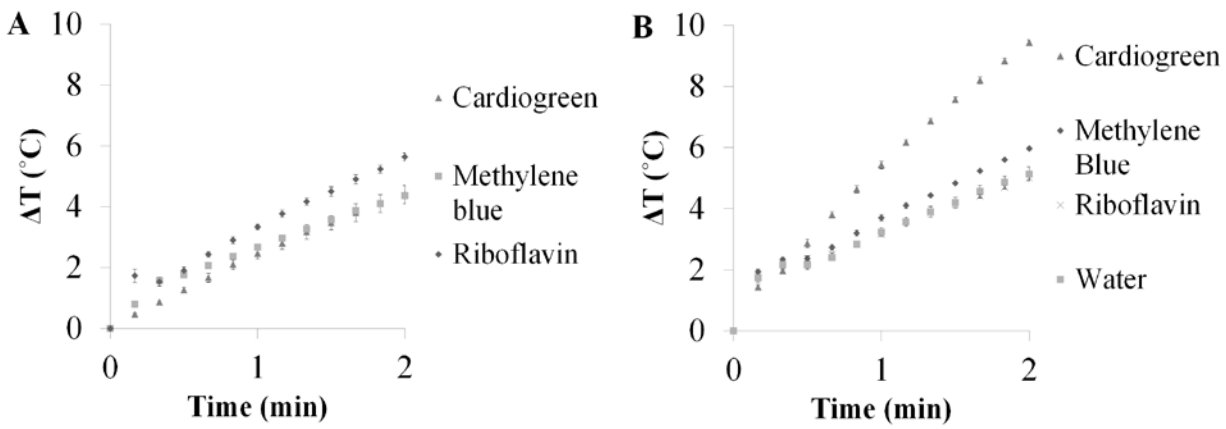

Figure 6. Comparing the rate of temperature change from 0.1mg/mL solutions of cardiogreen, methylene blue and riboflavin exposed to (A) 600mW of light (450 nm for riboflavin, 650 nm for methylene blue, and 715 nm for cardiogreen) (volume = 1mL), and (B) 750mW of NIR light (715 nm, bandwidth = 30 nm) (volume = 500µL) (n=3).

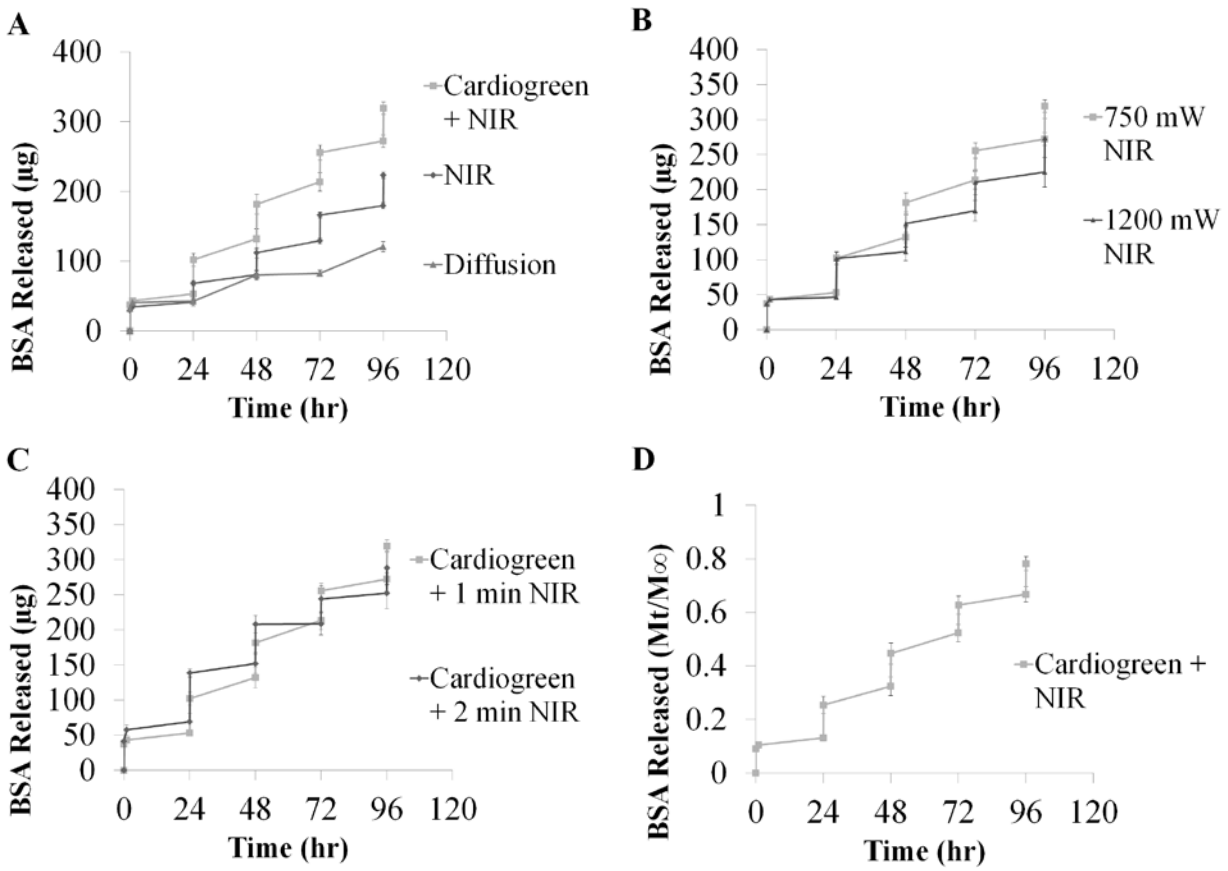

Figure 7. The cumulative release (µg, A-C) and percent release (D) of BSA (66kDa) from NiPAAm hydrogels (diameter = 9mm, thickness = 4mm) via the photothermal response of cardiogreen irradiated with NIR light. Cardiogreen is loaded into NiPAAm hydrogel via electrophoresis (see Supplement Figure 1 for amount of cardiogreen loaded), and NIR light irradiation occurred every 24 hours starting at t=24hr. (A) Comparing the triggered release versus diffusion of BSA from NiPAAm hydrogels (n=4). 'Cardiogreen + NIR' and 'NIR' samples were irradiated with 750mW NIR light for 1 minute. (B) Comparing the BSA release from cardiogreen-loaded NiPAAm hydrogels irradiated with 750mW and 1200mW NIR light for 1 minute (n=4). (C) Comparing the BSA release from cardiogreen-loaded NiPAAm hydrogels irradiated with 750mW NIR light for 1 and 2 minutes (n=4). (D) The percent release of BSA

from cardiogreen-loaded NiPAAm hydrogels irradiated with 750mW NIR light for 1 minute. M_t is cumulative release at time, t, and M_∞ is cumulative release after 14 days (n=4).

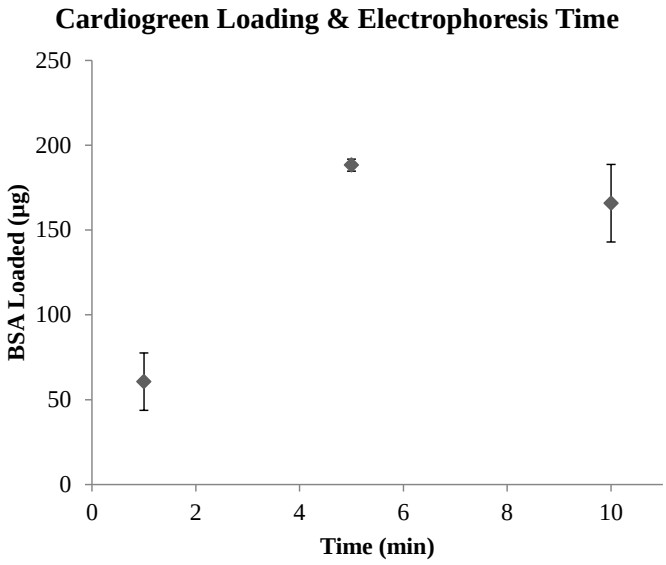

Supplement Figure 1. The amount of cardiogreen (µg) loaded into NiPAAm hydrogels via electrophoresis with 1, 5 and 10 minutes run time (n=3). The 5 minute run time was used to load the NiPAAm hydrogels for the experiments in this study.

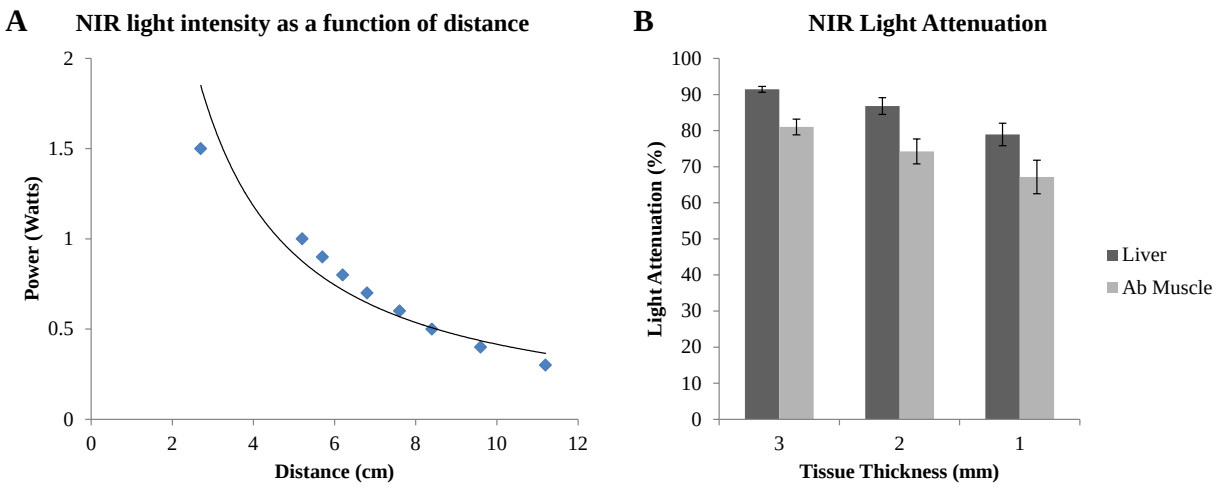

Supplement Figure 2. (A) Light intensity is proportional to the inverse square of the distance from the light source. (B) Light attenuation of NIR light in biological tissues increases with tissue thickness due to absorption by water in tissue and scattering by collagen fibers (n=3).

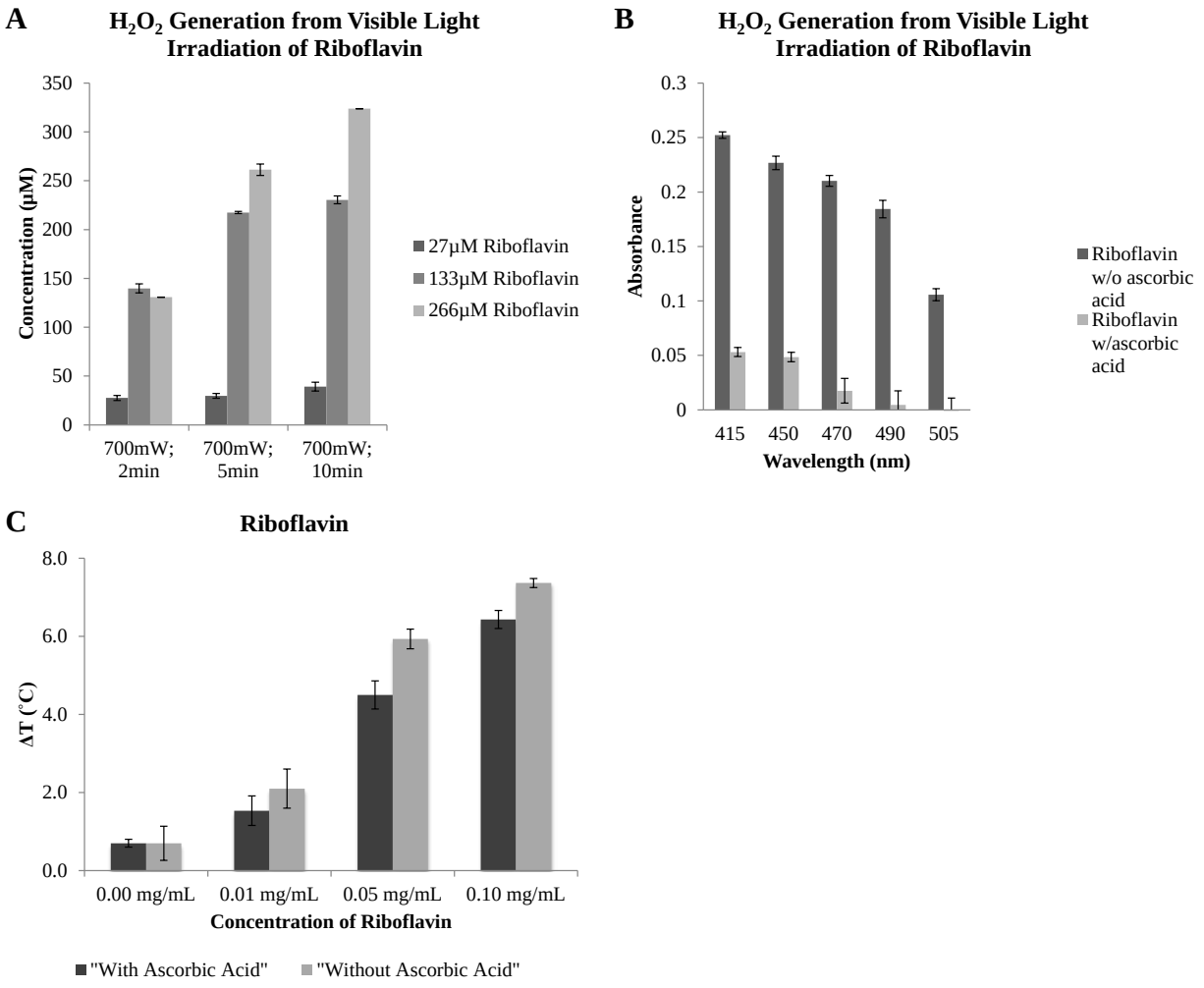

Supplement Figure 3. (A) Various concentrations (27, 133 and 266μM) of riboflavin were irradiated with 700mW of 450nm light for 2, 5 and 10 minutes and the concentration of hydrogen peroxide generated by each solution was determined using hydrogen peroxide assay kit (National Diagnostics, Georgia, USA) (n=6). (B) Effect of 2.5mM ascorbic acid on hydrogen peroxide generation by riboflavin (0.01 mg/mL) irradiated with visible light (600mW, 450nm) for 5 minutes (n=6). The addition of ascorbic acid to the solution results in a decrease in hydrogen peroxide generation. (C) The measured temperature change of 1mL aqueous solutions of riboflavin after 4 minutes of 450nm light (500mW) exposure with and without 2.5mM ascorbic acid (n=6). Addition of ascorbic acid slightly weakened the photothermal response.

2.8 TABLES

Table 1. Summary of chromophore properties and photothermal response

Chromophore	**Riboflavin**	**Methylene Blue**	**Cardiogreen**
Molecular weight	376.36 g/mol	319.85 g/mol	774.96 g/mol
λ_{abs} max.	445 nm	665 nm	775 nm
Quantum efficiency for fluorescence	0.25	0.04	0.19
Solubility in H_2O	84.7 mg/L	$4.36x10^4$ mg/L	$1x10^3$ mg/L
Max. ΔT after 2 min. exposure at 600mW; C = 0.1 mg/mL; (λ)	5.6˚C (450 nm)	4.3˚C (650 nm)	5.5˚C (780 nm)
ΔT of H_2O after 2 min. exposure at 600mW (λ)	1.2˚C (450 nm)	1.9˚C (650 nm)	3.2˚C (780 nm)

Table 2. Summary of select near infrared light actuated delivery-on-demand systems

Wavelength	Power	Time	Chromophore	Outcome	Ref.
808 nm (CW diode laser)	2.56W/cm^2	10 min	PEG-PLGA-Au half-shell nanoparticles (120 nm diameter)	0.25 mg/kg DOX released 24 hr post-injection by NIR irradiation. DOX persisted for 72 hr in tumor	[55]
808 nm (CW diode laser)	600mW	5, 10 min	Gold nanorods (50 x 10 nm)	All DOX released with 10 min exposure. Very little at 5 min. despite $\Delta T = 40^{\circ}C$ within 1 min.	[56]
1064nm (Nd:YVO_4 laser)	750mW	30 sec	Gold nanorods (65 x 11 nm)	Rapid release of rhodamine-labeled dextran from NiPAAm hydrogels (d = 140 μm)	[57]
980 nm (NIR laser)	0.7W/cm^2	20 min	Hallow CuS nanoparticles (0.1 mg/mL)	60% of camptothecin released after 3x 20 min (4.5% to 18.8% bursts) NIR light exposures over 80 hrs.	[58]
980 nm (CW NIR laser)	2.8W/cm^2	12 min	NIR-to-UV upconversion nanoparticles	siRNA for GFP photocaged by 4,5-dimethoxy-2-nitroacetophenone significantly decreased GFP fluorescence intensity 32 hr. post-exposure to NIR	[59]
980 nm (CW diode laser)	1W	5 min	water	70% release of fluorescein after 5x 5 min NIR light exposures from PLGA delivery vehicle (size =0.5 μm; $T_g = 42^{\circ}C$) over 90 min.	[47]
658 nm (laser)	300mW	4 min	(HPPH)-lipids	Minimal release of DOX for 2 days when soaked in 10% serum; 100 % release of DOX after 4 min of exposure to NIR light.	[60]
900 nm (non-coherent light)	750mW	1 min	cardiogreen	80% of BSA released from NiPAAm after 4x 1 min (11-12% bursts) NIR light exposures over 96 hrs (4 days).	

Acronyms: continuous wave, CW; polyethylene glycol, PEG; poly (lactic-co-glycolic acid), PLGA; doxorubicin, DOX; near infrared, NIR; poly (N-isopropylacrylamide), NiPAAm; ultraviolet, UV; small interfering ribonucleic acid, siRNA; green fluorescent protein, GFP; devinyl hexyloxyethy-pyropheophorbide, HPPH; bovine serum albumin, BSA.

Supplement Table 1. POLILIGHT® PL500 Specifications

Wavelength (nm)	Bandwidth (nm)
415	40
450	100
470	40
490	40
505	40
530	40
555	27
590	40
620	40
650	40
900 (NIR)	400

2.9 REFERENCES

[1] C. Alvarez-Lorenzo, L. Bromberg, A. Concheiro, Light-sensitive Intelligent Drug Delivery Systems, Photochemistry and Photobiology, 85 (2009) 848-860.

[2] D.A. LaVan, T. McGuire, R. Langer, Small-scale systems for in vivo drug delivery, Nature Biotechnology, 21 (2003) 1184-1191.

[3] J. Kost, R. Langer, Responsive polymeric delivery systems, Advanced Drug Delivery Reviews, 46 (2001) 125-148.

[4] S. Sershen, J. West, Implantable, polymeric systems for modulated drug delivery, Advanced Drug Delivery Reviews, 54 (2002) 1225-1235.

[5] I. Tomatsu, K. Peng, A. Kros, Photoresponsive hydrogels for biomedical applications, Advanced Drug Delivery Reviews, 63 (2011) 1257-1266.

[6] T. Tadokoro, N. Kobayashi, B.Z. Zmudzka, S. Ito, K. Wakamatsu, Y. Yamaguchi, K.S. Korossy, S.A. Miller, J.Z. Beer, V.J. Hearing, UV-induced DNA damage and melanin content in human skin differing in racial/ethnic origin, Faseb Journal, 17 (2003) 1177-1179.

[7] R.M. Lavker, G.F. Gerberick, D. Veres, C.J. Irwin, K.H. Kaidbey, Cumulative effects from repeated exposures to suberythemal doses of UVB and UVA in human skin, Journal of the American Academy of Dermatology, 32 (1995) 53-62.

[8] J.M. Joseph, H. Destaillats, H.M. Hung, M.R. Hoffmann, The sonochemical degradation of azobenzene and related azo dyes: Rate enhancements via Fenton's reactions, Journal of Physical Chemistry A, 104 (2000) 301-307.

[9] R.R. Anderson, J.A. Parrish, The optics of human-skin, Journal of Investigative Dermatology, 77 (1981) 13-19.

[10] R. Philip, A. Penzkofer, W. Baumler, R.M. Szeimies, C. Abels, Absorption and fluorescence spectroscopic investigation of indocyanine green, Journal of Photochemistry and Photobiology A: Chemistry, 96 (1996) 137-148.

[11] H. Mohr, B. Bachmann, A. KleinStruckmeier, B. Lambrecht, Virus inactivation of blood products by phenothiazine dyes and light, Photochemistry and Photobiology, 65 (1997) 441-445.

[12] L.M. Williamson, R. Cardigan, C.V. Prowse, Methylene blue-treated fresh-frozen plasma: what is its contribution to blood safety?, Transfusion, 43 (2003) 1322-1329.

[13] A. Guyton, J. Hall, Textbook of Medical Physiology, Elsevier, Philidelphia, 2006.

[14] G. Oster, B. Holmstrom, J.S. Bellin, Photochemistry of riboflavin, Experientia, 18 (1962) 249-253.

[15] W.J.M. Vanderputten, J.M. Kelly, Laser flash spectroscopy of methylene-blue with nucleic-acids - Effects of ionic-strength and pH, Photochemistry and Photobiology, 49 (1989) 145-151.

[16] X.Z. Zhang, R.X. Zhuo, Y.Y. Yang, Using mixed solvent to synthesize temperature sensitive poly(N-isopropylacrylamide) gel with rapid dynamics properties, Biomaterials, 23 (2002) 1313-1318.

[17] S.-H. Kim, C.-C. Chu, Visible light induced dextran-methacrylate hydrogel formation using (-)-riboflavin vitamin B2 as a photoinitiator and L-arginine as a co-initiator, Fibers and Polymers, 10 (2009) 14-20.

[18] S.G. Bertolotti, C.M. Previtali, A.M. Rufs, M.V. Encinas, Riboflavin triethanolamine as photoinitiator system of vinyl polymerization. A mechanistic study by laser flash photolysis, Macromolecules, 32 (1999) 2920–2924.

[19] R.A. Floyd, J.E. Schneider, D.R. Dittmer, Methylene blue photoinactivation of RNA viruses, Antiviral Research, 61 (2004) 141-151.

[20] T.H. Kim, Y.P. Chen, C.W. Mount, W.R. Gombotz, X.D. Li, S.H. Pun, Evaluation of Temperature-Sensitive, Indocyanine Green-Encapsulating Micelles for Noninvasive Near-Infrared Tumor Imaging, Pharmaceutical Research, 27 (2010) 1900-1913.

[21] J. Rao, A. Dragulescu-Andrasi, H. Yao, Fluorescence imaging in vivo: recent advances, Current Opinion in Biotechnology, 18 (2007) 17-25.

[22] V. Ntziachristos, A.G. Yodh, M. Schnall, B. Chance, Concurrent MRI and diffuse optical tomography of breast after indocyanine green enhancement, Proceedings of the National Academy of Sciences of the United States of America, 97 (2000) 2767-2772.

[23] R.H. Patel, A.S. Wadajkar, N.L. Patel, V.C. Kavuri, K.T. Nguyen, H.L. Liu, Multifunctionality of indocyanine green-loaded biodegradable nanoparticles for enhanced optical imaging and hyperthermia intervention of cancer, Journal of Biomedical Optics, 17 (2012) 10.

[24] M.W. Dewhirst, B.L. Viglianti, M. Lora-Michiels, M. Hanson, P.J. Hoopes, Basic principles of thermal dosimetry and thermal thresholds for tissue damage from hyperthermia, International Journal of Hyperthermia, 19 (2003) 267-294.

[25] R.B. Roemer, Engineering aspects of hyperthermia therapy, Annual Review of Biomedical Engineering, 1 (1999) 347-376.

[26] R. Weissleder, A clearer vision for in vivo imaging, Nature Biotechnology, 19 (2001) 316-317.

[27] J.A. Curcio, C.C. Petty, The Near Infrared Absorption Spectrum of Liquid Water, Journal of the Optical Society of America, 41 (1951) 302.

[28] B.H. Tonnessen, L. Pounds, Radiation physics, Journal of Vascular Surgery, 53 (2011) 6S-8S.

[29] K. Bergmann, C.T. Okonski, A spectroscopic study of methylene blue monomer, dimer, and complexes with montmorillonite, Journal of Physical Chemistry, 67 (1963) 2169-2177.

[30] F. Liebel, S. Kaur, E. Ruvolo, N. Kollias, M.D. Southall, Irradiation of Skin with Visible Light Induces Reactive Oxygen Species and Matrix-Degrading Enzymes, Journal of Investigative Dermatology, 132 (2012) 1901-1907.

[31] W. Holzer, M. Mauerer, A. Penzkofer, R.M. Szeimies, C. Abels, M. Landthaler, W. Baumler, Photostability and thermal stability of indocyanine green, Journal of Photochemistry and Photobiology B-Biology, 47 (1998) 155-164.

[32] M.L.J. Landsman, G. Kwant, G.A. Mook, W.G. Zijlstra, Light-absorbing properties, stability, and spectral stabilization of indocyanine green, Journal of Applied Physiology, 40 (1976) 575-583.

[33] J.P. Tardivo, A. Del Giglio, C.S. de Oliveira, D.S. Gabrielli, H.C. Junqueira, D.B. Tada, D. Severino, R.d.F. Turchiello, M.S. Baptista, Methylene blue in photodynamic therapy: From basic mechanisms to clinical applications, Photodiagnosis and Photodynamic Therapy, 2 (2005) 175-191.

[34] S.D.M. Islam, A. Penzkofer, P. Hegemann, Quantum yield of triplet formation of riboflavin in aqueous solution and of flavin mononucleotide bound to the LOV1 domain of Photl from Chlamydomonas reinhardtii, Chemical Physics, 291 (2003) 97-114.

[35] I. Ahmad, Q. Fasihullah, A. Noor, I.A. Ansari, Q.N.M. Ali, Photolysis of riboflavin in aqueous solution: a kinetic study, International Journal of Pharmaceutics, 280 (2004) 199-208.

[36] I. Ahmad, M.A. Sheraz, S. Ahmed, S.H. Kazi, T. Mirza, M. Aminuddin, Stabilizing effect of citrate buffer on the photolysis of riboflavin in aqueous solution, Results in Pharma Sciences, 1 (2011) 11-15.

[37] R. Chen, X. Wang, X.K. Yao, X.C. Zheng, J. Wang, X.Q. Jiang, Near-IR-triggered photothermal/photodynamic dual-modality therapy system via chitosan hybrid nanospheres, Biomaterials, 34 (2013) 8314-8322.

[38] J. Hu, Y. Hou, H. Park, B. Choi, S. Hou, A. Chung, M. Lee, Visible light crosslinkable chitosan hydrogels for tissue engineering, Acta Biomaterialia, 8 (2012) 1730-1738.

[39] A. Grzelak, B. Rychlik, G. Baptosz, Light-dependent generation of reactive oxygen species in cell culture media, Free Radical Biology and Medicine, 30 (2001) 1418-1425.

[40] S.D. Varma, S. Kumar, R.D. Richards, Light-induced damage to ocular lens cation pump: prevention by vitamin C, Proceedings of the National Academy of Sciences, 76 (1979) 3504-3506.

[41] H.J. Hah, G. Kim, Y.-E.K. Lee, D.A. Orringer, O. Sagher, M.A. Philbert, R. Kopelman, Methylene Blue-Conjugated Hydrogel Nanoparticles and Tumor-Cell Targeted Photodynamic Therapy, Macromolecular Bioscience, 11 (2011) 90-99.

[42] M.A. Phelps, A.B. Foraker, W. Gao, J.T. Dalton, P.W. Swaan, A Novel Rhodamine−Riboflavin Conjugate Probe Exhibits Distinct Fluorescence Resonance Energy Transfer that Enables Riboflavin Trafficking and Subcellular Localization Studies, Molecular Pharmaceutics, 1 (2004) 257-266.

[43] R. Yoshida, K. Sakai, T. Okano, Y. Sakurai, Drug release profiles in the shrinking process of thermoresponsive poly(N-isopropylacrylamide-co-alkyl methacrylate) gels, Industrial & Engineering Chemistry Research, 31 (1992) 2339–2345.

[44] A. Gutowska, J.S. Bark, I.C. Kwon, Y.H. Bae, Y. Cha, S.W. Kim, Squeezing hydrogels for controlled oral drug delivery, Journal of Controlled Release, 48 (1997) 141-148.

[45] A.M. Alkilany, C.J. Murphy, Toxicity and cellular uptake of gold nanoparticles: what we have learned so far?, Journal of Nanoparticle Research, 12 (2010) 2313-2333.

[46] W.-S. Cho, M. Cho, J. Jeong, M. Choi, H.-Y. Cho, B.S. Han, S.H. Kim, H.O. Kim, Y.T. Lim, B.H. Chung, J. Jeong, Acute toxicity and pharmacokinetics of 13 nm-sized PEG-coated gold nanoparticles, Toxicology and Applied Pharmacology, 236 (2009) 16-24.

[47] M.L. Viger, W. Sheng, K. Dore, A.H. Alhasan, C.-J. Carling, J. Lux, C.d.G. Lux, M. Grossman, R. Malinow, A. Almutairi, Near-Infrared-Induced Heating of Confined Water in Polymeric Particles for Efficient Payload Release, Acs Nano, 8 (2014) 4815-4826.

[48] H. Malonne, F. Eeckman, D. Fontaine, A. Otto, L. De Vos, A. Moes, J. Fontaine, K. Amighi, Preparation of poly (N-isopropylacrylamide) copolymers and preliminary assessment of their acute and subacute toxicity in mice, European Journal of Pharmaceutics and Biopharmaceutics, 61 (2005) 188-194.

[49] Y. Pan, H. Bao, N.G. Sahoo, T. Wu, L. Li, Water-Soluble Poly(N-isopropylacrylamide)-Graphene Sheets Synthesized via Click Chemistry for Drug Delivery, Advanced Functional Materials, 21 (2011) 2754-2763.

[50] M. Patenaude, T. Hoare, Injectable, Degradable Thermoresponsive Poly(N-isopropylacrylamide) Hydrogels, Acs Macro Letters, 1 (2012) 409-413.

[51] H. Vihola, A. Laukkanen, L. Valtola, H. Tenhu, J. Hirvonen, Cytotoxicity of thermosensitive polymers poly(N-isopropylacrylamide), poly(N-vinylcaprolactam) and amphiphilically modified poly(N-vinylcaprolactam), Biomaterials, 26 (2005) 3055-3064.

[52] A.S. Wadajkar, B. Koppolu, M. Rahimi, K.T. Nguyen, Cytotoxic evaluation of N-isopropylacrylamide monomers and temperature-sensitive poly(N-isopropylacrylamide) nanoparticles, Journal of Nanoparticle Research, 11 (2009) 1375-1382.

[53] S.H. Park, B.G. Choi, H.J. Moon, S.-H. Cho, B. Jeong, Block sequence affects thermosensitivity and nano-assembly: PEG-L-PA-DL-PA and PEG-DL-PA-L-PA block copolymers, Soft Matter, 7 (2011) 6515-6521.

[54] M.H. Park, M.K. Joo, B.G. Choi, B. Jeong, Biodegradable Thermogels, Accounts of Chemical Research, 45 (2012) 424-433.

[55] S.-M. Lee, H. Park, K.-H. Yoo, Synergistic Cancer Therapeutic Effects of Locally Delivered Drug and Heat Using Multifunctional Nanoparticles, Advanced Materials, 22 (2010) 4049-4053.

[56] Z. Xiao, C. Ji, J. Shi, E.M. Pridgen, J. Frieder, J. Wu, O.C. Farokhzad, DNA Self-Assembly of Targeted Near-Infrared-Responsive Gold Nanoparticles for Cancer Thermo-Chemotherapy, Angewandte Chemie-International Edition, 51 (2012) 11853-11857.

[57] A. Shiotani, T. Mori, T. Niidome, Y. Niidome, Y. Katayama, Stable incorporation of gold nanorods into N-isopropylacrylamide hydrogels and their rapid shrinkage induced by near-infrared laser irradiation, Langmuir, 23 (2007) 4012-4018.

[58] K. Dong, Z. Liu, Z. Li, J. Ren, X. Qu, Hydrophobic Anticancer Drug Delivery by a 980 nm Laser-Driven Photothermal Vehicle for Efficient Synergistic Therapy of Cancer Cells In Vivo, Advanced Materials, 25 (2013) 4452-4458.

[59] M.K.G. Jayakumar, N.M. Idris, Y. Zhang, Remote activation of biomolecules in deep tissues using near-infrared-to-UV upconversion nanotransducers, Proceedings of the National Academy of Sciences of the United States of America, 109 (2012) 8483-8488.

[60] K.A. Carter, S. Shao, M.I. Hoopes, D. Luo, B. Ahsan, V.M. Grigoryants, W. Song, H. Huang, G. Zhang, R.K. Pandey, J. Geng, B.A. Pfeifer, C.P. Scholes, J. Ortega, M. Karttunen, J.F. Lovell, Porphyrin-phospholipid liposomes permeabilized by near-infrared light, Nature Communications, 5 (2014) 1-11.

CHAPTER THREE: LIGHT ACTUATED RELEASE FROM A MODULAR DRUG DELIVERY-ON-DEMAND SYSTEM

3.1 ABSTRACT

The advantages of light actuated drug delivery-on-demand systems include being able to control the timing, dosage, and location of drug release. Additionally, release can be repeatedly achieved in a noninvasive manner. Previously, a new light actuated drug delivery-on-demand strategy that used safe wavelengths of light and biocompatible chromophores to trigger release from a responsive delivery vehicle was reported. However, the system had a short useful timeline as both drug and chromophore were quickly eliminated from the matrix-type system. The goal of this study was to address these shortcomings by designing a modular, reservoir-type drug delivery-on-demand system that could trigger the release of biologically active molecules over an extended period of time via light actuation. Using a design that combined a drug reservoir and thermally-responsive valve spiked with chromophore-loaded liposomes, increased release rates of the model small molecule drug were achieved over 7 days upon light irradiation. However, release due to diffusion is a dominate release mechanism and novel materials and system designs that eliminate the release due to diffusion in the ‘off’ state will enhance light actuated drug delivery-on-demand systems efficacy.

3.2 INTRODUCTION

Increasing interest in drug delivery-on-demand systems is driven by the desire to improve drug efficacy by exacting control over the timing, duration, dosage and location of drug release. For instance, the delivery of human parathyroid hormone fragment (1-34) [hPTH(1-34)], which has been FDA approved since 2002 to treat osteoporosis, is one case where it is better to have intermittent exposure to the drug rather than continuous exposure. It was demonstrated in the

mid-1990's that *sustained* exposure to hPTH(1-34) promoted osteoclast activity whereas *intermittent* injections promoted osteoblast activity [1, 2]. As such, patients being treated with hPTH(1-34) require daily injections. In 2012, clinical trials began for an implantable, wirelessly controlled drug delivery device that would deliver hPTH(1-34) in a pulsatile manner in lieu of daily injections for osteoporosis treatment. In another example, researchers designed magneto-electric nanoparticles that would release an anti-human immunodeficiency virus (anti-HIV) drug to brain tissue when a low alternating current magnetic field is applied [3]. The blood-brain barrier (BBB) acts to protect the sensitive neuronal extracellular environment by regulating the influx of molecules from the peripheral circulatory system [4]. Unfortunately, it can also hinder the delivery of beneficial therapeutic molecules and is a challenge for drug delivery systems that wish to target the brain. In the treatment of HIV, this means that there are tissues where the virus can persist. To overcome this challenge, a delivery-on-demand strategy was utilized through the application of an alternating low: 1) magnetic field to deliver the particles across the BBB [5] and 2) electric field to quickly release the drug from the nanoparticle [3].

Despite the advantages of the delivery-on-demand approach, there are significant limitations to current systems. Recall the delivery-on-demand device for hPTH(1-34). The device is made of non-biodegradable materials (i.e. silicone and titanium) and requires removal after the drug reservoirs are depleted. Currently, the device is implanted subcutaneously in the abdomen and is capable of delivering 40 µg daily doses for 3 weeks [2]. This means multiple replacement procedures over the approved 2-year treatment period for hPTH(1-34) would be required [6]. Additionally, the limitations of other delivery-on-demand systems, which have used various external stimuli to trigger release (i.e. irradiation, heat, electrical and magnetic fields, mechanical compression and ultrasound), have included problems with the delivery vehicle's

toxicity, stability, safety risks associated with the stimulus as well as requiring complex equipment setups [7-9]. Light has been an attractive choice for the external stimulus due to its non-invasive nature, high spatial resolution and temporal control, convenience and ease of use. However, light actuated systems in particular have been limited to *in vitro* applications due to problems with toxicity of the photo-responsive materials at therapeutically relevant concentrations [10]. As such, improvements are needed for light actuated drug delivery-on-demand systems to reach the clinic.

Chapter 2 described a new light actuated drug delivery-on-demand strategy that uses visible and near infrared (NIR) light and biocompatible chromophores – cardiogreen, methylene blue and riboflavin – to trigger release from a thermally responsive delivery vehicle via the photothermal effect. There are several advantage of this strategy, including the safety of visible and NIR light as external stimuli for remote actuation, the therapeutic application of NIR in deeper tissues due to limited light attenuation, and the selection of biomaterials that have a long history of use in FDA approved products. However, there are shortcomings to the reported delivery-on-demand system. First, the thermally responsive delivery vehicle acted as both a drug reservoir and a valve for drug release. This limits its application to candidate drugs that can either withstand the delivery vehicle's fabrication conditions or be readily loaded at high efficiency post fabrication. Additionally, while pulsatile release of the model drug upon NIR exposure from the delivery vehicle was achieved over multiple cycles, it was limited to 4 cycles due to the loss of the photothermal effect caused by chromophore diffusion from the delivery vehicle into the surrounding medium. Therefore, the goal of this study was to address these shortcomings by designing a modular drug delivery-on-demand system that can control the release of biologically active molecules over an extended period of time.

Modular systems offer several advantages, including flexibility in design, increased versatility in applications and less customization. For instance, there are challenges unique to delivering both biologics and small molecule drugs, including issues with solubility, encapsulation, biological half-life and biodistribution [11, 12]. Rather than having to design an entirely new drug delivery-on-demand system for each new drug, a modular delivery-on-demand system only requires changes to independent modules that fit into an overall system. This chapter reports on a reservoir-based design for the modular light actuated drug delivery-on-demand system. The influence of both reservoir material and hydrogel valve mesh size on the release of model small molecule drugs is characterized. Additionally, liposomes have been included to act as chromophore depots that delay chromophore diffusion from the delivery system, thereby prolonging the lifetime for both the photothermal effect and light actuated release. The proof-of-concept for this strategy is poly (ethylene glycol) reservoirs loaded with riboflavin as a model small molecule drug. Thermally responsive poly (N-isopropylacrylamide) hydrogels act as valves and are spiked with methylene blue-loaded liposomes to act as a heat source via the photothermal effect upon light irradiation.

3.3 MATERIALS AND METHODS

3.3.1 Chromophores and model small molecule drugs

Cardiogreen (CAS number 3599-32-4) and fluorescein (CAS number 518-47-8) were purchased from Sigma-Aldrich (Missouri, USA). Methylene blue was purchased from Thermo Fisher Scientific (CAS number 61-73-4; Massachusetts, USA). Riboflavin was purchased from Acros Organics (CAS number 83-88-5; New Jersey, USA). All materials were used without further purification.

3.3.2 Thermally responsive NiPAAm hydrogel synthesis and mass swelling ratio

Poly (N-isopropylacrylamide) (NiPAAm) (CAS number 25189-55-3, Sigma-Aldrich, Missouri, USA) hydrogels were fabricated using the procedure previously described by Zhang, et al [13]. Briefly, NiPAAm was dissolved in 50:50 water and acetone solution along with the crosslinker N, N'-methylenebisacrylamide (MBA) (CAS number 110-26-9, Sigma-Aldrich, Missouri, USA). This mixture was polymerized with N, N, N', N'-tetramethylethylenediamine (TEMED) (CAS number 110-18-9, Acros Organics, New Jersey, USA) and 10% (w/v) ammonium persulfate (APS) (CAS number 7727-54-0, Sigma-Aldrich, Missouri, USA), and then soaked and stirred in deionized water (dH_2O) for at least 24-hours to leach away unreacted products. To incorporate chromophore-loaded liposomes (see *Section 3.3.4*) into the NiPAAm hydrogels, liposomes suspended in Tris-buffered saline (TBS, pH 8.8) were used in lieu of dH_2O alone.

To determine the swelling ratio of the NiPAAm hydrogels, the hydrogels were soaked in dH_2O at room temperature for at least 24 hours. Excess water was removed from the swelled hydrogel surface with a moist Kim-wipe and then weighed (W_s). The hydrogels were frozen to -80˚C for 12 hours and lyophilized overnight. At the conclusion of lyophilization, the dry weight was determined (W_d). The mass swelling ratio (Q_m) was calculated as follows:

$$Q_m = \frac{W_s}{W_d} \quad (1)$$

3.3.3 Polymeric reservoir synthesis and drug loading

Reservoirs made of gelatin from bovine skin, type B (CAS number 9000-70-8, Sigma-Aldrich, Missouri, USA) were prepared by dissolving the gelatin powder in dH_2O at 60˚C with continuous stirring until it was a homogenous solution. The gelatin solution was poured into cylindrical molds and transferred to a refrigerator to cool for at least 30 minutes. To load the

model small molecule drugs, aqueous solutions of model drug were prepared using dH_2O and subsequently used to dissolve the gelatin powder in lieu of dH_2O alone.

Poly (ethylene glycol) diacrylate (PEGDA) (MW 700, CAS number 26570-48-9, Sigma-Aldrich, Missouri, USA) reservoirs were prepared by diluting stock PEGDA solution with dH_2O and bubbling the solution with nitrogen for 10 minutes to remove excess oxygen. Free radical polymerization was initiated with the addition of TEMED and 10% (w/v) APS. To load the model small molecule drugs, aqueous solutions of model drug were prepared using dH_2O and subsequently used to dilute the stock PEGDA solution in lieu of dH_2O alone.

3.3.4 Chromophore-loaded liposome synthesis

A method previously described by Cui, et al [14] was tailored to prepare chromophore-loaded palmitic acid/cholesterol liposomes. Briefly, 3/7 molar ratio mixtures of palmitic acid (CAS number 57-10-3, Sigma-Aldrich, Missouri, USA) and cholesterol (CAS number 57-88-5, Sigma-Aldrich, Missouri, USA) were dissolved in 90/10 (v/v) benzene/methanol and frozen in liquid nitrogen and lyophilized for 16 hours to completely remove the organic solvent. The freeze-dried samples were hydrated with aqueous chromophore solutions prepared with TBS (pH 8.8) and underwent five cycles of vortex-freeze-and-thaw (liquid nitrogen to 70˚C water bath). Finally, the solution underwent sonication using an ultrasonic homogenizer for 20 minutes total run time (20% amplitude, pulse on 20 seconds, and pulse off 5 seconds). Particle size distribution was determined by dynamic light scattering (173˚ back scattering) using a Zetasizer Nano-ZS ZEN3600 (Malvern Instruments, UK).

3.3.5 Measuring drug release

To measure the release of model drugs from the modular delivery system, modified conical tube setups were used (Figure 1). Briefly, the NiPAAm matrix was first placed at the

mouth of a 15mL conical tube body followed by the reservoir matrix. The stack was gently positioned to be flush with the mouth of the 15mL conical tube body and the cap was screwed into place (Figure 1A). The bottom of the conical tube had been removed to add and remove supernatant. At designated time points, supernatant samples (1 mL) were collected and 1 mL of fresh PBS was added to keep the supernatant volume constant during the course of the experiment.

For samples exposed to light, the reservoir matrix was first placed at the mouth of a 15mL conical tube body (Figure 1B). Next, a NiPAAm hydrogel was stacked on top of the reservoir matrix and gently positioned to be flush with the mouth of the 15mL conical tube body to ensure one surface was exposed to the supernatant for the duration of the experiment (Figure 1C). The conical tube was inverted to submerge the exposed surface of the NiPAAm hydrogel in 10 mL of PBS in a transparent petri dish and a modified petri dish cover was used to hold the conical tube body in place (secured by rubber O-rings) (Figure 1D). The light source was positioned below the setup and starting at the 24 hour time point, the NiPAAm hydrogels were irradiated with 590 nm light at 600mW for 2 minutes. Supernatant samples (1 mL) were collected at designated time points and to keep the supernatant volume constant at 10 mL, 1 mL of fresh PBS was added to replace the volume taken at each time point. Additionally, every 24 hours – prior to light irradiation – the whole supernatant was collected and replaced with fresh supernatant that was heated to 27˚C – 5˚C below the lower critical solution temperature (LCST) of NiPAAm.

The amount of model drug released at each time point was determined by measuring the absorbance (methylene blue: 630 nm) or fluorescent intensity (fluorescein and riboflavin: 485 nm excitation, 535 nm emission) on an Infinite F200 plate reader (Tecan, Männedorf,

Switzerland). The experiments were conducted in triplicates for each experimental group and the average values are represented with the standard deviation.

3.4 RESULTS

3.4.1 Mesh size of NiPAAm hydrogels

One of the ways to control the structural and mechanical properties of NiPAAm hydrogels is to change the concentration of crosslinker and monomer during polymerization. In this study, the molar ratio between NiPAAm monomer and MBA crosslinker was altered by changing the amount of MBA and keeping the NiPAAm concentration constant. The mesh size (ξ) was calculated using the following formula [15]:

$$\xi = Q^{1/3}(\overline{r_o^2})^{1/2} \quad (2)$$

where $(\bar{r}_o^2)^{1/2}$ is the root-mean-squared end-to-end distance of network chains between two adjacent crosslinks, and Q is the volumetric swollen ratio. The volumetric swelling ratio was determined using Q_m, calculated from Equation (1):

$$Q = \frac{\left(Q_m/\rho_1\right)+\left(1/\rho_2\right)}{1/\rho_2} \quad (3)$$

where ρ_1 is the density of solvent (water, 1 g/cm^3) and ρ_2 is the density of polymer (1.07 g/cm^3). The root-mean-squared end-to-end distance was determined using the following relationship:

$$\left(\overline{r_o^2}\right)^{1/2} = l\left(C_n \frac{2\overline{M_c}}{M_r}\right)^{1/2} \quad (4)$$

where C_n is the Flory characteristic ratio (6.9 for acrylates [16]), l is the bond length along the polymer backbone (carbon-carbon bond length = 0.154 nm [17]), and M_r is the molecular weight of the repeating monomer (113.18 g/mol). The average molecular weight between crosslinks (M_c) was calculated using the following equation [18]:

$$\overline{M_C} = \frac{n_r}{n_l} M_r + M_l \quad (5)$$

where M_l is the molecular weight of the crosslinker (154.17 g/mol), n_r and n_l are the moles of NiPAAm and MBA used in the experiments, respectively. The equilibrium volumetric swelling ratio and network mesh size are given in Table 1. Increasing the concentration of crosslinker decreased the average molecular weight between crosslinks and subsequently decreased the volumetric swelling ratio and the calculated mesh size of the NiPAAm hydrogels.

3.4.2 Drug diffusion from polymeric reservoirs and through NiPAAm hydrogels

The release profiles of model drugs from polymeric matrices depend upon the structural properties of the matrix as well as the physiochemical interactions between the polymeric matrix and the drug. Accordingly, the release of model small molecule drugs with similar molecular weights but different charges (riboflavin: 376.36 g/mol, no charge; fluorescein: 332.31 g/mol, negatively charged; methylene blue: 319.85 g/mol, positively charged) from two different polymeric reservoirs commonly used in biomedical applications (gelatin, a biopolymer and PEG, a synthetic polymer) and through NiPAAm hydrogels with varying crosslinking densities was studied.

Figure 2A compares the release profiles of the model drugs due to diffusion through NiPAAm hydrogels prepared with 32:1 M ratio of NiPAAm to MBA. There is ≤5% release of all model drugs by the 24 hour timepoint. Specifically, there was 5µg (±1µg) of riboflavin released, 2µg (±0.5µg) of methylene blue, and 5µg (±2µg) of fluorescein. After 7 days, 73% (±5%) of riboflavin was released by diffusion from 10% (w/v) gelatin reservoirs and through NiPAAm hydrogels compared to 53% (±4%) and 35% (±3%) of methylene blue and fluorescein, respectively. Figure 2B compares the release the model drugs release through NiPAAm hydrogels prepared with 8:1 M ratio of NiPAAm to MBA. Again, all samples have very little release in the first 24 hours. Methylene blue and fluorescein have 1% release and riboflavin has 3% release. Similar to 32:1 samples, riboflavin had the greatest release after 7 days with 70% (±4%) total release. Methylene blue had 36% (±3%) and fluorescein had the 21% (±5%).

Figure 3A compares the release of riboflavin from 10% and 20% (w/v) gelatin reservoirs and through NiPAAm hydrogels prepared with 32:1 M ratio of NiPAAm to MBA. There is very little release in the first 24 hours. As previously mentioned, riboflavin release from 10% (w/v) reservoirs was 5%. Increasing the reservoir concentration to 20 % (w/v) gelatin, decreased the release of riboflavin to 3% in the first 24 hours. Compared to the 73% (±5%) riboflavin released from 10% (w/v) gelatin reservoirs, there was 65% (±1%) from 20% (w/v) gelatin reservoirs after 7 days. Figure 3B compares the release of riboflavin from gelatin reservoirs at different concentrations but through NiPAAm hydrogels prepared with 8:1 M ratio of NiPAAm to MBA. In the first 24 hours, riboflavin release from 10% (w/v) reservoirs was 3%, and decreased to 1% when the concentration of the reservoir was increased to 20 % (w/v) gelatin. After 7 days, 70% (±4%) of riboflavin was released from 10% (w/v) gelatin reservoirs and 52% (±6%) from 20% (w/v) gelatin reservoirs.

Figures 3C and 3D compare the release of model drugs from PEG reservoirs and through NiPAAm hydrogels prepared with 8:1 M ratio of NiPAAm to MBA. Overall, there is a decrease in each model drug's release over time compared to the release from gelatin reservoirs. Specifically, riboflavin release was 2μg (±0.5μg) while <1μg of both methylene blue and fluorescein was released in the first 24 hours. After 7 days, riboflavin had the greatest release with 36% (±3%) total release, methylene blue had 7% (±1%) total release, and fluorescein had 4% (±1%) total release. Figure 3D is a zoomed-in view of methylene blue and fluorescein's release profiles for better visualization.

3.4.3 Light actuated release from modular drug delivery system

To demonstrate light actuated release from a modular drug delivery system, PEG reservoirs were loaded with riboflavin as a model small molecule drug and the NiPAAm valves

were spiked with methylene blue-loaded liposomes to act as a heat source upon irradiation with 600mW 590 nm light via the photothermal effect. Liposomes were added to delay the release of chromophore from the NiPAAm valve by acting as a chromophore depot. The overall goal being to increase the number of days a photothermal response could be generated and light actuated release achieved. The sizes of palmitic acid/cholesterol liposomes loaded with the various chromophores are summarized in Table 2 and are significantly larger than the calculated mesh sizes of the NiPAAm hydrogels reported in Table 1. Additionally, the liposomes loaded with cardiogreen and riboflavin are stable over 21 days and remain intact after light irradiation. Methylene blue-loaded liposomes are less stable over time and after light irradiation; however, absorption of the laser light by the chromophore could be skewing the results.

Figures 4A and 4B compare the release rate of riboflavin (bar graph) to cumulative release (line graph) due to light irradiation from modular delivery systems with and without chromophore, respectively. The release rate at the first light exposure (t = 24 hrs.) was the slowest for both systems at $2x10^{-2}$ µg/min from the chromophore loaded system and $9x10^{-3}$ µg/min from the system without chromophore. Additionally, ~1 µg of drug was released within the first 24 hours from both systems. After light irradiation, the cumulative release increased to 1.2 µg from the chromophore system and 1.05 µg from the control system. The release rates increased to 1.6, 1.8, 1.6, 1.9, 2.2, and $2.5x10^{-1}$ µg/min for the remaining six exposures in the chromophore system, respectively. These increased release rates correspond with small spikes in the cumulative release of riboflavin upon light exposure. The release rates of riboflavin from the control system are an order of magnitude slower with rates of 3.1, 1.8, 2.4, 1.9, 1.8, $3.5x10^{-2}$ µg/min for the remaining six exposures, respectively. The cumulative release of riboflavin from both systems is compared head-to-head in Figure 4C. The total amount of model drug released

after 7 days from the chromophore-loaded system was 19.2 µg (±0.8 µg) and 16.8 µg (±2 µg) from the control system. Figure 4D presents the percent of riboflavin released from the modular reservoir-valve system spiked with methylene blue-loaded liposomes. To calculate the percent released, the mass released at each timepoint, M_t, was divided by the mass initially loaded at the start of the experiment, M_∞. The first light exposure triggered the release of <1% of riboflavin while the second, third, fourth, fifth, sixth and seventh exposures triggered the release of 1.3%, 1.4%, 1.2%, 1.5%, 1.8% and 2% of riboflavin from the modular systems with chromophore, respectively. All light exposures triggered the release of <1% of riboflavin from the modular systems without chromophore. For comparison, the percent of riboflavin released between the light exposures, starting after the first light exposure, was 4%, 5%, 2%, 3%, 3% and 2%, respectively. After 7 days of visible light exposure every 24 hours, 31% (±1%) of the riboflavin was released from the modular systems with chromophore versus 27% (±3%) from the modular systems without chromophore.

3.5 DISCUSSION

Chapter 2 described a novel light actuated drug delivery-on-demand strategy that used safe visible and near infrared (NIR) light and biocompatible chromophores to trigger release from a thermally responsive delivery vehicle via the photothermal effect. However, the thermally responsive delivery vehicle acted as both a drug reservoir and a valve for drug release. These matrix-type devices exhibit a first-order release profile where a constant percent of the remaining drug was released per unit time [19]. As a result, drug was quickly eliminated from the system with 80% of the drug released after 4 days. Additionally, the photothermal response only lasted for 4 cycles due to chromophore diffusion from the delivery vehicle into the surrounding medium. Therefore, the goal of this study was to address these shortcomings by designing a

reservoir-type modular drug delivery-on-demand system that could release biologically active molecules over an extended period of time via light actuation.

The advantage of a reservoir-type modular delivery system is release rate is independent of the starting drug concentration rather it is dependent on diffusion through a membrane (zero-order release). This is explained by Fick's first and second laws of diffusion:

$$J = -D\frac{dC}{dx} \tag{6}$$

$$\frac{\partial C}{\partial t} = D\left(\frac{\partial^2 C}{\partial x^2}\right) \tag{7}$$

where *J* is flux, *D* is the diffusion coefficient, *C* is concentration, *x* is position, and *t* is time [20]. At steady-state the change in concentration over time is zero. Equation (7) then simplifies to:

$$\left(\frac{\partial^2 C}{\partial x^2}\right) = 0 \tag{8}$$

Performing the integrations on Equation (8) yields:

$$c(x) = A_1 x + A_2 \tag{9}$$

where A_1 and A_2 are constants of integration. To solve for the constants of integration requires knowing two boundary conditions. First, just inside the membrane wall closest to the reservoir (x = 0) the drug concentration is proportional to partition coefficient of the molecule, *K*, and the concentration of drug in the reservoir, C_R. Second, just inside the membrane wall closest to the supernatant (x = the membrane thickness, *h*) the drug concentration is again proportional to partition coefficient of the molecule and the concentration of drug in the supernatant, C_S. Substituting these boundary conditions into Equation (9) gives:

$$c(x) = \frac{K(C_S - C_R)}{h}x + KC_R \tag{10}$$

Equation (10) can be plugged into the equation for Fick's first law (Equation (6)) to solve for the particle flux through the membrane:

$$J = \frac{KD}{h}(C_S - C_R) \quad (11)$$

In other words, the flow of drug is driven by a difference in concentration and the rate is proportional to the permeability of the membrane [21]. It is important to note that at the end of the delivery system's lifetime, when the reservoir drug concentration begins to approach zero, the steady state assumption does not apply since changes in the reservoir concentration with time will impact the release profile. As a result, the system will not exhibit zero-order release.

Clearly, the permeability of the valve and reservoir materials can impact the final release profile. Specifically, in remote actuated drug delivery systems, it is desirable for drug release due to diffusion to be minimal in the 'off' state while still allowing for the expulsion of drug upon actuation. This is especially true for thermally responsive NiPAAm valves used in the reported modular delivery-on-demand system which undergoes a rapid volume phase transition upon heating. The consequence of this transition is a decrease in permeability with increasing temperatures [22]. In an effort to limit diffusion in the 'off' state while still allowing for photothermally triggered release, the effect NiPAAm crosslinking density had on the diffusion of model small molecule drug was studied. The results showed that increasing the crosslinking density – subsequently decreasing the mesh size from 9.3 nm to 4.2 nm – did little to change riboflavin's release profile due to diffusion, and slightly decreased the diffusion of methylene blue and fluorescein. A similar pattern in the release profiles of the model drugs was observed when the reservoir material was switched to PEG with riboflavin release due to diffusion being greatest and fluorescein the least. However, there is a significant decrease in total drug released from systems with PEG reservoirs compared to systems with gelatin reservoirs for all model drugs. This can be attributed to differences in the reservoir mesh sizes and how they compare to the drugs' sizes. The mesh size of PEG (MW = 700) is ~1 nm [23] while the mesh size of 16%

(w/v) gelatin is 33.8 nm [24]. Compared to the size of the model drugs (riboflavin's hydrodynamic radius, R_H = 5.8 Å [25]; methylene blue R_H = 4.9 Å [26]; fluorescein R_H = 8 Å [27]), gelatin's mesh size – and the calculated mesh sizes of the NiPAAm hydrogel valves – is an order of magnitude larger. As a result, changes in the mesh sizes had little influence on the permeation of drugs unlike the PEG reservoir, which have mesh sizes only slightly larger than the model drugs that impeded drug diffusion. Interestingly, there is a significant difference in the release profiles of the model drugs despite their sizes being similar, regardless of the reservoir material or NiPAAm crosslinking density. Given these observations, the release profiles cannot be fully explained by size exclusion.

Factors such as the physicochemical properties of the drugs, materials in the delivery system, the release environment, and interactions between these factors complicate the release profiles [19]. Both methylene blue and fluorescein are ionic molecules; consequently, ionic interactions and binding are possible. As a protein, gelatin contains both positively and negatively charged amino acids that could bind with negatively charge fluorescein and positively charged methylene blue, respectively. This has been seen in previous studies where fluorescein has been shown to bind to plasma proteins with a low affinity [28], and methylene blue's ability to bind to biopolymers, like DNA, has been used for photo-inactivation applications [29]. In addition to ionic interactions, there are other weak intermolecular forces impacting the drug release profiles. Case in point, PEG is a non-ionic polymer yet the results showed a similar pattern of the ionic drugs being released at a slower rate than riboflavin (neutral). The charges on methylene blue and fluorescein can polarize atoms in the polymer to create short-ranged attractions between the polymer and drug – termed van der Waals forces [20]. While weak, van der Waals forces slow drug diffusion. Additionally, PEG is a ubiquitous polymer in the

biomaterials field due to its extremely hydrophilic nature from its ability to hydrogen bond water. As such, it is likely fluorescein and riboflavin are involved in hydrogen bonding with PEG to varying degrees; however, methylene blue lacks a hydrogen bonding donor group and PEG can only act as a hydrogen bond acceptor.

As a proof-of-concept for light actuated release from a modular, reservoir-type drug delivery-on-demand system, NiPAAm hydrogels acted as a valve to regulate the release of riboflavin from PEG reservoirs. Additionally, NiPAAm was spiked with methylene blue-loaded liposomes, which served as both a heat source upon light irradiation via the photothermal effect of methylene blue, and as a way to delay chromophore diffusion from the delivery system. The results show that the release rates were an order of magnitude greater in the systems with chromophore compared to systems without chromophore. The increasing temperature from the photothermal response of methylene blue causes a rapid phase transition in NiPAAm that results in the polymer collapsing and increasing the diffusive transport rates by hydrostatically expelling drug [30, 31]. This increased release rate was observed over 7 days indicating a prolonged photothermal response from modular release system, and suggesting the liposomes successfully delayed the loss of chromophore from the system due to diffusion. Consistent with the overarching objective of designing a light actuated drug delivery-on-demand system from biocompatible materials, palmitic acid and cholesterol are both safe, naturally derived materials. Additionally, chromophore-loaded liposomes have shown good stability – consistent with what has been previously reported [14]. However, comparing the release profiles from the chromophore loaded system and the control system shows similar cumulative release after 7 days, signifying diffusion remains as a dominate mechanism for release. The advantage of

delivery-on-demand systems is the explicit control over when and where a drug is released, and as such, in the 'off' state drug release should be negligible [32].

Despite the improved lifetime for light actuated release from 4 days (Chapter 2) to one week, diffusion remains as the dominating release mechanism as evident by the significant amount of release between light exposures. As such, improvements to the design of the modular delivery-on-demand system are needed. Specifically, the system needs to block drug release in the absence of light. Switching the thermally-responsive polymer to a polymer that has an upper critical solution temperature (UCST) at physiologically relevant temperatures is one possible approach. At body temperature, the UCST polymer valve would create an impermeable skin over the drug reservoir and block the drug from being released. To trigger release, the temperature would be increased via the photothermal effect and cause the skin layer to become a hydrogel that then allows the drug to diffuse out. However, the major limitation to UCST polymers is that very few polymers exhibit a UCST in water at physiologically relevant temperatures [33, 34]. Additionally, there is no universal UCST polymer that demonstrate a stable phase separation that has little-to-no dependence on environmental conditions (i.e. pH, ionic species and strength) like the LCST polymer, NiPAAm [35]. Recently, Agarwal and coworkers reported a strategy to synthesize clinically relevant polymers (i.e. polymethacrylamide) that show a UCST, and identified rules for designing UCST polymers: 1) the polymer must be able to reversibly form intramolecular hydrogen bonds; 2) little-to-no ionic groups should be present; and 3) a hydrophilic-hydrophobic balance that results in a phase transition at the desired temperature range [33]. While polymers fabricated using this approach demonstrated an UCST, they suffer from hysteresis, and more work is needed before they'll become strong candidates for rapidly responding drug delivery-on-demand systems.

Another possible solution is to reconfigure the design and have the deswelling of NiPAAm open small pores that allows drug to be released. This is in contrast to the current study which had the drug diffusing through a NiPAAm membrane and the deswelling of NiPAAm increasing the rate of diffusion. Specifically, an elastomeric membrane that has NiPAAm microgels uniformly distributed throughout the membrane would prevent the diffusion of drug to the supernatant. Dispersed within this membrane is a photothermally responsive chromophore, and upon light irradiation, heat generated from the chromophore would cause the NiPAAm microgels to shrink and open small pores within the membrane to allow the drug to release. Critical elements of this modular system are 1) an impermeable membrane that does not allow the either the drug or chromophore to diffuse through it; 2) a reservoir that rapidly allows drug to diffuse through the small pores that open from the photothermal response of the irradiated chromophore; and 3) the use of biocompatible materials. One potential membrane materials is poly(trimethylene carbonate) (PTMC). It is biocompatible as well as biodegradable via surface erosion [36]. Additionally, previous studies have shown that the degradation rate can be controlled by the number average molecular weight with high molecular weight rods undergoing 60 weight percent mass loss 8 weeks after implantation *in vivo* compared to 20 weight percent mass loss at the same timepoint for lower molecular weight rods [37]. The advantage of a modular system that utilizes a biodegradable membrane is the entire delivery-on-demand system can be cleared from the body without being explanted including the non-biodegradable NiPAAm microgels, which can be cleared by macrophages via phagocytosis at the end of the devices lifetime.

3.6 CONCLUSION

This study describes a modular reservoir-valve delivery-on-demand system for the triggered release of small molecule drugs via light actuation. The data shows the rapid release of riboflavin – the model small molecule drug – upon light exposure from the modular delivery system over 7 cycles with 24 hours between light exposures. Despite the increased release rate of the model drug with light exposure, diffusion between exposures remains as a dominating release mechanism. Ultimately, innovative system designs and novel materials that eliminate the release due to diffusion in the 'off' state will enhance the efficacy of light actuated drug delivery-on-demand systems.

3.7 FIGURES

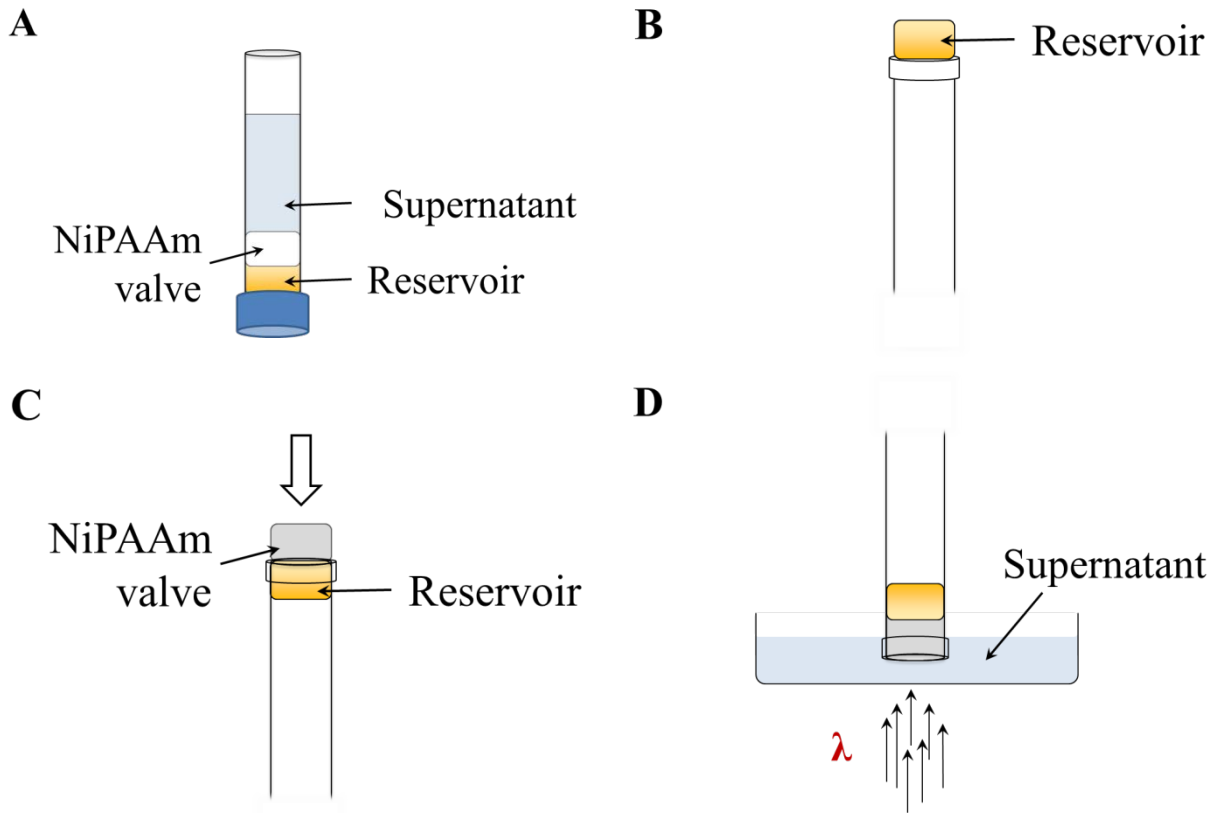

Figure 1. Illustrations of (A) the experimental setup for characterizing the release of model small molecule drugs from a polymeric reservoir and through a NiPAAm hydrogel valve; and (B-D) the sample preparation and experimental setup for measuring the light actuated release of model small molecule drugs from the modular drug delivery system.

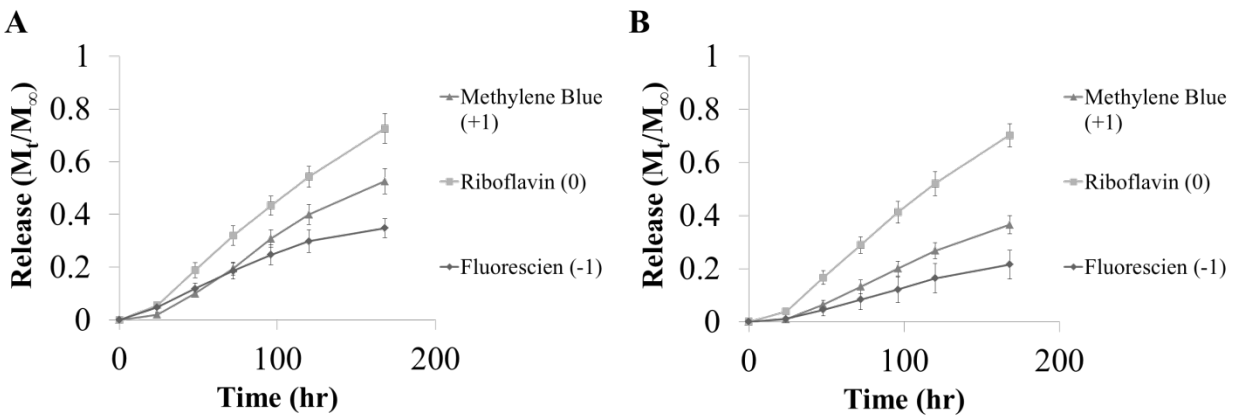

Figure 2. The percent release of model drugs from 10% (w/v) gelatin reservoirs over 7 days through NiPAAm hydrogels prepared with (A) [32:1] molar ratio NiPAAm to MBA; (B) [8:1] molar ratio NiPAAm to MBA. M_t is cumulative release at time, t, and M_∞ is initial loading amount (n=3).

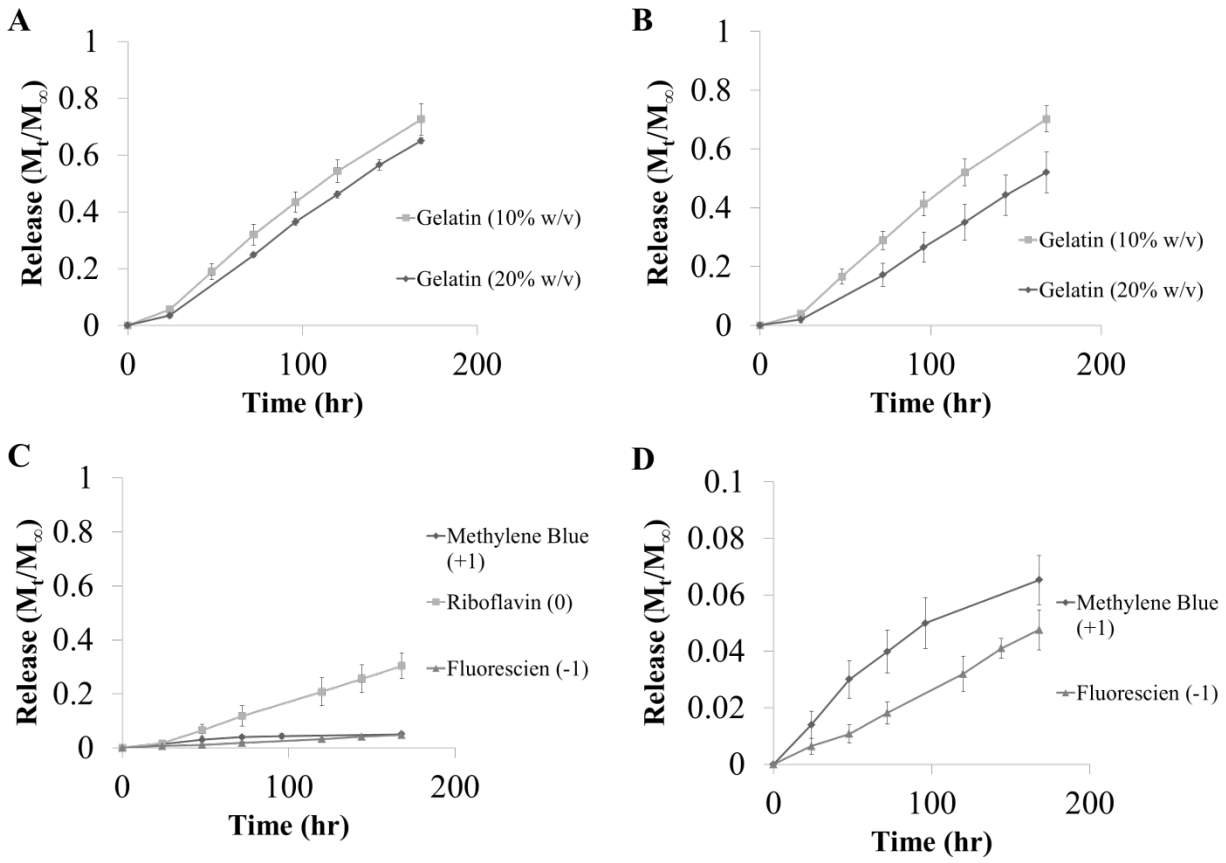

Figure 3. The percent release of riboflavin from 10% and 20 % (w/v) gelatin reservoirs over 7 days through NiPAAm hydrogels prepared with (A) [32:1] molar ratio NiPAAm to MBA; (B) [8:1] molar ratio NiPAAm to MBA. (C-D) The release of model drugs from 30% (v/v) PEG reservoirs through NiPAAm hydrogels prepared with [8:1] molar ratio NiPAAm to MBA. M_t is cumulative release at time, t, and M_∞ is initial loading amount (n=3).

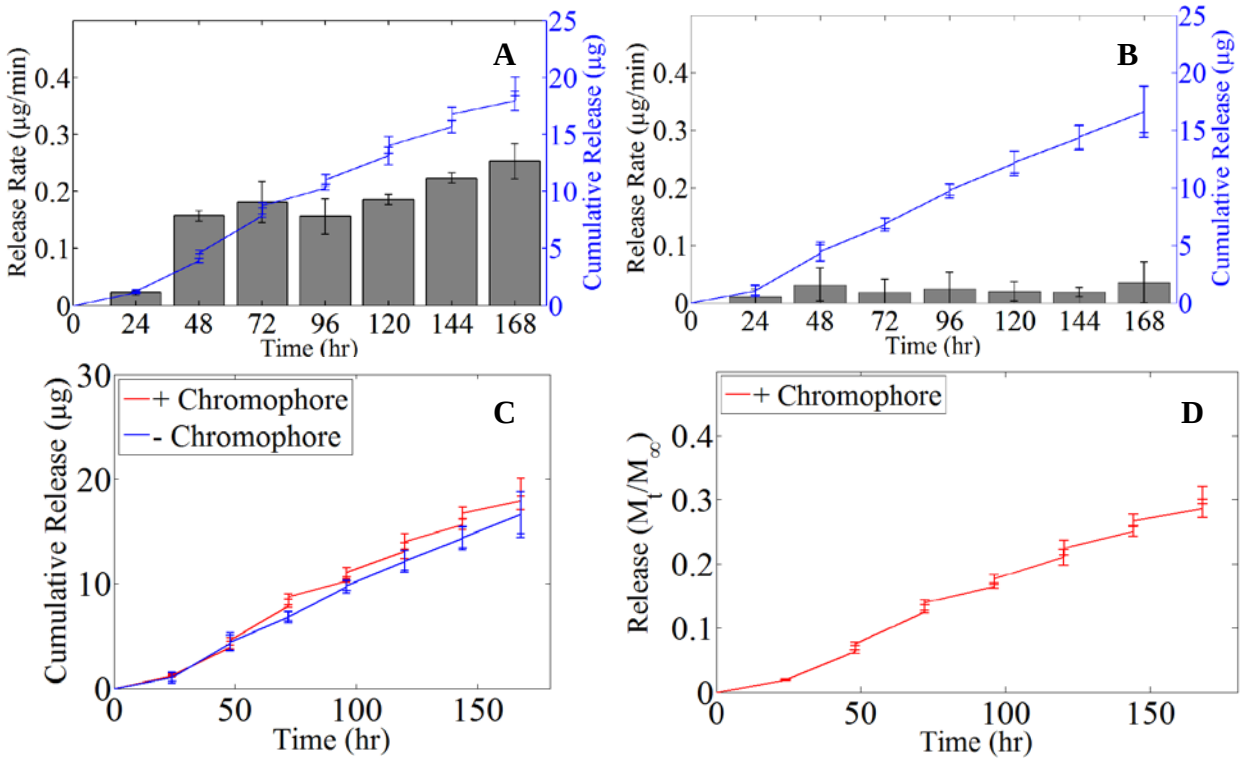

Figure 4. Release rate (bar graph) and cumulative release (line graph) of model drug (Riboflavin, 376.36 g/mol) from PEG reservoirs through NiPAAm hydrogel valves (diameter = 9mm, thickness = 4mm) spiked with methylene blue-loaded liposomes (A) and without chromophore-loaded liposomes (B). Samples were irradiated 600mW 590nm light for 2 minutes every 24 hours starting at t=24hr. The release rate of riboflavin increases upon light exposure from the modular delivery system when chromophore is present whereas the release rate is nearly an order of magnitude lower from the modular system without chromophore added. (C) Comparing the cumulative release profiles of model drug from modular delivery systems with chromophore to systems without chromophore. (D) The fraction of riboflavin released from the modular delivery system with chromophore via light actuation. M_t is cumulative release at time, t, and M_∞ is initial loading amount (n=3).

3.8 TABLES

Table 1. The volumetric swelling ratio (Q), average molecular weight between crosslinks (M_c) and mesh size (ξ) of NiPAAm hydrogels

NiPAAm:MBA *(Molar Ratio)*	**Q**	**M_c ($g \cdot mol^{-1}$)**	**ξ (nm)**
8:1	13.5	1096.32	4.25
16:1	19.7	2038.47	6.5
32:1	21.6	3922.77	9.38

Acronyms: poly (N-isopropylacrylamide), NiPAAm; N, N'-methylenebisacrylamide, MBA.

Table 2. Chromophore-loaded palmitic acid/cholesterol liposome size and homogeneity

Chromophore	T_0		T_7		T_{21}		λ*	
	Size (nm)	**PDI**	**Size (nm)**	**PDI**	**Size (nm)**	**PDI**	**Size (nm)**	**PDI**
Cardiogreen	113.7 *±0.85*	0.109 *±0.01*	120.6 *±4.15*	0.091 *±0.02*	120.5 *±6.06*	0.161 *±0.04*	121.3 *±1.05*	0.116 *±0.02*
Methylene Blue	145.3 *±4.25*	0.129 *±0.03*	140.25 *±0.49*	0.254 *±0.01*	122.2 *±1.76*	0.393 *±0.04*	–	–
Riboflavin	108.1 *±2.65*	0.091 *±0.01*	112.2 *±3.47*	0.134 *±0.04*	110.4 *±3.96*	0.188 *±0.01*	117.2 *±0.71*	0.139 *±0.004*
Blank	123.9 *±1.70*	0.173 *±0.04*	110.6 *±1.21*	0.060 *±0.01*	115.2 *±1.84*	0.10 *±0.003*	118.4 *±1.98*	0.11 *±0.02*

Acronyms: polydispersity, PDI; Time, $T_{(day)}$.

**Light irradiation for 5 minutes at 600mW: cardiogreen – near infrared light; methylene blue – 590 nm; riboflavin – 450 nm; empty liposomes – white light.*

± *Standard deviation*

3.9 REFERENCES

[1] T. Uzawa, M. Hori, S. Ejiri, H. Ozawa, Comparison of the effects of intermittent and continuous administration of human parathyroid hormone(1-34) on rat bone, Bone, 16 (1995) 477-484.

[2] R. Farra, N.F. Sheppard, Jr., L. McCabe, R.M. Neer, J.M. Anderson, J.T. Santini, Jr., M.J. Cima, R. Langer, First-in-Human Testing of a Wirelessly Controlled Drug Delivery Microchip, Science Translational Medicine, 4 (2012).

[3] M. Nair, R. Guduru, P. Liang, J. Hong, V. Sagar, S. Khizroev, Externally controlled on-demand release of anti-HIV drug using magneto-electric nanoparticles as carriers, Nature Communications, 4 (2013).

[4] B.T. Hawkins, T.P. Davis, The blood-brain barrier/neurovascular unit in health and disease, Pharmacological Reviews, 57 (2005) 173-185.

[5] Z.M. Saiyed, N.H. Gandhi, M.P.N. Nair, Magnetic nanoformulation of azidothymidine 5 '-triphosphate for targeted delivery across the blood-brain barrier, International Journal of Nanomedicine, 5 (2010) 157-166.

[6] C. Deal, J. Gideon, Recombinant human PTH 1-34 (Forteo): An anabolic drug for osteoporosis, Cleveland Clinic Journal of Medicine, 70 (2003) 585-586.

[7] S. Mura, J. Nicolas, P. Couvreur, Stimuli-responsive nanocarriers for drug delivery, Nature Materials, 12 (2013) 991-1003.

[8] S.R. Sirsi, M.A. Borden, State-of-the-art materials for ultrasound-triggered drug delivery, Advanced Drug Delivery Reviews, 72 (2014) 3-14.

[9] Wahajuddin, S. Arora, Superparamagnetic iron oxide nanoparticles: magnetic nanoplatforms as drug carriers, International Journal of Nanomedicine, 7 (2012) 3445-3471.

[10] C. Alvarez-Lorenzo, L. Bromberg, A. Concheiro, Light-sensitive Intelligent Drug Delivery Systems, Photochemistry and Photobiology, 85 (2009) 848-860.

[11] K.S. Soppimath, T.M. Aminabhavi, A.R. Kulkarni, W.E. Rudzinski, Biodegradable polymeric nanoparticles as drug delivery devices, Journal of Controlled Release, 70 (2001) 1-20.

[12] T.M. Allen, Drug Delivery Systems: Entering the Mainstream, Science, 303 (2004) 1818-1822.

[13] X.Z. Zhang, R.X. Zhuo, Y.Y. Yang, Using mixed solvent to synthesize temperature sensitive poly(N-isopropylacrylamide) gel with rapid dynamics properties, Biomaterials, 23 (2002) 1313-1318.

[14] Z.-K. Cui, G. Bastiat, C. Jin, A. Keyvanloo, M. Lafleur, Influence of the nature of the sterol on the behavior of palmitic acid/sterol mixtures and their derived liposomes, Biochimica Et Biophysica Acta-Biomembranes, 1798 (2010) 1144-1152.

[15] C.-C. Lin, A.T. Metters, Hydrogels in controlled release formulations: Network design and mathematical modeling, Advanced Drug Delivery Reviews, 58 (2006) 1379-1408.

[16] T. Canal, N.A. Peppas, Correlation between mesh size and equilibrium degree of swelling of polymeric networks, Journal of Biomedical Materials Research, 23 (1989) 1183-1193.

[17] D. Eisenberg, D. Crothers, Physical Chemistry with Applications to the Life Sciences, The Benjamin/Cummings Publishing Company, Menlo Park, 1979.

[18] C. Fanger, H. Wack, M. Ulbricht, Macroporous poly (N-isopropylacrylamide) hydrogels with adjustable size "cut-off" for the efficient and reversible immobilization of biomacromolecules, Macromolecular Bioscience, 6 (2006) 393-402.

[19] Y. Fu, W.J. Kao, Drug release kinetics and transport mechanisms of non-degradable and degradable polymeric delivery systems, Expert Opinion on Drug Delivery, 7 (2010) 429-444.

[20] K. Dill, S. Bromberg, Molecular driving forces: statistical thermodynamics in chemistry and biology, Garland Science, New York, 2003.

[21] M. Goldberg, I. Gomez-Orellana, Challenges for the oral delivery of macromolecules, Nature Reviews Drug Discovery, 2 (2003) 289-295.

[22] M. Palasis, S.H. Gehrke, Permeability of responsive poly(N-isopropylacrylamide) gel to solutes, Journal of Controlled Release, 18 (1992) 1-11.

[23] G.M. Cruise, D.S. Scharp, J.A. Hubbell, Characterization of permeability and network structure of interfacially photopolymerized poly(ethylene glycol) diacrylate hydrogels, Biomaterials, 19 (1998) 1287-1294.

[24] J.W. Mwangi, C.M. Ofner, Crosslinked gelatin matrices: release of a random coil macromolecular solute, International Journal of Pharmaceutics, 278 (2004) 319-327.

[25] H.S. Shin, S.Y. Kim, Y.M. Lee, K.H. Lee, S.J. Kim, C.E. Rogers, Permeation of solutes through interpenetrating polymer network hydrogels composed of poly(vinyl alcohol) and poly(acrylic acid), Journal of Applied Polymer Science, 69 (1998) 479-486.

[26] M. Majumder, P. Sheath, J.I. Mardel, T.G. Harvey, A.W. Thornton, A. Gonzago, D.F. Kennedy, I. Madsen, J.W. Taylor, D.R. Turner, M.R. Hill, Aqueous Molecular Sieving and Strong Gas Adsorption in Highly Porous MOFs with a Facile Synthesis, Chemistry of Materials, 24 (2012) 4647-4652.

[27] D.S. Banks, C. Fradin, Anomalous diffusion of proteins due to molecular crowding, Biophysical Journal, 89 (2005) 2960-2971.

[28] W. Li, J.H. Rockey, Fluorescein binding to normal human-serum proteins demonstrated by equilibrium dialysis, Archives of Ophthalmology, 100 (1982) 484-487.

[29] E.M. Tuite, J.M. Kelly, Photochemical interactions of methylene-blue and analogs with DNA and other biological substrates, Journal of Photochemistry and Photobiology B-Biology, 21 (1993) 103-124.

[30] H.G. Schild, Poly (N-isopropylacrylamide) - Experiment, theory and application, Progress in Polymer Science, 17 (1992) 163-249.

[31] A.S. Hoffman, A. Afrassiabi, L.C. Dong, Thermally reversible hydrogels II. Delivery and selective removal of substances from aqueous solutions, Journal of Controlled Release, 4 (1986) 213-222.

[32] B.P. Timko, T. Dvir, D.S. Kohane, Remotely Triggerable Drug Delivery Systems, Advanced Materials, 22 (2010).

[33] J. Seunng, S. Agarwal, First Example of a Universal and Cost-Effective Approach: Polymers with Tunable Upper Critical Solution Temperature in Water and Electrolyte Solution, Macromolecules, 45 (2012) 3910-3918.

[34] D. Roy, W.L.A. Brooks, B.S. Sumerlin, New directions in thermoresponsive polymers, Chemical Society Reviews, 42 (2013) 7214-7243.

[35] J. Seuring, S. Agarwal, Polymers with Upper Critical Solution Temperature in Aqueous Solution: Unexpected Properties from Known Building Blocks, Acs Macro Letters, 2 (2013) 597-600.

[36] B.D. Ulery, L.S. Nair, C.T. Laurencin, Biomedical Applications of Biodegradable Polymers, Journal of Polymer Science Part B-Polymer Physics, 49 (2011) 832-864.

[37] Z. Zhang, R. Kuijer, S.K. Bulstra, D.W. Grijpma, J. Feijen, The in vivo and in vitro degradation behavior of poly(trimethylene carbonate), Biomaterials, 27 (2006) 1741-1748.

CHAPTER FOUR: CONCLUSIONS AND FUTURE DIRECTIONS

The objective of this project was to design a light actuated drug delivery-on-demand system that uses biocompatible chromophores and safe wavelengths of light. This was achieved by characterizing the photothermal response of biocompatible visible light and near infrared (NIR)-responsive chromophores for drug delivery-on-demand applications, and demonstrating the feasibility and functionality of the light actuated on-demand drug delivery system in vitro. Specifically, cardiogreen, methylene blue and riboflavin were shown to be capable of significantly increasing the temperature of aqueous solutions upon exposure to visible light or NIR, and this temperature change was dependent upon light intensity, wavelength, and chromophore concentration. Furthermore, cardiogreen irradiated with NIR triggered the rapid release of a model biologic drug from a thermally responsive delivery vehicle over multiple NIR exposures. The results from Chapter 2 advanced the biomedical application of cardiogreen, methylene blue and riboflavin by using them as a tool for light-actuated drug delivery-on-demand systems. However, the system described in Chapter 2 had a short useful timeline as both drug and chromophore were quickly eliminated from the thermally responsive delivery vehicle. To address these shortcomings, a modular, reservoir-type drug delivery-on-demand system that would release biologically active molecules over an extended period of time via light actuation was designed. Using a design that combined a drug reservoir and thermally-responsive valve spiked with chromophore-loaded liposomes, pulsatile release of the model small molecule drug riboflavin was achieved over 7 days. Despite the improved lifetime for light actuated release, diffusion between light exposures remains as a dominating release mechanism. As such, novel designs that eliminate drug release between exposures will enhance light actuated drug delivery-on-demand systems efficacy

Ultimately, this drug delivery strategy has potential for clinical applications that require explicit control over the presentation of biologically active molecules. Further research into the design and fabrication of novel biocompatible thermally responsive delivery vehicles will aid in the advancement of the light actuated drug delivery-on-demand approach described here. Additionally, in vivo studies that demonstrate the feasibility and functionality of this strategy to treat clinical indications are required. These studies are also needed to confirm the in vivo biocompatibility.

4.1 ENGINEERING BIOCOMPATIBLE PHOTO-RESPONSIVE MATERIALS

There is a lack of biocompatible photo- and photothermally-responsive materials to serve as delivery vehicles for light actuated drug delivery-on-demand systems. This bottleneck limits these systems to proof-of-concept models and presents a significant obstacle to clinical translation. To overcome this bottleneck, work is needed to design and fabricate delivery vehicles made entirely of materials that are already used in Food and Drug Administration (FDA) approved applications, but incorporated to produce unique features that have not been reported with said materials. A successful delivery vehicle will be biocompatible, rapidly respond to light actuation, and demonstrate little-to-no release in the absence of light.

Using oligonucleotides as photothermally-responsive tethers is one possible approach. DNA de-hybridizes at elevated temperatures, and the temperature that de-hybridization occurs at can be modulated to physiologically relevant temperatures by changing the number of base pairings between the two DNA strands as well as the guanine-cytosine content [1]. Indeed, this strategy to use oligonucleotides as heat liable tethers for the controlled release of biologically active molecules has been previously reported [2, 3]. For example, previous studies have conjugated DNA tethers to gold nanoparticles, which generate heat upon exposure to NIR, in

order to de-hybridize the double stranded DNA thereby releasing single stranded DNA [4]. This capability makes DNA tethers an attractive option for delivery-on-demand systems. By conjugating these tethers to various biomaterials, a stimuli-responsive delivery vehicle can be fabricated out of traditionally non-responsive biomaterials, and addition of the non-toxic, biocompatible chromophore characterized in Chapter 2 can be used to trigger release via the photothermal effect.

Fibrin is a traditionally non-stimuli-sensitive biomaterial with a long history of use in FDA approved products that these DNA tethers can be attached to, thereby making it photothermally responsive. Fibrin has previously been functionalized with exogenous peptides by enzymatic incorporation to alter its bioactivity [5]. This was accomplished by attaching the substrate for Factor XIIIa – a transglutaminase that crosslinks glutamine and lysine residues within the fibrin network – to the molecule to be released. For example, previous studies have enzymatically incorporated VEGF into fibrin scaffolds and then control the growth factor release as endothelial cells migrate into the fibrin scaffold and degrade it [6-8]. Utilizing this strategy to functionalize fibrin with DNA tethers, a light sensitive drug delivery-on-demand system can be engineered out of materials with proven biocompatibility.

Specifically, DNA tethers can be functionalized with peptides of the Factor XIIIa substrate (peptide sequence: NQEQVSPL) in order to enzymatically incorporate them into the fibrin network. Preliminary data (Figure 1) shows that the swelling ratio of fibrin gels increases with the addition of 100 μg/mL of Factor XIIIa substrate peptide, indicating a disruption in the crosslinking of the fibrin network and, therefore, enzymatic incorporation of the peptide sequence. The lower concentration of peptide added (50 μg/mL) did not change the swelling ratio compared to control fibrin hydrogels. This suggests that the concentration of peptide added

was negligible and any change to the fibrin network as a result of enzymatic incorporation is not detectable. It seems unlikely that the peptide failed to incorporate since there is a measurable difference in swelling ratios when a higher concentration of peptide is added. Regardless, further characterization is required. This includes testing for changes in the fibrin hydrogel's mechanical properties via rheometry, measuring the peptide's incorporation efficiency and subsequently studying the effect on cellular response. Ultimately, the ability of this strategy to enzymatically incorporate DNA tethers and photothermally release a payload needs to be demonstrated.

There are other biomaterials that can be fitted with DNA tethers and engineering photothermally-responsive fibrin is only one possibility. As seen in Figure 2, there are numerous possible delivery vehicles that qualify as biocompatible – each with unique advantages and disadvantages. For instance, alginate is biocompatible and demonstrates long term stability in vivo [9], but lacks cell binding sites and requires modification with RGD to promote cell survival if the delivery vehicle is supposed to act as a scaffold as well [10]. Additionally, each biomaterial will have unique properties that can be exploited for the incorporation of heat sensitive linkers, and there are numerous payloads that can be delivered on-demand. Identifying novel ways to engineer biomaterials that demonstrate thermal-sensitivity and can be utilized in the delivery-on-demand strategy reported here would help overcome obstacles to clinical translation for light-actuated delivery-on-demand systems.

4.2 DESIGNING A LOW POWER, MULTIPLE-BEAM NEAR INFRARED SOURCE

The advantage of NIR (700-1100 nm) for light actuated delivery-on-demand systems is the deep tissue penetration that is achievable, which is why this range of wavelengths has been coined the "optical window" [11]. The reason for this is that the major endogenous absorbers that limit the penetration depth of visible and ultraviolet light – oxyhemoglobin, deoxyhemoglobin,

melanin, bilirubin, β-carotene, etc. – have absorption minima in the NIR region [12]. Rather, water is the major absorber in living tissue, but it has a low absorption coefficient ($\leq$0.1 cm^{-1}) in this range [13]. The resulting differences in light attenuation at various wavelengths are highlighted in Supplement Figure 1. Specifically, the transmittance percent of visible light through ~200 μm section of tissue (Supplement Figure 1A) is comparable to the transmittance percent of NIR through a tissue section millimeters thick (Supplement Figure 1B).

Tissues are not, however, completely transparent to NIR, and the greatest cause of NIR attenuation is from scattering. Both cellular and extracellular components contribute to scattering due to differences in refractive indices as well as Mie scattering, but collagen is the predominate scatterer [14]. Consequently, a greater number of photons from the NIR source are required for deeper tissue applications of the reported drug delivery-on-demand system (Figure 3A). Unfortunately, despite water's low absorption coefficient in the NIR, significant temperatures changes can be achieved via NIR absorption by water with enough intensity as seen in the Chapter 2 results. As seen in Figure 3B, this can cause significant temperature changes in the overlying tissue as native water absorbs NIR photons, which can result in tissue damage from excessive heating.

One solution to achieve greater penetration depth without damaging the overlying tissue is to use multiple low-power light sources for light actuation. Preliminary data, shown in Figure 3C, demonstrates that a single low-power (~350mW) beam of NIR is unable to produce a significant photothermal effect, but when two low-power beams are used, a photothermal response comparable to a sample irradiated with a single 700mW NIR beam is produced. As such, two low-power light sources can be used to protect the superficial tissue from thermal

damage while the location where the NIR beams converge will have a sufficient power to produce a significant photothermal effect (Figures 3D and 3E).

A similar strategy is used in other clinical applications in order to achieve significant penetration depths into the body. For example, stereotactic radiosurgery is one strategy used to increase the radiation dose to brain tumors while surrounding healthy tissue receives a clinically insignificant dosage of radiation. This is achieved by creating a shell with 192 individual radiation sources and internal channels to focus the radiation – all under the control of a computer [15]. In this way, the point where the beams converge receives a high dose of photon energy while the energy from each individual beam is under the harmful limit as it travels through tissue [16]. The added benefit of using multiple low-power light sources for light-actuated delivery-on-demand, where the drug delivery vehicles are distributed throughout the body, is release would only occur in areas where intense light is applied, thereby reducing the likelihood of off-target release.

4.3 IN VIVO VALIDATION: SAFETY AND EFFICACY

The reported in vitro studies have demonstrated the feasibility and functionality of the drug delivery-on-demand system for biologically active molecules; however, in vivo studies are needed that demonstrate a favorable clinical outcome. For instance, the light actuated delivery-on-demand of chemotherapeutic drugs should reduce tumor sizes if not completely eliminate the tumor in cancer treatment applications. In addition to studying the effectiveness, the safety of the system needs to be evaluated. For instance, cells can exhibit a stress response when exposed to excessive amounts of heat via the bystander effect [18]. These increased temperatures can denature cellular proteins, adversely affect mitochondrial function, and lead to the accumulation of perichromatin granules in the nucleus [19]. Fortunately, cells have mechanisms in place to

protect against the adverse effects of excessive heat generation. One such mechanism is the expression of stress proteins. There are numerous proteins categorized as stress proteins and they serve a number of functions, such as assisting in the folding and unfolding of other proteins, transporting proteins, and triggering an immune response [19]. However, if the cell is exposed to too much heat, apoptosis and necrosis will occur. Clearly, it is necessary to understand the heating profile and general response of the drug delivery-on-demand system upon light irradiation in a living system.

Based on the photothermal response data from Chapter 2 and the ex vivo data from Chapter 3, it is expected that a significant photothermal response from irradiated chromophores can be achieved in vivo. However, the heating profile is likely to be different due to perfusion in living tissues and differences in the thermal properties. Previously, heat transfer in tissue has been modeled by the Pennes's Bioheat Equation, seen here:

$$\rho c \frac{\partial T}{\partial t} = k\nabla^2 T + h_m + \mathrm{V}\rho_b c_b (T_a - T) \quad (1)$$

where ρ is density of tissue, c is specific heat of tissue, k thermal conductivity of tissue, T local tissue temperature, h_m rate of metabolic heat production per unit volume of tissue, V perfusion rate per unit volume of tissue, ρ_b density of blood, c_b is specific heat of blood, and T_a is temperature of arterial blood [20]. In Chapter 2, water was the medium used in the temperature change results; however, the thermal conductivity of tissue is lower than that of water. For example, many internal organs have thermal conductivities around 0.49 W/m/K compared to water at 0.60 W/m/K [21]. Further, the final heating profile will be dependent on the surrounding tissue. Skin and fat, for instance, have low thermal conductivities at 0.37 and 0.21 W/m/K, respectively while tissues like the eye and the lumen of the small intestines have thermal conductivities >0.50 W/m/K [22]. As such, it is likely that the in vivo environment is going to

have an insulating effect with less heat lost while heat is being generated. The presence of a heat sink can further complicate the heating profile (represented by the third term in Equation 1). The blood in perfused tissues can absorb the heat generated from chromophore irradiation and carry it away [23]. Therefore, in vivo evaluation and characterization of the heating profiles generated from chromophore irradiation are required for safe application of the designed drug delivery-on-demand system.

Chapter 2 discussed that chromophores are capable producing reactive oxygen species such as singlet oxygen and other free radicals upon light irradiation, which can be cytotoxic and lead to irreversible damage [24]. In particular, the hydroxyl radical is a highly reactive species with diffusion-controlled reaction rates [25]. Specifically, free radicals, such as hydroxyl radicals, and reactive oxygen species target sulfhydryl bonds in proteins, the unsaturated bonds in membrane fatty acids and nucleic acids [26]. For example, the double bonds in heterocyclic DNA bases are one target of hydroxyl radicals and the addition of hydroxyl radicals contributes to the generation of additional free radical species that culminate in strand breaks and DNA-protein crosslinks [27]. Furthermore, singlet oxygen can react directly with cholesterol and fatty acids in the cell membrane via Type II lipid peroxidation reaction, which leads to a loss of membrane flexibility, permeability and structural integrity in vivo [28, 29]. However, it is important to note that cells produce a number of different free radicals species naturally during electron transfer reactions, and there are innate defense mechanisms in vivo, such as enzymes and free radical scavengers, to protect against oxidative damage [25]. For instance, the human eye has excess ascorbic acid present to scavenge free radicals produced by photochemical oxidation due to light entering the aqueous humor [30]. One goal of future animal studies will therefore need to be to determine whether free radicals generated during light irradiation of the

drug delivery-on-demand system overwhelms the these innate defense mechanisms leading to tissue damage. In which case, additional features to protect against the generation of excess reactive species will need to be included in the delivery system design.

While many clinical applications require protection against both excessive free radical generation as well as excessive heat generation, there are cases where it would be advantageous to allow free radical generation and/or excessive tissue heating to occur in combination with drug delivery-on-demand. For instance, photodynamic therapy (PDT) utilizes photosensitizers to produce cytotoxic species for treating oncological, cardiovascular, ophthalmic and dermatological diseases [31, 32]. Clinical trials using PDT to treat choroidal neovascularization (blood vessel growth that results in damage to the retina) showed sustained visual acuity in 53% of patients compared to 38% of patients treated with the placebo [33]. A recent study combined PDT with anti-vascular endothelial growth factor (VEGF) injections and found improved vision and decreased retinal thickness in patients who had failed anti-VEGF monotherapy [34]. In the case of excessive heat generation, thermal energy has been used to induce cell death in small, unresectable tumors [35], and enhanced tumor destruction has been observed with combined thermal ablation and doxorubicin delivery compared to thermal ablation alone [36]. Clearly, there are clinical applications that would benefit from combined PDT or thermal ablation with drug delivery-on-demand and the resulting combination products would become powerful tools in the treatment of disease.

4.4 CONCLUDING REMARKS

The future is bright for light actuated drug delivery-on-demand systems, but there is still much to do. In addition to designing new delivery vehicles and performing in vivo validation studies, more evidence supporting delivery-on-demand over conventional methods (i.e. sustained

controlled release, bolus injections) for applications ranging from tissue engineering to cancer treatment is required to engineer optimal delivery-on-demand systems with release profiles that maximize clinical outcomes. Furthermore, the complexity of these systems is a challenge to scale-up and reduces its chances of reaching patients. Going forward, one of the goals needs to be: simplify.

4.5 FIGURES

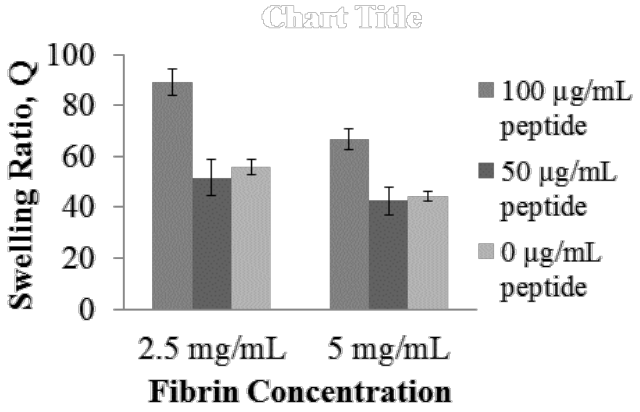

Figure 1. Swelling Ratio of 300µL fibrin hydrogels (2.5 and 5 mg/mL final fibrinogen concentration prepared with 10 IU/mL thrombin) with and without Factor XIIIa substrate peptide (n=3).

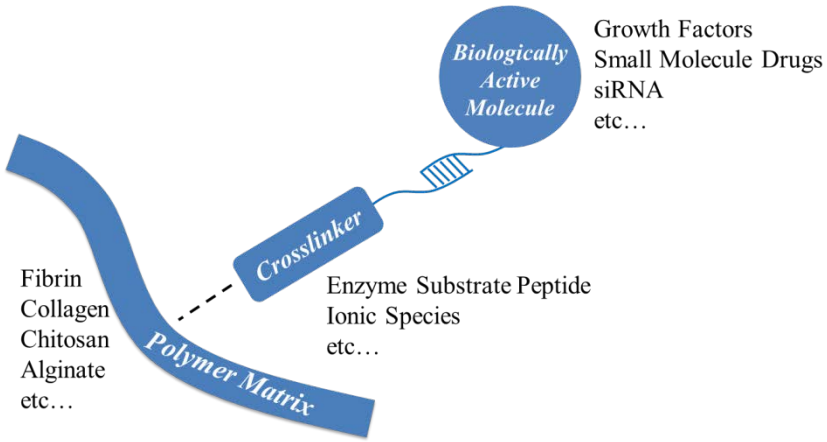

Figure 2. Schematic illustration of the strategy to functionalize traditionally non-thermally responsive materials with thermally responsive linkers. Biomaterials have unique properties that can be used to incorporate of heat sensitive linkers for the delivery-on-demand of various biologically active molecules.

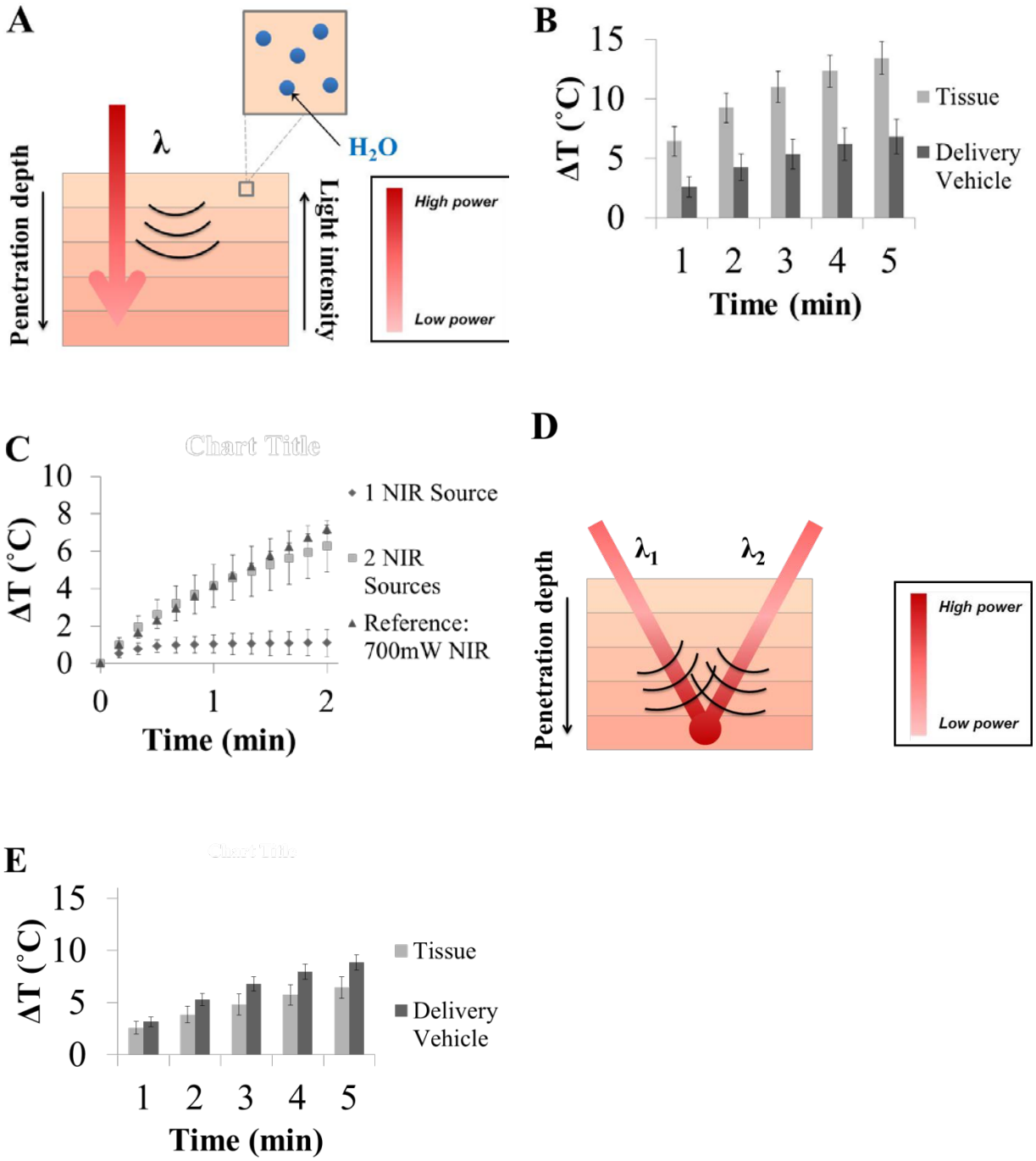

Figure 3. (A) Illustration of single light source setup which requires a high power light source for deeper tissue penetration due to light attenuation. The high power can cause heating in superficial tissue because of moderate NIR absorption by water in the tissue. (B) The measured

temperature change of chicken muscle tissue (thickness = 2mm) in the NIR beam path and a cardiogreen-spiked NiPAAm delivery vehicle (see Chapter 2 – Materials and Methods for loading protocol) beneath the tissue (NIR initial light intensity ~ 1W; n=9). (C) The measured temperature change of cardiogreen-spiked NiPAAm delivery vehicle irradiated with a single low-power (~350mW) beam of NIR and dual low-power (combined ~700mW) beams of NIR light. A single beam of NIR at 350mW is unable to produce a significant photothermal effect, but a photothermal response comparable to a sample irradiated with a single 700mW NIR beam is produced when two low-power NIR beams are used to irradiate the samples (n=9). (D) Illustration of dual light source setup which using converging low-power NIR beams to deliver a high dose of NIR photons to deeper tissue without heating the superficial tissue. (E) The measured temperature change of chicken muscle tissue (thickness = 2mm) in the NIR beam path and a cardiogreen-spiked NiPAAm delivery vehicle beneath the tissue ($\lambda_{NIR\text{-}1}$ = 350mW, $\lambda_{NIR\text{-}2}$ = 350mW; n=9).

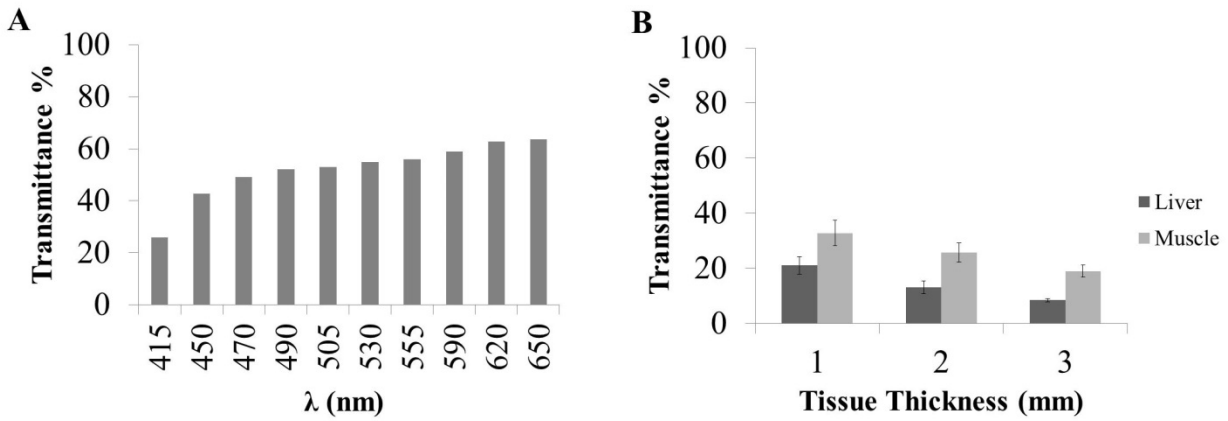

Supplement Figure 1. Transmittance percent of (A) visible light through rat pup skin (thickness = 0.23mm); and (B) near infrared light through 1-3mm thick rat tissue (n=3).

4.6 REFERENCES

[1] R.C. Jin, G.S. Wu, Z. Li, C.A. Mirkin, G.C. Schatz, What controls the melting properties of DNA-linked gold nanoparticle assemblies?, Journal of the American Chemical Society, 125 (2003) 1643-1654.

[2] A.M. Derfus, G. von Maltzahn, T.J. Harris, T. Duza, K.S. Vecchio, E. Ruoslahti, S.N. Bhatia, Remotely triggered release from magnetic nanoparticles, Advanced Materials, 19 (2007) 3932-3936.

[3] E. Ruiz-Hernandez, A. Baeza, M. Vallet-Regi, Smart Drug Delivery through DNA/Magnetic Nanoparticle Gates, Acs Nano, 5 (2011) 1259-1266.

[4] S. Yamashita, H. Fukushima, Y. Akiyama, Y. Niidome, T. Mori, Y. Katayama, T. Niidome, Controlled-release system of single-stranded DNA triggered by the photothermal effect of gold nanorods and its in vivo application, Bioorganic & Medicinal Chemistry, 19 (2011) 2130-2135.

[5] J.C. Schense, J. Bloch, P. Aebischer, J.A. Hubbell, Enzymatic incorporation of bioactive peptides into fibrin matrices enhances neurite extension, Nature Biotechnology, 18 (2000) 415-419.

[6] M. Ehrbar, A. Metters, P. Zammaretti, J.A. Hubbell, A.H. Zisch, Endothelial cell proliferation and progenitor maturation by fibrin-bound VEGF variants with differential susceptibilities to local cellular activity, Journal of Controlled Release, 101 (2005) 93-109.

[7] A.H. Zisch, U. Schenk, J.C. Schense, S.E. Sakiyama-Elbert, J.A. Hubbell, Covalently conjugated VEGF-fibrin matrices for endothelialization, Journal of Controlled Release, 72 (2001) 101-113.

[8] M. Ehrbar, V.G. Djonov, C. Schnell, S.A. Tschanz, G. Martiny-Baron, U. Schenk, J. Wood, P.H. Burri, J.A. Hubbell, A.H. Zisch, Cell-demanded liberation of VEGF(121) from fibrin implants induces local and controlled blood vessel growth, Circulation Research, 94 (2004) 1124-1132.

[9] T. Andersen, B.L. Strand, K. Formo, E. Alsberg, B.E. Christensen, Alginates as biomaterials in tissue engineering, Carbohydrate Chemistry: Chemical and Biological Approaches, Vol 37, 37 (2012) 227-258.

[10] J.A. Rowley, G. Madlambayan, D.J. Mooney, Alginate hydrogels as synthetic extracellular matrix materials, Biomaterials, 20 (1999) 45-53.

[11] K. Konig, Multiphoton microscopy in life sciences, Journal of Microscopy, 200 (2000) 83-104.

[12] S.L. Jacques, Optical properties of biological tissues: a review, Physics in Medicine and Biology, 58 (2013) R37-R61.

[13] G.M. Hale, M.R. Querry, Optical-constants of water in 200-nm to 200-mum wavelength region, Applied Optics, 12 (1973) 555-563.

[14] S. Thomsen, D. Tatman, Physiological and pathological factors of human breast disease that can influence optical diagnosis, Advances in Optical Biopsy and Optical Mammography, 838 (1998) 171-193.

[15] J.H. Suh, Stereotactic Radiosurgery for the Management of Brain Metastases, New England Journal of Medicine, 362 (2010) 1119-1127.

[16] S. Kim, J. Palta, The Physics of Stereotactic Radiosurgery, in: L.S. Chin, W.F. Regine (Eds.) Principles and Practice of Stereotactic Radiosurgery, Springer New York, 2008 pp. 33-50.

[17] V. Ntziachristos, Going deeper than microscopy: the optical imaging frontier in biology, Nature Methods, 7 (2010) 603-614.

[18] M. Purschke, H.-J. Laubach, R.R. Anderson, D. Manstein, Thermal Injury Causes DNA Damage and Lethality in Unheated Surrounding Cells: Active Thermal Bystander Effect, Journal of Investigative Dermatology, 130 (2010) 86-92.

[19] W.J. Welch, Mammalian stress response - Cell physiology, structure-function of stress proteins, and implications for medicine and disease, Physiological Reviews, 72 (1992) 1063-1081.

[20] H. Arkin, L.X. Xu, K.R. Holmes, Recent Developments in Modeling Heat-Transfer in Blood-Perfused Tissues, Ieee Transactions on Biomedical Engineering, 41 (1994) 97-107.

[21] J.W. Valvano, J.R. Cochran, K.R. Diller, Thermal-conductivity and diffusivity of biomaterials measured with self-heated thermistors, International Journal of Thermophysics, 6 (1985) 301-311.

[22] P. Hasgall, E. Neufeld, M. Gosselin, A. Klingenböck, N. Kuster, IT'IS database for thermal and electromagnetic parameters of biological tissues, in, 2012.

[23] M.B. Ducharme, P. Tikuisis, Role of blood as heat-source or sink in human limbs during local cooling and heating, Journal of Applied Physiology, 76 (1994) 2084-2094.

[24] R. Chen, X. Wang, X.K. Yao, X.C. Zheng, J. Wang, X.Q. Jiang, Near-IR-triggered photothermal/photodynamic dual-modality therapy system via chitosan hybrid nanospheres, Biomaterials, 34 (2013) 8314-8322.

[25] K.H. Cheeseman, T.F. Slater, An introduction to free-radical biochemistry, British Medical Bulletin, 49 (1993) 481-493.

[26] L.J. Machlin, A. Bendich, Free-radical tissue-damage - Protective role of antioxidant nutrients, Faseb Journal, 1 (1987) 441-445.

[27] M. Dizdaroglu, P. Jaruga, M. Birincioglu, H. Rodriguez, Free radical-induced damage to DNA: Mechanisms and measurement, Free Radical Biology and Medicine, 32 (2002) 1102-1115.

[28] A.W. Girotti, Photodynamic lipid-peroxidation in biological-systems, Photochemistry and Photobiology, 51 (1990) 497-509.

[29] J.M.C. Gutteridge, Lipid-peroxidation and antioxidants as biomarkers of tissue-damage, Clinical Chemistry, 41 (1995) 1819-1828.

[30] S.D. Varma, S. Kumar, R.D. Richards, Light-induced damage to ocular lens cation pump: prevention by vitamin C, Proceedings of the National Academy of Sciences, 76 (1979) 3504-3506.

[31] H.J. Hah, G. Kim, Y.-E.K. Lee, D.A. Orringer, O. Sagher, M.A. Philbert, R. Kopelman, Methylene Blue-Conjugated Hydrogel Nanoparticles and Tumor-Cell Targeted Photodynamic Therapy, Macromolecular Bioscience, 11 (2011) 90-99.

[32] Y.N. Konan, R. Gurny, E. Allemann, State of the art in the delivery of photosensitizers for photodynamic therapy, Journal of Photochemistry and Photobiology B-Biology, 66 (2002) 89-106.

[33] M.S. Blumenkranz, N.M. Bressler, M.J. Potter, S.B. Bressler, J.M. Mones, P. Harvey, L.J. Singerman, E.S. Gragoudas, J.W. Miller, U. Schmidt-Erfurth, D. Treatment Age Related Macular, Photodynamic therapy of subfoveal choroidal neovascularization in age-related macular degeneration with verteporfin - Two-year results of 2 randomized clinical trials - TAP report 2, Archives of Ophthalmology, 119 (2001) 198-207.

[34] K. Tozer, A.B. Roller, L.P. Chong, S. Sadda, J.C. Folk, V.B. Mahajan, S.R. Russell, H.C. Boldt, E.H. Sohn, Combination Therapy for Neovascular Age-related Macular Degeneration Refractory to Anti-Vascular Endothelial Growth Factor Agents, Ophthalmology, 120 (2013) 2029-2034.

[35] K.F. Chu, D.E. Dupuy, Thermal ablation of tumours: biological mechanisms and advances in therapy, Nature Reviews Cancer, 14 (2014) 199-208.

[36] S.N. Goldberg, I.R. Kamel, J.B. Kruskal, K. Reynolds, W.L. Monsky, K.E. Stuart, M. Ahmed, V. Raptopoulos, Radiofrequency ablation of hepatic tumors: Increased tumor destruction with adjuvant liposomal doxorubicin therapy, American Journal of Roentgenology, 179 (2002) 93-101.